Recommendations for clinical electron beam dosimetry: Supplement to the recommendations of Task Group 25

Bruce J. Gerbi[a)]
University of Minnesota, Minneapolis, Minnesota 55455

John A. Antolak
Mayo Clinic, Rochester, Minnesota 55905

F. Christopher Deibel
Cleveland Clinic, Cleveland, Ohio 44195

David S. Followill
The University of Texas M. D. Anderson Cancer Center, Houston, Texas 77030

Michael G. Herman
Mayo Clinic, Rochester, Minnesota 55905

Patrick D. Higgins
University of Minnesota, Minneapolis, Minnesota 55455

M. Saiful Huq
University of Pittsburgh Cancer Institute, Pittsburgh, Pennsylvania 15232

Dimitris N. Mihailidis
Charleston Radiation Therapy Consultants, Charleston, West Virginia 25304

Ellen D. Yorke
Memorial Sloan-Kettering Cancer Center, New York, New York 10021

Consultants:

Kenneth R. Hogstrom
Louisiana State University, Baton Rouge, Louisiana 70803-4001

Faiz M. Khan
University of Minnesota, Minneapolis, Minnesota 55455

(Received 13 October 2008; revised 17 March 2009; accepted for publication 1 April 2009; published 18 June 2009)

The goal of Task Group 25 (TG-25) of the Radiation Therapy Committee of the American Association of Physicists in Medicine (AAPM) was to provide a methodology and set of procedures for a medical physicist performing clinical electron beam dosimetry in the nominal energy range of 5–25 MeV. Specifically, the task group recommended procedures for acquiring basic information required for acceptance testing and treatment planning of new accelerators with therapeutic electron beams. Since the publication of the TG-25 report, significant advances have taken place in the field of electron beam dosimetry, the most significant being that primary standards laboratories around the world have shifted from calibration standards based on exposure or air kerma to standards based on absorbed dose to water. The AAPM has published a new calibration protocol, TG-51, for the calibration of high-energy photon and electron beams. The formalism and dosimetry procedures recommended in this protocol are based on the absorbed dose to water calibration coefficient of an ionization chamber at ^{60}Co energy, $N_{D,w}^{^{60}\mathrm{Co}}$, together with the theoretical beam quality conversion coefficient k_Q for the determination of absorbed dose to water in high-energy photon and electron beams. Task Group 70 was charged to reassess and update the recommendations in TG-25 to bring them into alignment with report TG-51 and to recommend new methodologies and procedures that would allow the practicing medical physicist to initiate and continue a high quality program in clinical electron beam dosimetry. This TG-70 report is a supplement to the TG-25 report and enhances the TG-25 report by including new topics and topics that were not covered in depth in the TG-25 report. These topics include procedures for obtaining data to commission a treatment planning computer, determining dose in irregularly shaped electron fields, and commissioning of sophisticated special procedures using high-energy electron beams. The use of radiochromic film for electrons is addressed, and radiographic film that is no longer available has been replaced by film that is available. Realistic stopping-power data are incorporated when appropriate along with enhanced tables of electron fluence data. A larger list of clinical applications of electron beams is included in the full TG-70 report available at http://www.aapm.org/pubs/reports. Descriptions of the techniques in the clinical sections are not exhaustive but do describe key elements of the procedures

and how to initiate these programs in the clinic. There have been no major changes since the TG-25 report relating to flatness and symmetry, surface dose, use of thermoluminescent dosimeters or diodes, virtual source position designation, air gap corrections, oblique incidence, or corrections for inhomogeneities. Thus these topics are not addressed in the TG-70 report. © *2009 American Association of Physicists in Medicine.* [DOI: 10.1118/1.3125820]

Key words: electrons, quality assurance, clinical dosimetry, TG-25

TABLE OF CONTENTS

I. INTRODUCTION

The goal of Task Group 25 (TG-25) of the Radiation Therapy Committee of the American Association of Physicists in Medicine (AAPM) was to provide a methodology and a set of procedures for the practicing clinical physicist for performing clinical electron beam dosimetry in the nominal energy range from 5 to 25 MeV.[1] Specifically, the task group recommended procedures and measurement techniques for acquiring basic information required for acceptance testing and treatment planning of new accelerators with therapeutic electron beams. TG-25 also provided information on many aspects of clinical electron beam dosimetry including, but not limited to, thermoluminescent dosimetry (TLD), diode dosimetry, film dosimetry, electron source position, field shaping and shielding, measurements of percentage depth dose, and beam flatness and symmetry. Since the publication of this report, significant advances have taken place in the field of electron beam dosimetry. For example, the major emphasis in primary standards laboratories around the world has shifted from standards for exposure or air kerma to those for absorbed dose to water. Accredited dosimetry calibration laboratories now provide calibrations of ionization chambers in terms of absorbed dose to water at the radiation quality of ^{60}Co gamma rays. The AAPM has published a new calibration protocol, TG-51, for the calibration of high-energy photon and electron beams.[2] The formalism and dosimetry procedures recommended in this protocol are based on the absorbed dose to water calibration coefficient of an ionization chamber at ^{60}Co, $N_{D,w}^{60\mathrm{Co}}$, together with theoretical beam quality conversion factors k_Q for the determination of absorbed dose to water in high-energy photon and electron beams.

In light of these changes, Task Group 70 was charged to reassess those recommendations given in the TG-25 report that need to be updated because of the recommendations given in the TG-51 protocol and to recommend new methodologies and procedures that would allow the practicing medical physicist to initiate and continue a high quality program on clinical electron beam dosimetry. This TG-70 report is thus a supplement to the TG-25 report and is meant to enhance the material given in the TG-25 report by the inclusion of either new topics or topics that were not covered in depth in the TG-25 report. These topics include, but are not limited to, procedures for obtaining data to commission a treatment planning computer to determine dose in irregularly shaped electron beam fields and the procedures for commissioning of sophisticated special procedures using high-energy electron beams. The use of radiochromic film for electrons has been addressed while radiographic film no longer available has been replaced by films currently commercially available. Realistic stopping-power data are incorporated when appropriate along with enhanced electron fluence ratio tables. A much larger list of clinical applications of electron beams is also included in the full TG-70 report which is available on the AAPM website (http://www.aapm.org/pubs/reports). The descriptions of the techniques in the clinical sections are not exhaustive but give direction on the key elements of the procedure and how to proceed toward initiation of these programs. There have been no major changes since the TG-25 report relating to flatness and symmetry, surface dose, use of thermoluminescent dosimeters or diodes, virtual source position designation, air gap corrections, oblique incidence, or corrections for inhomogeneities. Thus these topics are not readdressed in this new report.

This report is not intended for regulatory use. Allowances must be made for improved techniques, more accurate information, and advances in equipment after the date of publication of this material. Rather, this report aims to provide guidance for the practicing medical physicists in the area of high-energy electron beam treatments.

II. NOTATION AND DEFINITIONS

- *%dd*: Central-axis percentage depth dose.
- *%di*: Central-axis percentage depth ionization.
- $D_{\max}$: Absorbed dose at the depth of dose maximum.
- D/U: Dose per monitor unit.
- $d_{\max}$: Depth at which the absorbed dose (not ionization) is maximum.
- d_{med}: Depth in plastic or other nonwater media.
- d_{ref}: Reference depth for measurement of absorbed dose for beam calibration given as $d_{\mathrm{ref}}=0.6R_{50}-0.1$, where R_{50} is in cm. This is the depth at which the point of measurement of the ion chamber is placed to measure the absorbed dose. Unit: cm.

- d_w: Depth in water.
- $\overline{E}_d$: Mean energy of an electron beam at depth d. Unit: MeV.
- $\overline{E}_0$: Mean energy of an electron beam at the surface of the water phantom. Unit: MeV.
- $E_{p,0}$: Most probable energy (kinetic) of an electron beam at the surface of a water phantom for an electron beam. Unit: MeV.
- ϕ^w_{med}: Factor that corrects the difference in electron fluence between a solid phantom (i.e., plastic medium) and water phantom at water equivalent depths.
- I_{50}: Depth in water along the central axis in an electron beam at which the ionization chamber reading is 50% of its maximum value. Unit: cm.
- k_Q: Beam quality conversion factor, which corrects for the effects of the differences between the reference beam quality for which the absorbed dose to water calibration coefficient applies (usually ^{60}Co) and the actual user quality Q. k_Q is a function of the beam quality Q (specified by R_{50}) and is chamber specific.
- $k_{R_{50}}$: Component of k_Q in an electron beam (i.e., $k_Q = k_{R_{50}} P^Q_{\mathrm{gr}}$). $k_{R_{50}}$ is a function of the beam quality Q (specified by R_{50}), is chamber specific, and is independent of the ionization gradient at the point of measurement. $k_{R_{50}}$ is a function of the electron beam quality specified by R_{50}.
- $k'_{R_{50}}$, k_{ecal}: Electron quality conversion factor and photon-electron conversion factor, respectively. For electron beams, $k_{R_{50}} = k'_{R_{50}} k_{\mathrm{ecal}}$ where k_{ecal} is needed to convert $N^{^{60}\mathrm{Co}}_{D,w}$ into an electron beam absorbed-dose calibration factor $N^{Q_{\mathrm{ecal}}}_{D,w}$ for a selected beam quality Q_{ecal} and $k'_{R_{50}}$ is needed to convert $N^{Q_{\mathrm{ecal}}}_{D,w}$ into $N^{Q}_{D,w}$ for any beam quality Q. k_{ecal} is fixed for a given chamber model and $k'_{R_{50}}$ is a function of the electron beam quality specified by R_{50}.
- $(\overline{L/\rho})^w_{\mathrm{air}}$: Ratio of Spencer-Attix mean restricted collision mass stopping power of water to that of air averaged over the electron spectrum.
- $M_{\mathrm{raw}}(d)$: Uncorrected reading of an ionization chamber with the point of measurement of the chamber placed at the point of interest at a depth d in the medium. If no sign is indicated, the measurement is made collecting the same charge as during calibration. If a sign is indicated (+ or −), it is the sign of the charge collected. Unit: C or rdg (meter reading).
- M: Reading of the ionization chamber with the point of measurement of the chamber placed at the point of interest, corrected for ion recombination, polarity effect, electrometer calibration coefficient, and standard environmental conditions of temperature, pressure, and relative humidity of the air in the ion chamber for which the chamber calibration coefficient applies. Unit: C or rdg.
- $N^{^{60}\mathrm{Co}}_{D,w}$: Absorbed dose to water calibration coefficient for an ionization chamber in a reference beam of quality ^{60}Co. Unit: Gy/C or Gy/rdg.
- $N^{Q}_{D,w}$: Absorbed dose to water calibration coefficient for an ionization chamber in a photon or electron beam of quality specified by Q. Unit: Gy/C or Gy/rdg.
- P^Q_{gr}: Correction factor which accounts for the fact that a cylindrical chamber positioned with its cavity center at a reference depth does not sample the same electron fluence present at that depth in an undisturbed medium. It depends on the ionization gradient at the point of measurement. For cylindrical chambers P^Q_{gr} is a function of the radius of the cavity, r_{cav}, and the local gradient. P^Q_{gr} is unity for plane-parallel chambers.
- P_{fl}: Factor that corrects the response of an ionization chamber for the perturbation of the electron fluence that occurs because of differences in the scattering properties between the air cavity and the phantom material it replaces. The perturbation effect consists mainly of in scattering of electrons which makes the observed fluence inside the cavity too large compared to that in the medium in the absence of the cavity.
- P_{repl}: Product of P^Q_{gr} and P_{fl}.
- P_{ion}: Factor that corrects the response of an ionization chamber for the incomplete collection of charge in the cavity volume owing to ion recombination.
- P_{pol}: Factor that corrects the response of an ionization chamber for any differences in readings which result from the application of a polarizing potential of opposite polarity to a chamber under the same irradiation conditions.
- P_{TP}: Factor that corrects the response of an ionization chamber for any difference between the air density in the chamber at the time of measurement and the standard environmental conditions for which the calibration coefficient applies.
- P_{wall}: Factor that accounts for the difference in material between the chamber wall and the phantom.
- Point of measurement: Defined in the TG-51 protocol as "the point at which the absorbed dose is measured. For cylindrical ion chambers used for clinical reference dosimetry the point of measurement is on the central axis of the cavity at the center of the active volume of the cavity, and for plane-parallel chambers the point of measurement is at the front (upstream side) of the air cavity at the center of the collecting region." When used in this specific sense, the phrase "point of measurement" is set out in the text as point of measurement.
- Q: General notation used to specify beam quality for both photon and electron beams. For electron beams the beam quality is specified in terms of R_{50}.
- r_a: Applicator/insert size for measurements of output factors in clinical electron beams.
- r, r_d: Side of the equivalent square for the field size defined at the surface of the patient and at depth d, respectively.
- r_{cav}: Radius of the air cavity of a cylindrical ionization chamber. Unit: cm.
- r_0: Side of the equivalent square for the reference field size for clinical electron beam dosimetry. The reference field size within this protocol is taken to be 10×10 cm^2, defined at the nominal treatment distance.

- R_{50}: Depth in water along the beam central axis in a 10×10 cm^2 or larger beam of electrons at a source-to-surface distance (SSD) of 100 cm at which the absorbed dose is 50% of the maximum value. The field size should be large enough to ensure that the measured value of absorbed dose is independent of field size. For beams with $R_{50}>8.5$ cm (i.e., with energy greater than roughly 20 MeV), a 20×20 cm^2 or greater field size is needed. Unit: cm.
- R_p: Practical range of an electron beam, determined from the depth-dose curve as the depth of the point where the tangent at the inflection point of the falloff portion of the curve intersects the bremsstrahlung background.
- S_e: Output factor for electron beams.
- $(S/\rho)_{\text{coll}}$: Mass collision stopping power which includes all energy losses in particle (electron) collisions leading to the production of secondary electrons and atomic excitations. It includes energy losses due to the production of Cerenkov radiation and is a component of the total mass stopping power, S/ρ.[3]
- SSD: Usually a nominal distance since the position of the source is not well defined in many cases. Unit: cm.
- T: Temperature of the air inside an ion chamber, taken as the temperature of the surrounding water when in thermal equilibrium. Unit: °C.
- U: Monitor unit.

III. DOSE MEASUREMENTS

III.A. Calibration protocol, TG-51

TG-51 describes the steps required to calibrate megavoltage clinical electron beams of nominal energy ranging from 4 and 50 MeV. It defines a procedure for determining the absorbed dose to water at the reference depth d_{ref} in a water phantom. As with all protocols, exact adherence to the recommended procedure is essential in obtaining the correct dose per monitor unit at the calibration point. TG-51 has two main objectives: (1) Incorporate the absorbed dose to water standard into the calibration protocol and (2) simplify the calibration formalism. The major differences between TG-51 and both TG-21 and TG-25 are that the TG-51 calibration protocol takes advantage of the use of an ionization chamber that has been calibrated in terms of the standards of absorbed dose (to water), and the protocol uses realistic electron beam data for the determination of restricted stopping-power ratios for water compared to air.[4] The full calibration must be done in water but output constancy measurements can be done in plastic phantom materials provided that a transfer factor has been established. Use of the standard of absorbed dose to water has several advantages. It is more accurate and robust and clinical reference dosimetry is directly related to absorbed dose to water.

III.B. Electron beam quality specification

From TG-51, beam quality in electron beams is specified by R_{50}, the depth in water (in cm) at which the absorbed dose falls to 50% of the maximum dose for a beam which has a field size on the phantom surface $\geq10\times10$ cm^2 ($\geq20\times20$ cm^2 for $R_{50}>8.5$ cm, i.e., $E>20$ MeV) at a SSD of 100 cm.[2] The central-axis percentage depth-dose curve can be determined using cylindrical or plane-parallel ionization chambers, diode detectors, or radiographic film for measurements of central-axis depth-dose curves; however, their accuracies should be verified by comparison against the depth-dose curves generated using ionization chambers. Other detectors are acceptable if their response has been shown to be accurate in comparison to ionization chambers.

Several acceptable methods to determine R_{50} with ionization chambers have been described in TG-51. The depth of 50% of the ionization maximum on the depth-ionization curve, I_{50}, can be converted to R_{50} using Eqs. (16) and (17) in TG-51.[2,5,6] The above procedure is for the determination of R_{50} only and does not describe a procedure for the determination of the entire central-axis percentage depth-dose curve in water. Otherwise, the percentage depth-ionization curve measured using an ionization chamber can be converted to a percentage depth-dose curve and R_{50} obtained from those data. Alternatively, the percentage depth-dose curve can be measured directly using diode detectors and R_{50} can be obtained directly from the measured data. The following sections will give detailed information on how to make these measurements using various detectors and media.

III.C. Dosimetry equipment

III.C.1. Ionization chambers, diodes, radiographic film

Cylindrical and well-guarded plane-parallel ionization chambers along with diodes and radiographic film are acceptable for relative dosimetry for electron beams in this report. The response characteristics of plane-parallel ionization chambers differ from those of cylindrical chambers and offer certain advantages in comparison to cylindrical ionization chambers. For example, well-guarded plane-parallel ionization chambers are designed to minimize scattering perturbation effects, and the replacement perturbation correction factor P_{repl} can be taken as unity for some chambers.[1,7,8] Additionally, the effective point of measurement of the chamber is the inner surface of the entrance window, at the center of the window for all beam qualities and depths. Thus the "effective point of measurement" is the same as the point of measurement. These advantages of plane-parallel ionization chambers make them well suited for measurements of percentage depth dose and output factors. However, the polarity effect can lead to inaccuracies in the measurement of percentage depth dose when using plane-parallel chambers. The polarity effect depends on the energy and the angular distribution of the incident radiation and both the depth of the measurement and the field size. The effect can even reverse sign as a function of depth since forward ejected electrons near the surface create a region with a net loss of electrons whereas a higher negative charge is accumulated at deeper depths where electrons stop in the medium. The charge deposition in the collecting electrode may either in-

crease or decrease due to these effects based on the polarizing voltage of the chamber.[9] The type and thickness of the material behind the collecting electrode also can affect significantly the total accumulated charge.

Cylindrical ionization chambers are more widely used for the measurement of central-axis depth-dose distributions. To obtain the most accurate clinical data, they need to be positioned appropriately and require the application of correction factors. For electron beam measurements, the effective point of measurement of a cylindrical chamber is at a point $0.5r_{cav}$ (where r_{cav} is the radius of the air cavity of a cylindrical ionization chamber) distance upstream from the central electrode of the chamber for electron beam measurements. Cylindrical chambers provide dosimetry data as accurate as plane-parallel chambers at depths greater than 0.5 cm but measurements in the buildup region have to be carefully evaluated. The appropriate procedure for the use of both plane-parallel and cylindrical chambers is described in the following sections.

Diode detectors and radiographic film[10] can also be used for the collection of electron data but ionization chambers remain the gold standard against which the response of both of these detectors needs to be evaluated. Their use has been described in TG-25 and will be discussed in a later section of this report.

III.C.2. Phantoms

As stipulated by TG-51, water is the required medium for absolute dose calibration. This task group further recommends the use of water as the measurement medium for clinical dosimetry whenever possible. The water phantom should extend at least 5 cm beyond all four sides of the largest field size employed at the depth of measurement. However, nonwater phantoms can be used with appropriate caution for relative electron beam dosimetry in situations when accurate chamber positioning in water is not possible; a water phantom presents difficulties or is inadequate or inconvenient for the clinical situation. In these cases, the physicist should strive to use well-characterized materials to minimize uncertainty due to composition or density variations between different samples of the same nominal material.[11,12] Use of nonwater phantoms is described in Sec. III H.

III.D. Measurement of central-axis percentage depth dose in water

III.D.1. Measurements using cylindrical ionization chambers in water

Beam scanning systems using cylindrical ion chambers are commonly used for clinical electron beam percentage depth-dose measurements. Following is a step-by-step method for determining percentage depth doses in water using integrated charge readings with a discussion of the parameters involved. The procedure assumes that R_{50} for the electron beam has already been determined. It is appropriate for cylindrical ionization chamber used for electron beam dosimetry and is consistent with recommendations given in the TG-51 protocol[2] and TG-25 report [in TG-25 the most probable energy at the surface of the phantom is $E_{p,0}=0.22+1.98R_p+0.0025R_p^2$, where R_p is given by Eq. (5) in the current report]. Although the use of pinpoint chambers for measurements in electron beams has not been described in the literature, certain chambers have exhibited a strong field size dependence of the polarity effect and stem effect in photon beam measurements.[13] As such, their use for measurements in electron beams should be done with caution and their response should be verified using other detectors of known response in electron beams.

(i) Select an ionization chamber whose stability and leakage characteristics have been documented. The leakage should not exceed 0.1% of the maximum signal.[1] All measurements should be performed in a water phantom with the surface of the phantom positioned at the SSD to be used clinically. Position the central axis of the ionization chamber (i.e., the point of measurement) at the depth to be measured. Allow sufficient time (1–4 min for water) for the chamber to come to equilibrium with the temperature of the medium.[14] Irradiate the chamber for a certain number of monitor units and record the raw electrometer reading M_{raw} at depth d.

(ii) The raw measurement of charge, M_{raw}, should be corrected for ion recombination (P_{ion}) and polarity (P_{pol}) effects. As a minimum, both of these effects should be measured near the surface, at the depth of maximum ionization, at the depth of 50% ionization, and near the practical range (at approximately the depth of 10% ionization). If the values of P_{ion} and P_{pol} are such that they cause the percentage depth-ionization curve to shift by more than 2 mm then these corrections should be included to correct M_{raw}. Software provided with automated scanning systems cannot currently apply this correction so this has to be done independently of the scanning system. Otherwise, they are of little clinical consequence and can be "ignored." The two voltage technique recommended in the TG-51 protocol should be used for the determination of P_{ion} (Eq. (11) for continuous radiation, Eq. (12) for pulsed or pulsed-swept beams). Equation (9) of the TG-51 protocol should be used to correct for the polarity effect, P_{pol}.[2] For measurements made over a short period of time, temperature and pressure corrections are seldom needed but they should be kept in mind for long measurement sessions. P_{wall} is assumed to be unity for electron beams and low atomic number thin-walled chambers.[15] However, recent data show that P_{wall} for cylindrical chambers cannot be assumed to be unity for either photon or electron beams.[16] At the TG-51 reference depth for electrons, the P_{wall} values can differ from unity by as much 0.6% and exhibit a change with depth as great as 2.5% for a graphite-walled cylindrical chamber between a depth of 0.5 cm and R_{50} for 6 MeV electrons. Other chambers at higher energies exhibit smaller deviations from unity.[16] It is recommended that the user check the response of their chambers versus

TABLE I. Chamber replacement factor P_{repl} for cylindrical chambers.

$\overline{E}_d$ [a] (MeV)	Inner diameter (mm)			
	3	5	6	7
2	0.977	0.962	0.956	0.949
3	0.978	0.966	0.959	0.952
5	0.982	0.971	0.965	0.960
7	0.986	0.977	0.972	0.967
10	0.990	0.985	0.981	0.978
15	0.995	0.992	0.991	0.990
20	0.997	0.996	0.995	0.995

[a] $\overline{E}_d = \overline{E}_0(1 - d/R_p)$. $\overline{E}_0$ is the mean incident electron energy, $\overline{E}_d$ is the mean energy as a function of depth d in water, and R_p is the practical range of the electron beam.

the literature, such as data provided by Buckley and Rogers, to ensure that the variation in P_{wall} versus depth will introduce a less than 2% error. If published data are not available, then P_{wall} as a function of depth should be determined to ensure that this effect does not introduce a more than 2% error into the determination of percentage depth dose. The corrected ion chamber reading M at depth d is then given by

$$M(d) = M_{raw}(d) \cdot P_{ion} \cdot P_{pol}. \quad (1)$$

.

(iii) Determine the chamber replacement correction factor P_{repl}. For electron beams, P_{repl} is composed of two parts, the gradient correction (P_{gr}) and the electron fluence correction (P_{fl}). Correct for the gradient effect by shifting the measured ionization curve upstream by 0.5 times the radius of the air cavity An alternative method is to set the point of measurement of the chamber $0.5r_{cav}$ deeper than the point of interest in the phantom. The fluence correction accounts for changes in the primary electron fluence spectrum—due to the presence of the chamber air cavity and is needed if the ion chamber (cylindrical) is in a region where full or transient charged particle equilibrium has not been established, such as anywhere in an electron beam. Thus, following the procedure for the measurement of the depth-ionization curve outlined above, $P_{repl} = P_{fl}$ and depends on the chamber cavity radius and energy of the electrons at depth. A detailed analysis of the topic has been given by Rogers.[17,18] We recommend values from Table I (same as Table V from TG-25) for P_{fl} of the appropriate chamber diameter and electron energy for every depth. Note that Table V from TG-25 is a reproduction of Table VIII from the TG-21 report with header describing electron fluence corrections for cylindrical chambers.[15] Selection of P_{fl} from the table requires a determination of $\overline{E}_d$, the mean electron energy at the depth of measurement which is approximately given by[19]

$$\overline{E}_d = \overline{E}_0\left(1 - \frac{d}{R_p}\right), \quad (2)$$

where $\overline{E}_0$ is the mean energy at the surface of the phantom, and R_p is the practical range of the electron beam. $\overline{E}_0$ (mean incident energy) can be determined via a second-order polynomial in terms of R_{50} (in cm):[20]

$$\overline{E}_0 = 0.656 + 2.059R_{50} + 0.022R_{50}^2 \quad (\text{MeV}), \quad (3)$$

or using I_{50} (in cm):

$$\overline{E}_0 = 0.818 + 1.935I_{50} + 0.040I_{50}^2 \quad (\text{MeV}). \quad (4)$$

Use of the previously recommended relationship $\overline{E}_0 = 2.33R_{50}$ or $\overline{E}_0 = 2.4R_{50}$ by TG-25 produces values of mean electron energies within 0.4 MeV of those obtained from Eqs. (3) and (4). For the previous relationships, TG-25 allowed R_{50} to be either the depth of 50% maximum ionization or 50% of maximum dose. The practical range of R_p in terms of R_{50} can be obtained by using[21]

$$R_p = 1.271R_{50} - 0.23 \quad (\text{cm}). \quad (5)$$

This task group recommends Eqs. (2)–(5) for the determination of $\overline{E}_0$, $\overline{E}_d$, and R_p and the continued use of the Harder equation[19] even considering the Monte Carlo data in the literature.[5,22] Analysis of the results obtained for the measurement of central-axis percentage depth dose using either the Harder approach or the Monte Carlo derived data did not show clinically significant differences.[23]

(iv) Calculate the percentage depth-ionization ($\%di$) curve in water using the following equation:

$$\%di_w(d) = 100\frac{M(d)}{M(I_{max})}, \quad (6)$$

where M is the fully corrected ion chamber reading [Eq. (1)], and I_{max} is the depth of the maximum ionization reading.

(v) Use the following equation to calculate the water-to-air stopping-power ratios for realistic electron beams as a function of R_{50} (in cm) and depth d.[24] These stopping-power ratios are the same as the values used in the TG-51 protocol,

$$\left(\frac{\overline{L}}{\rho}\right)_{air}^{w}(R_{50}, d) = \frac{A + B(\ln R_{50}) + C(\ln R_{50})^2 + D(d/R_{50})}{1 + E(\ln R_{50}) + F(\ln R_{50})^2 + G(\ln R_{50})^3 + H(d/R_{50})}, \quad (7)$$

where $A = 1.0752$, $B = -0.508\,67$, $C = 0.088\,670$, $D = -0.084\,02$, $E = -0.428\,06$, $F = 0.064\,627$, $G = 0.003\,085$, and $H = -0.124\,60$. Rogers[25] showed that Eq. (7) can be used for the determination of the entire central-axis percentage depth-dose curve with accuracy to within 1% of the value at dose maximum (d_{max}). It can be used for a large number of clinical electron beams, with the exception of swept electron beams at shallow depths. For calculations in superficial regions where extreme accuracy is either desired

TABLE II. Chamber replacement factor P_{repl} for plane-parallel chambers. The Markus chamber data are derived from $P_{repl}=1-0.041e^{-0.4\overline{E}_d}$ (Ref. 203). For the Capintec chamber, the values are the average of the two data sets available in the literature normalized to unity at 20 MeV (Refs. 204 and 205) (reproduction of Table II, TG-39, Ref. 8).

$\overline{E}_d$ [a] (MeV)	Holt, NACP, Exradin	Markus	Capintec PS-033
2.5	1.000	0.985	0.956
3	1.000	0.988	0.961
4	1.000	0.992	0.970
5	1.000	0.994	0.977
6	1.000	0.996	0.982
7	1.000	0.997	0.986
8	1.000	0.998	0.989
10	1.000	0.999	0.994
12	1.000	1.000	0.996
15	1.000	1.000	0.998
20	1.000	1.000	1.000

[a] $\overline{E}_d=\overline{E}_0(1-d/R_p)$. $\overline{E}_0$ is the mean incident electron energy, $\overline{E}_d$ is the mean energy as a function of depth d in water, and R_p is the practical range of the electron beam.

or required, the restricted stopping-power ratios should be recalculated since they were originally calculated for a bin of 0.05 cm thickness.[25] This task group recommends the computation of percentage depth dose based on TG-51 using the following equation:

$$\%dd_w(d)=\%di_w(d)\times\frac{(\overline{L}/\rho)^w_{air}(R_{50},d)\cdot P_{fl}(E_d)}{(\overline{L}/\rho)^w_{air}(R_{50},d_{max})\cdot P_{fl}(E_{d_{max}})}. \quad (8)$$

III.D.2. Measurements using plane-parallel ionization chambers in water

Well-guarded thin-walled plane-parallel chambers are acceptable for the measurement of percentage depth-dose curves in water. The use of a thin-window plane-parallel chamber minimizes the error in the effective point of measurement determination. When measurements are performed using a plane-parallel ionization chamber, the inner surface of the front window is to be selected as the measurement point of interest. The thickness of the front window of plane-parallel chambers can be 1–2 mm so this thickness must be taken into account during the measurement setup. Also, care must be taken to determine the location of the inner surface of the front window for plane-parallel chambers that have protective or waterproofing caps.

Well-guarded plane-parallel chambers for relative electron dosimetry do not require a P_{gr} correction. The P_{fl} correction for some types of plane-parallel chambers is considered unity, except for the Markus chamber and the Capintec PS-033 chamber. Correction factors for these two chambers are provided in Table II.[8] These corrections for P_{fl} should be made using step (iii) above. For clinical measurements, P_{wall}, the wall correction factor for plane-parallel chambers, should be set equal to unity and be assumed to be independent of depth despite evidence that backscatter differences between the water phantom and the rear chamber wall may introduce a non-negligible effect. For plane-parallel chambers with polystyrene rear walls, the ratio of P_{wall} values from 6 to 20 MeV electron beams becomes larger than 1% for depths beyond R_{50}. For rear chamber walls made of polymethylmethacrylate (PMMA) and graphite, this correction (being the ratio of P_{wall} at two depths) is negligible for clinical purposes based on the same data above.[21] Buckley and Rogers[16] showed that for commonly used plane-parallel chambers (NACP-02, Roos, Markus, and Capintec PS-033), P_{wall} corrections can be 1.7% or larger for 6 MeV electrons at the reference depth. For the NACP-02 chamber (the only chamber for which P_{wall} versus depth was reported) at 6 MeV, P_{wall} increased up to 5% as the depth increased from d_{ref} to R_{50} and exhibited almost a 6% increase at the practical range of the beam. The change in P_{wall} versus depth for the NACP-02 was much less dramatic at 20 MeV, increasing by approximately 2.5% from d_{ref} to R_{50}. Recent calculations of P_{repl} by Wang and Rogers[26] who discussed issues with plane-parallel chamber usage in low-energy clinical electron beams suggest that in addition to P_{wall}, P_{repl} may not be unity as currently assumed. The impact of these variations from unity for P_{wall} and P_{repl} is clinically negligible (for measurements of output factors and percentage depth dose) since these factors are calculated from the ratio of two doses. The change in P_{wall} will be far less than 1% for measurements of output factor for unrestricted fields or small irregularly shaped fields and less than 2%–3% (less than a 1 mm change in the percentage depth-dose curve) for the measurement of percentage depth-dose for low-energy, 6 MeV beams. The effect will be even less for 20 MeV electron beams. Clinical physicists are advised to keep alert to new developments in the literature for information specific to their plane-parallel chamber.

III.D.3. Measurements using diodes in water

As stated in TG-25 and TG-51, diodes can also be used to measure directly percentage depth-dose curves, with the requirement that their performance be tested against percentage depth-dose curves obtained using an ion chamber.[1,27–29] This task group recommends the guidelines of TG-25 for diode usage in electron beams. The effective point of measurement is the die, the active part of the diode. Its position with respect to the front surface of the device should be taken into account based on the design specifications provided by the manufacturer. In cases where the effective point of measurement is not known, it should be determined using procedures described in TG-25 or by using high resolution x-ray images.[30] If it is known, then the effective point of measurement needs to be verified, as part of commissioning the diode. The user should be careful to use diode detectors specifically designed for electron beams and not ones designed for use in photon beams. The latter diodes have high atomic number material added close to the sensitive volume to improve their photon energy sensitivity and are not suitable for electron beam measurements. A quality control pro-

gram should be developed for checking diode versus ion chamber readings before taking any large data sets (such as at commissioning of a new linac), at least yearly in the clinical environment and more often if the diodes are used extensively.[12]

III.D.4. Considerations of automated water scanning systems

The report of AAPM Task Group 106 has an excellent description of scanning and data taking techniques for the commissioning of both photon and electron beams.[31] When a beam scanning system in water is used for *%dd* measurements, the scan direction should be toward the surface to reduce the effect of meniscus formation. Too fast a scan speed and/or too great a step size can affect the accuracy of the measurements. Therefore, the scan speed and step size should be optimized to ensure that the region near $d_{\max}$ is measured accurately. This is especially important for low-energy electron beams where the central-axis percentage depth-dose curve is highly peaked at the location of $d_{\max}$. Smoothing software should be applied to the measured data whenever possible to minimize noise and small variations in the readings. The smoothed data should be compared to the unsmoothed *%dd* curves to ensure that the process did not introduce artifacts. It is also good practice to compare a reference scan taken at the beginning of the measurement session (e.g., a 10×10 cm^2 scan) with one taken at the end of the measurement session to ensure that the scanning system operated in a consistent fashion throughout the measurement session.

Software that automatically converts percentage depth-ionization data to percentage depth-dose data should be commissioned before clinical use to ensure that this operation is being performed correctly. One should appreciate when using ionization chambers that the depth of maximum ionization may not be the depth of maximum dose, as the factors converting percentage depth ionization to percentage depth dose are depth dependent (Fig. 1). The reference scan should also be compared to central-axis percentage depth-dose data taken using integrated readings to provide an independent verification that the scanner is operating properly.[31] More scanning water phantom checks for evaluating total system performance are given in the literature.[32]

Commissioning data including the central-axis percentage depth doses and isodose curves are almost always measured using automated water scanning systems. Although many scanning systems correctly apply the corrections for the effective point of measurement for cylindrical ionization and the stopping-power ratio corrections (with the exception of fields smaller than 3×3 cm^2),[33] few systems apply the P_{repl} (P_{fl}) correction or corrections for polarity effect. In most instances, these corrections are small due to the small size of the cylindrical chambers employed and have little impact on clinical practice. However, it is strongly recommended that the algorithms and the correction factors applied by these automated systems be thoroughly understood and that the final data from the automated scanning system is checked against data that take all correction factors into account to ensure that the corrections are being applied correctly. Once the true accuracy of the automated scanner system is substantiated, the above check need only be done after a major system repair or after a system or software upgrade.

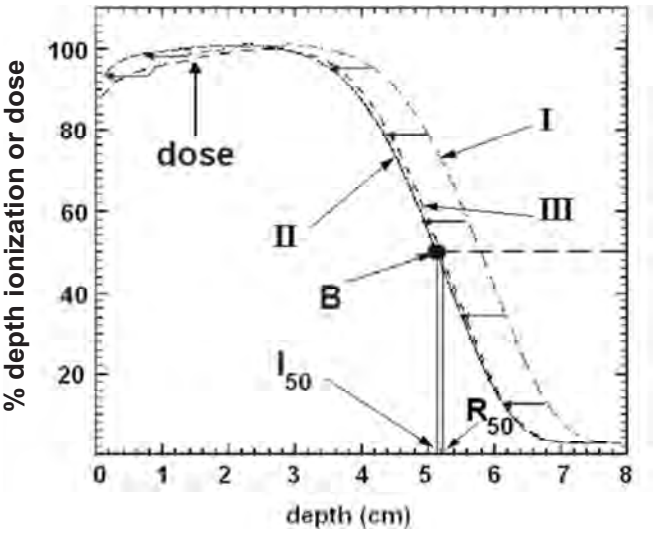

FIG. 1. Effect of shifting depth-ionization data measured with cylindrical chambers upstream by $0.5r_{\text{cav}}$ for electron beams (with $r_{\text{cav}}=1.0$ cm). The raw data are shown by curve I (long dashes) and the shifted data, which are taken as the depth-ionization curve, are shown by curve II (solid line). The value of the percentage ionization at B (solid curve, 50% ionization) in the electron beam gives I_{50} from which R_{50} can be determined. For electron beams, curve II must be further corrected to obtain curve III, the percentage depth-dose curve (short dashes).

III.E. Output factors for electron beams

For clinical applications, the determination of the dose per monitor unit for each electron treatment situation is crucial. Since this depends on many variables, measurements of electron beam output as a function of field size are needed for each standard applicator or cone at each electron energy over the range of SSDs in clinical use. Output factors should also be determined for the "standard" rectangular or circular cutouts that many clinics maintain for convenience and also for patient-specific irregularly shaped fields that differ strongly from these simple shapes. This task group recommends following the definition of output factor given in TG-25.

Specifically, the output factor S_e for a particular electron field size r_a at any treatment SSD_{r_a} is defined as the ratio of the dose per monitor unit, D/U (Gy/MU), on the central axis at the depth of maximum dose for that field, $d_{\max}(r_a)$, to the dose per monitor unit for the reference applicator, or field size r_0, and standard SSD_{r_0} at the depth of maximum dose for the reference field used in calibration, $d_{\max}(r_0)$. In equation form:

$$S_e(d_{\max}(r_a),r_a,\text{SSD}_{r_a})=\frac{D/U(d_{\max}(r_a),r_a,\text{SSD}_{r_a})}{D/U(d_{\max}(r_0),r_0,\text{SSD}_{r_0})}. \tag{9}$$

The determination of dose in water at $d_{\max}(r_0)$ from the dose at the calibration reference depth requires the use of clinical

percentage depth-dose data. For fields where the central axis is blocked or within 1 cm of the field edge, $D/U(d_{\max}(r_a), r_a)$ should be measured approximately at the center of the open part of the field. It is important to note that $d_{\max}(r_0)$ may occur at different depths for different field sizes. Specifically, for field sizes that are too small to produce lateral electronic equilibrium at the central axis, $d_{\max}$ occurs at a shallower depth than for the reference field size and the depth of $d_{\max}$ must first be determined from a central-axis depth-dose measurement. D/U is then measured at that depth for that field (defined by applicator with insert) and compared with D/U at the depth of maximum for the reference field (e.g., 10×10 or 15×15 cm^2 open applicator). If the measurement is made at the extended SSD SSD_{r_a}, the user must be extremely careful not to take the effect of distance into account twice when performing monitor unit calculations. Additionally, stopping-power ratios decrease when electron field sizes become smaller than about 3×3 cm^2.[33,34] This could amount to changes of the order of not more than 0.5% which may be clinically insignificant in most instances but could be important for small fields. More importantly, the $(\overline{L}/\rho)^{\text{water}}_{\text{air}}$ is depth dependent and ignoring the change in $(\overline{L}/\rho)^{\text{water}}_{\text{air}}$ due to the change in the depth of the measurement point, $d_{\max}$, as the field gets smaller can lead to overestimates of the output factor by up to 3%.[33]

III.F. Treatments at extended distance

An important aspect of many clinical applications of electron beams is the use of extended treatment distances (from 100 to 130 cm) to avoid collision between the patient and the applicator. This can lead to significant change in the output factor, degradation of dose uniformity within the field, and widening of the penumbra in comparison to measurements at the calibration SSD of 100 cm. Changes relative to standard SSD increase as SSD increases and are more dramatic for low beam energies and small fields. Treatment planning systems differ in their ability to accurately depict the effects of extended SSD and individual users should investigate the limitations of their planning systems before use on patients.

TG-25 (Sec. VIII) includes a thorough discussion of the dosimetric effects of increasing SSD and states that "all extended SSD treatments should be considered as potentially delivering a dose and/or dose distribution to the patient which is significantly different from that which the radiation therapist has intended" and advises that there should be "both well-defined guidelines for its use and methods for indicating when existing data can be used and when individual dose measurements are required." Publications since 1991 (Refs. 35–37) provide further evidence for the considerations cited in TG-25. TG-70 strongly advises that physicists review Sec. VIII of the TG-25 report when dealing with electron beam treatments at extended SSD.

III.G. Dose determination in small or irregular electron fields

Inherent problems exist in the dosimetry of small and/or irregular electron fields. When electron fields are smaller than or comparable to the radius required for lateral scattering equilibrium, the depth of $d_{\max}$ moves toward the surface, the central-axis percentage depth dose decreases, and the output (dose/monitor unit) decreases from that of the unrestricted applicator. Figure 2 shows the changes in the central-axis fractional depth-dose curves for restricted fields. In two dimensions, the isodose coverage is reduced in all directions as the field size shrinks from that of the unrestricted cone. Similar dosimetric changes occur in narrow, curved portions of irregular fields.

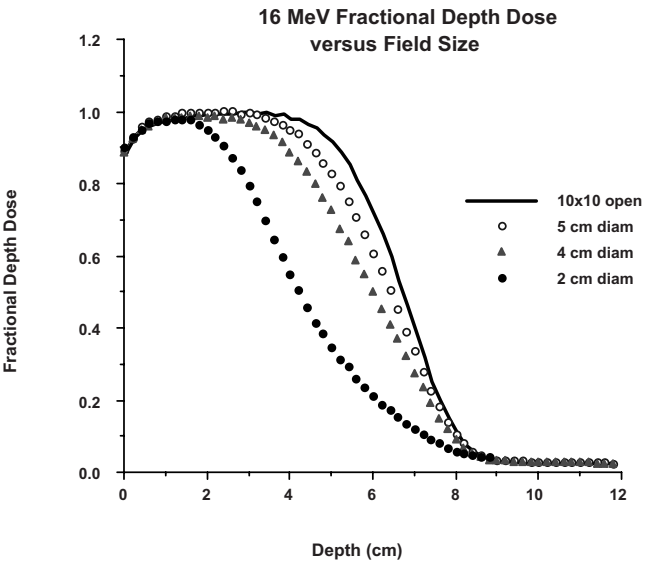

FIG. 2. The effect of electron field restriction on the fractional depth-dose curves for 9 and 16 MeV electron beams. All the curves are normalized to the 100% value of the 10×10 cm^2 open cone.

For such severely restricted fields, either custom measurements can be performed or analytical approaches presented in the literature can be used to describe these changes.[38–46] Special considerations apply when the minimum field size dimension is less than the minimum radius of the circular field that produces lateral scattered equilibrium. Basically, when the field radius is equal to or less than $0.88\sqrt{\overline{E_0}}$ cm, where $\overline{E_0}$ is given by Eqs. (3) and (4), then additional dosimetric measurements should be performed.[43] To characterize such restricted fields and ensure that the target is adequately covered, the central-axis depth dose should be measured, the output factor should be determined as described above, and the isodose distribution in a plane perpendicular to the central axis at either $d_{\max}$ or at a clinically relevant depth, such as D_{90}, should be measured.

Measurements of the depth dose, including the change in $d_{\max}$, can be done with an ionization chamber that is small enough such that its active volume fits in the flat portion of the beam, a diode, or by film dosimetry in a suitable phantom with the beam parallel to the film (see TG-25 Sec II.D and Sec. III H 4 of this report regarding film dosimetry). Once $d_{\max}$ is determined, then ionization chamber, diode dosimetry, or film dosimetry can be performed to determine the output of the beam. It is acceptable to maintain a library of small cutout information which includes information on the

depth of d_{max}, percentage depth-dose data, output factor, and penumbral and isodose information. This information must be marked clearly with electron cone, treatment distance, and linac information to ensure that it is being applied properly to the current clinical situation.

The use of validated computational approaches (analytical, numerical, or Monte Carlo) frees the physicist from having to do new measurements for each new cutout. There are several analytical approached in the literature.[38–46] The equivalent square technique and one-dimensional technique were detailed in TG-25. In brief, these techniques use square field data to determine both the output factor and the percentage depth-dose curves for rectangular fields to within a few percentage.

Hogstrom *et al.*[47] showed that the central-axis depth-dose curve for a rectangular electron field of sizes X and Y can be determined by taking the square root of the product of the depth doses for the square fields whose sides are X and Y:

$$\%dd(d,r_{X,Y}) = [\%dd(d,r_{X,X}) \times \%dd(d,r_{Y,Y})]^{1/2}. \quad (10)$$

In addition, it has been shown[48] that a similar relationship for output factors S_e for rectangular fields of dimensions X and Y also holds,

$$S_e(d_m,r_{X,Y}) = [S_e(d_m,r_{X,X}) \times S_e(d_m,r_{Y,Y})]^{1/2}. \quad (11)$$

However, the above techniques do not predict accurately the output factors or percentage depth-dose values for irregularly shaped electron fields. Algorithms that use a sector-integration technique[40–43,45,46,49] or discrete pencil-beam models[50–52] have been developed to calculate the outputs of arbitrarily shaped electron beams. Tests of pencil-beam algorithms were made for square, rectangular, and round fields and differences as great as ±2.7% were found between calculated and measured values.[53] Sector integration approaches have been shown to be accurate to within ±1%.[40–43,45,46,54] Table III (Ref. 41) shows the accuracy of the various techniques.

The model proposed by Khan *et al.*[42,43,45] using lateral buildup ratios (LBRs) is based on the electron pencil-beam model that uses a quantity $\sigma_r(d)$ to define the effective spread of the beam and only requires measurements for a single small cutout (2 cm diameter). The approach is able to predict the shift in d_{max}, the change in the output factor at d_{max}, and the change in the central-axis percentage depth doses for the restricted field. The lateral buildup ratio as a function of depth is calculated by dividing the percentage depth dose of the small field, r, by the percentage depth dose of the large (reference) field, r_∞. That is,

$$\mathrm{LBR}(d,r) = \frac{\%dd(d,r)}{\%dd_\infty(d,r_\infty)}. \quad (12)$$

The values of $\sigma_r(d)$ can then be derived from their relationship to the LBR:[42]

$$\sigma_r^2(d) = \frac{r_x^2}{\ln\left[\dfrac{1}{1-\mathrm{LBR}(r_x,d)}\right]}, \quad (13)$$

where r_x is the dimension of the field size x. The parametrization of $\sigma_r^2(d)$, derived from the reference field measurements, can then be used to calculate $\mathrm{LBR}(r,d)$ for any point in an electron field. For general application an effective LBR LBR_{eff} may be found by summing the pencil-beam contributions around the selected point, described by the following equation:

$$\mathrm{LBR}_{eff}(d,r) = 1 - \left(\frac{\Delta\theta}{2\pi}\right)\sum_{i=1}^{n} \exp\left[\frac{-r_i^2}{\sigma_r^2(d)}\right], \quad (14)$$

where r_i is the radial distance from the point of measurement to the field edge, $\Delta\theta$ is the angle increment, and n is the number of "sectors."

The output factor for any point j in the field and depth d relative to the central-axis depth dose of the large reference field is then

$$S_e(d,r_j) = S_e \times \mathrm{LBR}_{eff}(d,r_j) \times \%dd_\infty(d,r_\infty)/100. \quad (15)$$

The cone factor S_e is assumed to be the relative output factor for the electron applicator with standard insert. In comparison with measurements, this calculational approach agreed to within ±3% over a range of clinically significant depths.[42]

Such methods of modeling electron depth-dose distributions and output factors may enable irregular field calculations to be a viable option, eliminating or reducing greatly the need for many clinical measurements. Alternatively, treatment planning systems based on current models or on Monte Carlo code may be effective in calculating accurately the output factor, depth-dose characteristics, and penumbral characteristics of small and irregularly shaped electron fields.[55,56]

TABLE III. Comparison of the percentage difference between measured and calculated output factors for common methods of calculation in the literature. The measured and calculated output factors were for cutout shields that were shaped as squares, rectangles, circles, ellipses, and arbitrary shapes used in the clinic.

Calculation method	Percentage difference (≤ ± %)
Equivalent square	2.7,[a] 5.9,[b] 3.0[c]
Square root	3.0,[d] 2.3,[e] 4.6,[b] 3.0[f]
One dimensional	3.0,[d] 2.0,[e] 2.1[b]
Pencil beam	2.7,[g] 2.0[h]
Sector integration	3.0,[i] 1.5,[j] 1.0,[k]

[a]Reference 206.
[b]Reference 207.
[c]Reference 208.
[d]Reference 39.
[e]Reference 51.
[f]Reference 209.
[g]References 50 and 52.
[h]Reference 53.
[i]Reference 40.
[j]Reference 54.
[k]Reference 41.

III.H. Nonwater phantoms: Conversion of relative dose measurements from nonwater phantoms to water

This task group emphatically recommends the use of water as the standard phantom material for the absolute calibra-

TABLE IV. Recommended effective density ρ_{eff} of scaling depth from nonwater phantoms to water phantoms for electron beams.

Material	Mass density (g cm^{-3})	Recommended effective density ρ_{eff} [a]
Water[b]	1.00	1.00
Clear polystyrene[b]	1.045	0.975
High-impact polystyrene (white)[b]	1.055	0.99
Electron solid water[b]	1.04	1.00
PMMA[b]	1.18	1.115
Epoxy resin water substitute, photon formulation[c]	1.02	0.98
Epoxy resin water substitute, electron formulation[c]	1.04	1.00

[a]Given as *C*pl in Ref. 12.
[b]From Ref. 1, Table VII, p. 84.
[c]From Ref. 12, p. 2945.

tion of clinical electron beams as is required by TG-51 and strongly recommended by the IPEM 2003 protocol.[12] However, nonwater phantoms have a place in clinical electron beam dosimetry since they may be convenient to measure percentage depth dose, off-axis dose distributions, and output factors of small or irregular electron fields. Surface measurements for an electron beam may be difficult to perform in water compared to a nonwater phantom. Measurements of output of electron beams for total skin electron treatments (TSETs) are more easily performed using plastic phantoms. Finally, periodic constancy and quality control measurements are also conveniently made in nonwater phantoms.

The nonwater phantom material should be close to water equivalent, which requires that it possess a linear collision stopping power and scattering power close to that of water. Ideally, the phantom material should have the same effective atomic number and the same electron density as water.[1]

Any phantom material intended for clinical electron dosimetry should be tested by the user, comparing measurements in the plastic phantom with those in a water phantom. The commissioning should include checking the density, the thickness, and the variation of thickness of each slab, along with radiographic checks for air gaps inside the slabs.[57] One problem of standard off-the-shelf industrial plastics such as polystyrene and polymethylmethacrylate is that the reported characteristics of different samples of the same nominal material can vary greatly in terms of density and electron scattering power due to difference in composition caused by even small amounts of different additives or impurities. A second problem with these two plastics is that they are both good insulators giving rise to errors in ion chamber dosimetry due to charge storage effects of stopped electrons trapped in the phantom.[58–61] These effects influence primarily the response of cylindrical chambers while being practically insignificant for parallel plate chambers. Charge storage effects are more dramatic for thick slabs of plastic. Thus, this report recommends the use of thin sheets of these materials with no more than 12 mm thickness for the sheet that contains the cylindrical chamber if possible.[12]

Ion chamber measurements in nonwater equivalent phantom materials require that the air in the cavity of an ionization chamber in the nonwater phantom be traversed by the same electron fluence, in energy and in angular distribution as well as in magnitude, as that at the depth of interest in the undisturbed water phantom. The phantom should have a machined slot that holds the chamber snugly, without air gaps. The chamber and the plastic phantom should reach thermal equilibrium prior to making any measurements.[14] When measurements are made in nonwater equivalent plastic phantoms, the output factor to water can be determined by properly scaling the depth in the plastic phantom to its water equivalent depth and by applying fluence correction factors for converting the ionization measured in the solid phantom to that in water.

III.H.1. Measurements using cylindrical ionization chambers in nonwater phantoms

If a cylindrical ion chamber is used for the measurement of the relative output factor in nonwater phantoms, several corrections are required to convert the measurement to water. To determine the relative output factor for an electron field of size r, the depth of maximum dose $d_{\max}$ must first be found in the nonwater phantom. Thin slabs of phantom material and successive readings keeping the SSD constant need to be performed to determine the depth of the maximum reading. Application of depth scaling converts a depth in a solid phantom to its water equivalent depth. At these equivalent depths the mean energies of the electron beam are identical. Under these conditions the same chamber calibration coefficient can be used at the two positions in the two phantom materials.

Following the recommendations of TG-25, this task group recommends that the depth in plastic phantoms, d_{med}, be scaled to its water equivalent depth d_w using the following equation:

$$d_w = d_{\text{med}}\rho_{\text{eff}} = d_{\text{med}}\left(\frac{R_{50}^{w}}{R_{50}^{\text{med}}}\right), \tag{16}$$

where the effective density ρ_{eff} is given by the ratio of the R_{50} in water to that of the nonwater medium. Recommended values of the depth-scaling factors ρ_{eff} are given in Table IV. Since the values of ρ_{eff} are normalized to the quoted standard densities given in the table, it is recommended that the den-

sity of plastic should be measured for the batch of plastic in use rather than using a nominal value for the plastic type. Table IV also gives the quoted standard densities of the plastics for which the effective densities ρ_{eff} were determined. If the measured densities of the plastic phantoms are significantly different from the densities quoted as standard mass densities in the table, then the scale factor ρ_{eff} given in Table IV should be multiplied by the ratio of the measured density to the quoted standard density. Several studies describe more accurate methods for determining depth-scaling factors for the actual phantoms being used.[5,11,62–65] For more accurate depth-scaling factors between nonwater materials and water, Ding and Rogers[5] gave a detailed procedure to determine the depth-scaling factor for the actual phantom material in use over the entire range of the depth-dose curve.

Since the $d_w^{\max}(r_0)$, the depth of maximum dose for the reference *field size* in water, is known, it can be converted into equivalent depth in nonwater phantom, $d_{\text{med}}^{\max}(r_0)$, via Eq. (16). The relative output factor can be determined from Eq. (9) and the dose conversion relationship of TG-25:

$$D_w(d_w^{\max}) = D_{\text{med}}(d_{\text{med}}^{\max})[(\bar{L}/\rho)_{\text{coll}}]_{\text{med}}^{w}\phi_{\text{med}}^{w}. \tag{17}$$

$[(\bar{L}/\rho)_{\text{coll}}]_{\text{med}}^{w}$ is the ratio of the Spencer-Attix mean unrestricted mass collision stopping power in water to that in a nonwater medium, and ϕ_{med}^{w} is the fluence ratio scaling factor that accounts for the difference in the electron fluence in the nonwater phantom versus the water phantom at equal water equivalent depths. This is due primarily to the difference in the scattering power between the two materials. Strictly speaking, since the equivalent depths are at different distances from the virtual source, the fluence factor also contains an inverse square correction; this inverse square correction is negligible and thus can be neglected for clinical work. Table V (Ding *et al.*[66]) provides values of the electron fluence correction factors ϕ_{med}^{w} as a function of energy and depth. Thus, substituting Eq. (17) into Eq. (9) yields the expressions shown below where $S_{e,w}(d_w^{\max}, r)$ is the electron output factor in water:

$$S_{e,w}(d_w^{\max}, r) = S_{e,\text{med}}(d_{\text{med}}^{\max}, r) \cdot \frac{[\phi(d_{\text{med}}^{\max}, r)]_{\text{med}}^{w}}{[\phi(d_{\text{med}}^{\max}, r_0)]_{\text{med}}^{w}}. \tag{18}$$

As with TG-25, the most probable energy[1] should be used for selecting the proper data from these tables. Recently, new data for electron fluence factors for a variety of nonwater phantoms and electron energies have been published.[66,67] This task group recommends the values in Table V (Ding *et al.*[66]) since they are generated for realistic electron beams as represented by a variety of modern clinical linear accelerators.

Since the quantities to be determined are relative, the user should verify which corrections are significant and need to be included for the particular measurement and the particular nonwater material. For example, when the output factor of an irregular electron field is measured in PMMA, the ratio of the electron fluence factors and the ratio of the P_{repl} factors are approximately unity (to within 0.2%–0.5%) and only the restricted stopping-power ratios provide a clinically significant correction. The ratio of correction factors should be even less important if solid water material is used for the measurements.[1,12] Thus, in clinical practice we recommend that only the restricted stopping-power ratios be used for simplicity.

III.H.2. Measurements using plane-parallel ionization chambers in nonwater phantoms

Plane-parallel chambers can also be used in nonwater phantoms for relative electron dosimetry measurements. An important reason why parallel plate chambers are suited for such measurements in nonwater phantoms is that the correction factor P_{repl} is unity for some of the chambers.[8] We recommend the use of Task Group 39 (TG-39) of the American Association of Physicists in Medicine for the selection of the appropriate correction factors when a parallel plate chamber is to be used for relative measurements. Use data in Table II for P_{repl} as a function of E_d. This task group recommends that the user has good knowledge of the materials used in the construction of their plane-parallel chamber so that selection of appropriate correction factors can be made. Again, these correction factors may amount to a negligible value or may cancel out for relative measurements such as relative output factors and percentage depth doses. Thus, the incorporation of P_{repl} corrections is not recommended.

III.H.3. Ion chamber measurement of central-axis percentage depth dose using nonwater phantoms

Although we recommend water as medium to perform central-axis depth-dose measurements for clinical electron beams, we acknowledge instances that nonwater phantoms may be more convenient to be used. When an ionization chamber is used for measurements in a nonwater, the scaled data provide the depth-ionization distribution in a water phantom. To convert this depth-ionization distribution to depth-dose distribution, it is necessary to multiply the ionization current or charge at each depth by the appropriate water-to-air stopping-power ratios as described in Sec. III D 1. If cylindrical ionization chambers are used for measurement then measured data should also be multiplied by the appropriate fluence correction factors. The following measurement sequence can be followed:

(i) Place the point of measurement of the ionization chamber at the scaled reference depth in nonwater phantom with Eq. (16). This gives the equivalent depth in a water phantom where dose will be determined.
(ii) Irradiate. Convert the charge reading M_{raw} corrected for temperature, pressure, etc., measured in nonwater phantom to the charge reading M at the equivalent depth d_w in water by multiplying M_{raw} with the fluence correction factor ϕ_{med}^{w}. Steps (i) and (ii) essentially determine the corrected charge reading at a given depth d_w in a water phantom from measurements made in a plastic phantom.

TABLE V. Electron fluence ratio tables for clear polystyrene, high-impact polystyrene, and PMMA [from Ding *et al.* (Ref. 66)].

	Nominal energy									
	5	6	6	9	10	11	12	15	18	20
					R50					
Depth	2.1	2.3	2.6	4	4.1	4.2	5.2	6.5	7.7	8.1
					(a) Polystyrene					
0.25	1.019	1.018	1.018	1.012	1.012	1.009	1.009	1.009	1.012	1.012
0.50	1.031	1.029	1.026	1.016	1.014	1.012	1.011	1.011	1.012	1.012
0.75	1.044	1.041	1.034	1.019	1.018	1.015	1.011	1.011	1.013	1.012
1.00	1.046	1.047	1.042	1.023	1.020	1.020	1.013	1.013	1.013	1.013
1.25	1.042	1.046	1.044	1.027	1.025	1.024	1.016	1.016	1.014	1.013
1.50	1.034	1.039	1.046	1.031	1.028	1.028	1.020	1.020	1.016	1.014
1.75	1.029	1.030	1.047	1.033	1.032	1.033	1.025	1.025	1.015	1.015
2.00	1.039	1.026	1.033	1.036	1.035	1.035	1.028	1.028	1.015	1.017
2.25			1.028	1.037	1.037	1.035	1.033	1.034	1.018	1.017
2.50			1.038	1.039	1.036	1.037	1.034	1.034	1.018	1.017
3.00				1.036	1.030	1.030	1.034	1.034	1.020	1.018
3.50				1.028	1.023	1.024	1.034	1.034	1.024	1.020
4.00				1.034	1.031	1.026	1.026	1.026	1.026	1.022
5.00							1.027	1.026	1.024	1.023
6.00									1.016	1.019
7.00									1.011	1.014
8.00									1.022	1.012
					(b) High-impact polystyrene (white)					
0.25	1.019	1.016	1.015	1.010	1.011	1.006	1.009	1.009	1.007	1.009
0.50	1.030	1.026	1.022	1.012	1.014	1.009	1.012	1.010	1.008	1.009
0.75	1.039	1.036	1.031	1.019	1.017	1.015	1.011	1.010	1.009	1.010
1.00	1.040	1.042	1.035	1.021	1.018	1.018	1.014	1.012	1.010	1.010
1.25	1.034	1.039	1.036	1.025	1.022	1.022	1.014	1.013	1.010	1.011
1.50	1.025	1.031	1.035	1.029	1.026	1.025	1.018	1.014	1.011	1.012
1.75	1.020	1.023	1.038	1.031	1.030	1.029	1.021	1.016	1.012	1.013
2.00	1.029	1.018	1.023	1.032	1.031	1.031	1.022	1.018	1.013	1.013
2.25			1.018	1.033	1.032	1.032	1.025	1.019	1.013	1.014
2.50			1.022	1.034	1.032	1.032	1.027	1.020	1.015	1.014
3.00				1.030	1.027	1.026	1.024	1.022	1.016	1.015
3.50				1.024	1.022	1.016	1.023	1.026	1.018	1.019
4.00				1.030	1.024	1.019	1.020	1.026	1.019	1.019
5.00							1.013	1.021	1.023	1.020
6.00							1.025	1.014	1.016	1.019
7.00									1.011	1.014
8.00									1.022	1.012
					(c) PMMA					
0.25	1.009	1.011	1.008	1.004	1.003	1.003	1.000	1.000	1.000	1.001
0.50	1.012	1.014	1.009	1.005	1.004	1.003	1.001	1.002	1.001	1.003
0.75	1.016	1.015	1.012	1.006	1.004	1.003	1.001	1.003	1.001	1.002
1.00	1.017	1.016	1.014	1.008	1.005	1.005	1.002	1.004	1.001	1.002
1.25	1.016	1.015	1.016	1.008	1.007	1.007	1.001	1.004	1.001	1.001
1.50	1.011	1.013	1.014	1.012	1.010	1.008	1.004	1.004	1.001	1.000
1.75	1.008	1.007	1.018	1.010	1.013	1.010	1.004	1.003	1.000	1.000
2.00	1.017	1.007	1.009	1.010	1.012	1.009	1.004	1.003	0.999	1.001
2.25			1.008	1.010	1.012	1.009	1.005	1.004	1.000	1.001
2.50			1.013	1.010	1.011	1.011	1.003	1.003	1.000	1.001
3.00				1.007	1.008	1.007	1.000	1.002	1.001	1.000
3.50				1.006	1.006	1.002	1.001	1.003	1.000	1.002
4.00				1.010	1.008	1.007	0.998	1.002	0.999	1.000
5.00							0.996	0.996	0.995	0.998
6.00								0.996	0.989	0.993
7.00									0.994	0.992

TABLE V. (*Continued.*)

	Nominal energy									
	5	6	6	9	10	11	12	15	18	20
	R50									
Depth	2.1	2.3	2.6	4	4.1	4.2	5.2	6.5	7.7	8.1
8.00									1.014	0.998

(iii) Repeat steps (i) and (ii) above to determine the corrected reading at various depths.
(iv) Use Eqs. (7), (8), and (16) based on the equivalent depths in water to determine the entire central-axis depth-dose distribution in water.

The overall relationship for central-axis depth dose in a nonwater phantom is given below:[1]

$$\%dd_w(d^w) = \%di_{\text{med}}(d^{\text{med}}) \times \frac{\left(\frac{\bar{L}}{\rho}\right)^w_{\text{air}} (R^w_{50}, d^w) \cdot P_{\text{fl}}(E_{d^{\text{med}}})}{\left(\frac{\bar{L}}{\rho}\right)^w_{\text{air}} (R^w_{50}, d^w_{\text{max}}) \cdot P_{\text{fl}}(E_{d^{\text{med}}_{\text{max}}})} \times \frac{\phi^w_{\text{med}}(d^{\text{med}})}{\phi^w_{\text{med}}(d^{\text{med}}_{\text{max}})}. \quad (19)$$

As mentioned above, well-guarded plane-parallel ionization chambers can be used for measurements of depth-ionization curves to minimize the effects of the fluence perturbation correction factor (P_{repl}) for some of these chambers.

III.H.4. Film dosimetry

Radiographic film is one of the most practical detectors to use in nonwater phantoms to obtain relative measurements for clinical electron fields. It is particularly convenient for determining the central-axis depth-dose and isodose distributions of irregular fields to find the d_{max} and other therapeutically important factors, such as the depths of 90%, 80%, and 50% isodose levels. Depth-dose measurements can be done with a film placed parallel to the electron beam at the treatment SSD and with the shortest dimension of the field under investigation oriented along the edge of the film. Great care should be exercised to guard against the consequences of improper film placement in nonwater phantoms as described in TG-25 and by Dutreix and Dutreix.[68] Other issues regarding film orientation with respect to the electron beam are reported in the literature and correction techniques for them are recommended in the literature.[69] The report of TG-69 gives detailed guidance relating to general issues of film dosimetry.[10]

The uniformity and width of the isodose distribution at clinically relevant depths (e.g., d_{max}, R_{90}) provide an estimate of the clinically useful field width at those depths. For these measurements, the film is placed perpendicular to the beam direction at the depth of interest. This TG recommends following the TG-25 recommendations for perpendicular film placement. In addition, we recommend the use of high-impact (white polystyrene) or electron solid water phantoms for film dosimetry due to the high degree of water equivalency of those two materials so the film measured depth doses do not require corrections.

Having determined the d_{max} of the field under investigation from the data taken above, the relative output factor can be determined via film dosimetry relative to the reference 10×10 cm^2 cone. This is done by using pieces of film from the same batch for all of the specific measurements of relative output factor for the field under investigation, the reference field, and the background. This TG recommends the use of TG-25 for details on film calibration for electron film dosimetry and TG-69 for general information on film dosimetry.

TG-25 describes the response of various films available at the time of its publication, handling recommendations, and caveats associated with the placement of film in solid phantoms. Most of these recommendations are still appropriate. Industrex M2 film is no longer available although other industrial films from Kodak are available. Kodak XV-2 and XTL film are much more common in ordinary radiation therapy departments. Kodak EDR2 film, an extended range verification film, has become popular for the validation of intensity-modulated radiation treatments using photon beams. It has been shown to be a very reliable, convenient, and accurate dosimeter for this application. However, EDR2 responds differently to electron beams than to photons. A study done to characterize this film's response to electron beams[70] shows that EDR2 responds more strongly to electron radiation than to the same dose of x rays (Fig. 3). Additionally, the film responds more strongly to higher-energy electrons than to electrons of lower energy. Since the average energy of an electron beam is higher at the d_{max} normalization depth, the indicated dose at depth using this film is reduced from the expected level because of the lower film response to lower electron beam energies. The difference between R_{50} for EDR2 and measurements with ion chambers, diodes, or XV2 film changes linearly with energy from 0.15 to 0.49 cm for 6–20 MeV electrons. The change in the practical range R_p with energy is less dramatic, showing differences of 0.14 cm at 6 MeV and 0.32 cm at 20 MeV. These response characteristics should be kept in mind if Kodak EDR2 is used for electron beam dosimetry. This task group recommends using XV-2 film for electron beam dosimetry.

The use of radiochromic film has advanced markedly[71] since the 1998 report of TG-55,[72] driven, in part, by the move to filmless departments. A more sensitive product, GAFCHROMIC EBT, has been introduced that exhibits little

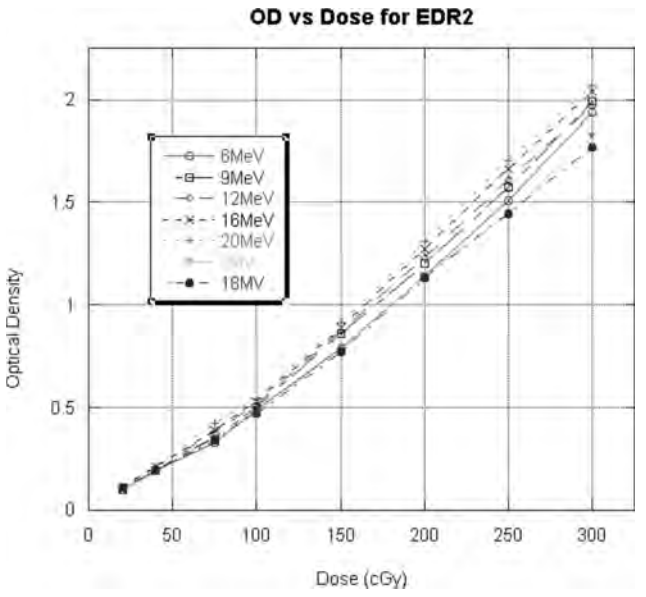

FIG. 3. The response of Kodak EDR2 film to high-energy electrons. The top curve shows the increase in response of the film with increase in electron beam energy. [Reprinted with permission from B. J. Gerbi and D. A. Dimitroyannis, Med. Phys. 30, 2702 (2003). Copyright 2003, American Association of Physicists in Medicine.].

energy dependence in either photon[73,74] or electron beams.[75] It has also been shown to be immune from the effects of fractionation, dose rate, and depth dependence in electron beams.[75] The effective atomic number (Z_{eff}) of the EBT film is 6.98, which is close to the corresponding value for water (7.3). It is comparable in cost to radiographic film and can be precisely read using a flat-bed document scanner.[76] There are several articles describing the use of radiochromic film for *in vivo* dosimetry,[77,78] for *in vivo* dosimetry in total skin electron treatments,[79] for intraoperative electron dosimetry,[80] and for experimentally validating a few leaf collimators for spatially and energy modulated electron beams.[81]

IV. ELECTRON BEAM ALGORITHMS

The development of clinical electron beam models for the determination of dose in inhomogeneous media and clinically relevant geometries has been a rich area of clinical investigation for many years. The accurate commissioning of an electron beam treatment planning system can be quite involved. By neglecting certain factors or tests or being unaware of the details and fine points associated with an algorithm, results can be unsuitable for clinical use. Task Group 53 of the AAPM has produced an extensive set of guidelines for the testing of treatment planning computer systems.[82] They address the issues of electron algorithm evaluation and describe tests of the Electron Contract Working Group (ECWG) for various planning situations.[83] They describe tests to be performed for electron beams in addition to tests that deal with the verification of the depth-dose data for open fields, tests for treatments at extended distances, tests for shaped electron fields, and output factor tests. These tests form a solid basis for evaluation of the accuracy of the algorithm, but additional tests may be needed to confirm that the dose calculation engine performs adequately over the entire range of clinical situations.

Most electron beam algorithms used clinically employ a pencil-beam approach based on the work of Hogstrom and co-workers[47,84] or Brahme *et al.*[85,86] The accuracy of these algorithms is well understood and documented and these algorithms have been shown to be clinically useful.[38,87–89] Algorithms that are more accurate than standard pencil-beam algorithms are available and are starting to appear in commercial treatment planning systems. For details of each algorithm, the reader is referred to several review articles and references contained therein.[90–93] It is not the purpose of this document to endorse one algorithm over another; rather, it is to offer guidance to the clinical medical physicist in implementing accurate electron dose planning. Given that accurate 3D dose calculation algorithms incorporating heterogeneity corrections have been implemented on many (if not all) modern treatment planning systems, the task group recommends that treatment planning for electron beams should use CT data and 3D heterogeneity corrections.

All electron treatment planning algorithms require measured input data for modeling (commissioning) the clinical electron beam. Monte Carlo dose calculations for electrons have been integrated into some treatment planning systems and may be more widely used in the future. The report of AAPM Task Group 105 describes basic techniques and issues relating to clinical use of Monte Carlo.[94] The medical physicist is advised to follow the vendor's recommendations as a minimum standard for commissioning the electron beams in their treatment planning system. Each vendor will have different recommended input data depending on the type of algorithm used and the implementation. The measured data usually include percentage depth doses for a range of field size, and off-axis profiles for selected field sizes at several depths. The range of field sizes included in the commissioning data should be similar to the range of field sizes used in the clinical practice. It is well known that for pencil-beam algorithms, percentage depth doses for large fields cannot be used to accurately predict percentage depth doses for small fields.[47,85] Off-axis profiles within the range of the electron beam are usually used to model nonflatness of the electron dose distributions. Off-axis profiles beyond the practical range are useful for modeling the bremsstrahlung component of the dose distribution. If monitor unit calculations are to be done within the treatment planning system, then output factors for a range of circular or square field sizes will also be part of the commissioning data set. For other required commissioning data, the physicist should refer to the commissioning instructions included with the treatment planning system.

At a given clinical installation, a medical physicist should be responsible for ensuring that the commissioning data are entered into the treatment planning system correctly. When a linear accelerator is put into clinical service, a range of dosimetric data will be measured covering a range of field sizes and SSDs for each energy. TG-53 provides a useful guide for the range of data that should be measured. It is important that

the measured data span the range of electron beams used in the clinical practice. Some or all of these data are entered into the treatment planning system. If the treatment planning algorithm is commissioned correctly and the vendor's implementation is correct, the treatment planning system should be able to reproduce all of the measured commissioning data to within the accuracy stated in TG-53. In essence, this ensures that the treatment planning system can return the input data, and that the input data are customized for the beams used in a given clinic.

The performance of the algorithm in the presence of heterogeneities or surface irregularities can be considered to be a property of the algorithm rather than a particular installation. Therefore, it only needs to be tested once (or a few times) for a particular implementation of an algorithm. The vendor's documentation should provide details regarding the algorithm's lineage, e.g., peer-reviewed articles describing the theory and implementation. References to peer-reviewed articles describing the performance of the implementation for "standard" heterogeneities and surface irregularities, such as the ECWG data set[83] or the more recent update of this data set by Boyd *et al.*,[95] should also be included in the vendor's documentation. It is very important that the documentation refers to a specific implementation, since different algorithm implementations may behave differently under the same circumstances.

If the user has verified that the treatment planning system can accurately calculate the dose per monitor unit, then the treatment monitor units can be taken directly from the treatment planning system if an independent check of the value is done. If the user has not verified the absolute dose per monitor unit in the treatment planning system, then the electron beam should be transferred onto a water phantom (in the planning system with the beam normally incident) so that the user can calculate the correspondence between the beam weight and the maximum dose delivered on the central axis to a water phantom at the same SSD. Then, the treatment monitor units can be verified by measuring the beam output or by calculating the monitor units using the clinical beam data tables.

The optimal treatment planning system would (1) calculate absolute dose per monitor unit throughout the calculation volume under all treatment conditions and (2) calculate absolute dose per monitor unit at the central-axis (or field center) maximum dose point in a water phantom at the same SSD as the patient. One could argue that the former implies the latter. While the latter can be obtained by transferring the electron beam to a water phantom in the treatment planning system, it would be very desirable to have the treatment planning system do this calculation automatically and report it as a standard part of the treatment planning output. Since the depth of maximum dose varies with field size, the depth of maximum dose in the water phantom should also be reported. The monitor unit second check would then compare the treatment planning dose output in a water phantom to a hand calculation (or MU calculation program) or measurement.

While the above recommendations are in common use, treatment planning implementations can make such dose specifications difficult to plan. Vendors are encouraged to allow for standard electron prescriptions in their treatment planning software. Similar to what is done for photon beams, beam parameters needed for secondary monitor unit calculations but specific to electron beams (e.g., size of equivalent rectangular field) should be included in the standard treatment planning hard-copy output.

Many vendor implementations are also incomplete in that they do not allow for beam modifiers such as skin collimation or customized bolus[96–98] or treatment planning of electron arc therapy.[87,99–101] This is a serious deficiency in the realistic application of electron beam treatment planning where a system should be able to represent accurately the actual treatment situation. Additional measurements in phantom to corroborate the results of the treatment planning system along with *in vivo* measurements during treatment are strongly encouraged for difficult treatment planning situations such as the determination of skin dose, rapidly changing contours, or scattering from high-Z materials.

V. PRESCRIBING, RECORDING, AND REPORTING ELECTRON BEAM THERAPY

V.A. Specification

The recommendations in the TG-25 report remain a sound basis for electron beam specification.[1] They were derived from the 1978 recommendations of the International Commission on Radiation Units and Measurements.[102] More recently, ICRU Report 71 on "Prescribing, recording, and reporting electron beam therapy" updates the 1978 recommendations.[103] ICRU Report 71 recommends the same general approach for both electron and photon dose prescription and reporting.[104,105] The concepts of gross tumor volume (GTV), clinical target volume (CTV), planning target volume (PTV), treated volume, organs at risk (OARs), and planning organ at risk volume (PRV) are defined as in previous ICRU reports and their use is recommended both by the ICRU and this task group. According to the TG-25 report, each beam's specification should include

- the electron beam radiation quality specified by the energy (MeV) and the type of radiation machine,
- the field size, as defined by the applicator (cone) size, aperture insert (or average dimensions or equivalent square area of the open area), and skin collimation,
- the nominal SSD, and
- any other beam modification devices such as energy moderators, patient bolus, or special devices.

Further, according to TG-25,

- the target dose should be specified at a point at the depth of maximum dose on the central axis or middle of the open part of the field in a water phantom for the field size and SSD used to treat the patient,
- the dose prescription point should not be in a high-dose gradient area, for example, near the edge of the field, and generally not in a blocked area,
- the energy and field sizes should be chosen and so

specified such that the target volume is encompassed within 90% (or any other appropriate minimum dose) of the prescribed dose, and
- the allowed variation of the dose across the target volume should be described relative to the target dose.

The ICRU also states that complete specification of the treatment should include its time-dose characteristics (total dose, dose per fraction, treatments per week, etc.) with no adjustments for differences in the relative biological effectiveness between photons and electrons.[103]

V.B. Prescription

There is a wide variety of acceptable methods for prescribing radiation dose for electron treatments. Those given by the ICRU have been defined and agreed upon by a group of experts in the field. This task group recommends planning using 3D CT-based dose calculations but recognizes that acceptable electron treatment fields can be established using basic clinical data, available diagnostic information, and clinical examination of the patient. All prescription methods can be classified as either prescribing dose to a point or to an isodose surface.

In developing the computerized treatment plan or prescribing dose to a point, the specifications listed in Sec. V A. should be followed. When prescribing dose to a patient without a CT-based dose plan, all of the above principles apply except that the patient is assumed to be water equivalent. Thus the impact of patient heterogeneities on dose cannot be assessed.

V.C. Dose reporting

Report 71 of the ICRU (Ref. 103) recommends the same general approach to report dose for electron treatments as those described for photons as specified in reports ICRU 50 and 62.[104,105] These publications indicate that the treatment should be specified completely including time-dose characteristics. No adjustments due to the differences in the relative biological effectiveness between photons and electrons are to be made. They recommend the selection of a reference point for reporting electron doses which is referred to as the "ICRU reference point." The location of this point should be clearly indicated and should always be at the center or in the central part of the PTV. The beam energy should be selected so that the maximum of the depth-dose curve on the beam axis is located at the center of the PTV. If the peak dose does not fall in the center of the PTV, then the ICRU reference point for reporting should be selected at the center of the PTV. The maximum absorbed dose to water should also be reported in this instance. The maximum and minimum doses in the PTV and dose(s) to OARs derived from dose distributions and/or dose-volume histograms should also be reported. For small and irregularly shaped beams, the peak absorbed dose should be reported. It is also recommended that when corrections for inhomogeneous material are applied, the application of these corrections should be reported.[103]

VI. CLINICAL APPLICATIONS OF ELECTRON BEAMS

VI.A. Heterogeneities in electron treatments

The discussion of the effect of heterogeneities in the TG-25 report was limited to a brief description of some of the effects of heterogeneities on electron dose distributions and the coefficient of equivalent thickness (CET) method for calculating depth dose behind slab heterogeneities. The CET method is useful for a quick estimate of penetration of electrons incident on a chest wall into lung or on one side of the nose to the septum. However, as pointed out in the TG-25 report, it is approximate even in slab geometry and cannot handle more complex inhomogeneities.

While fairly accurate electron dose calculations are now commercially available, a qualitative understanding of how heterogeneities affect the dose distribution is helpful in situations that the TPS cannot handle. Heterogeneities affect the penetration of the beam because of differences in stopping power, which are a result of different densities and tissue compositions. However, in most clinical situations, differences in scattering power have a much larger effect. Localized heterogeneities disrupt lateral scatter equilibrium, causing local hot and cold spots.

For a small (compared to field size) high-density heterogeneity, electrons are more likely to be scattered away from the high-density region than to be scattered toward it. Behind the heterogeneity, the fluence perturbation creates hot spots lateral to the heterogeneity and corresponding cold spots directly under the heterogeneity. A small low-density heterogeneity has the opposite effect. Figures 32 and 33 in the TG-25 report clearly show these effects.

The magnitude of the hot and cold spots depends on the electron energy and the size, density, depth, and composition of the heterogeneity and the surrounding tissue. The physicist needs to be alert to treatment sites such as the nose where complex dose distributions caused by inhomogeneities may be clinically important. Chobe *et al.*[106] described a patient who received a boost that was not CT planned to the nasal vestibule with an anterior, 13 MeV electron field. The patient developed maxillary necrosis, attributed in part to side scatter which produced an ~120% hot spot in the maxilla, according to a retrospective CT-based 2D pencil-beam calculation.

Another important site of tissue inhomogeneity is the chest wall, which also often involves opposed or junctioned electron beams.[107–109] Surgically produced and nonbiological inhomogeneities can also be problematic. Fontenla *et al.*[110] provided measurements and 2D pencil-beam calculations of the effects of approximately bone-density ocular implants on electron beam treatment of the orbit. The calculations account for the most clinically significant effect, 40% and 10% attenuations directly under the implant for 6 and 12 MeV electrons, respectively, but do not reproduce small hot spots. Yorke *et al.*[111] presented phantom measurements showing a complex dose distribution for 9 and 12 MeV electron stoma boosts, with small 130%–150% hot spots in soft tissue under

TABLE VI. Percentage depth dose at the surface and superficial regions of high-energy electron beams for a Varian 2300 C/D for a 10×10 cm^2 cone at 100 cm SSD. Also shown are the depths at which D_{max} and D_{90} occur.

	Electron percentage depth dose[a] (%)					
Depth	6 MeV	9 MeV	12 MeV	15 MeV	18 MeV	22 MeV
Surface[b]	70.8	76.5	82.0	86.6	88.4	89.1
0.5 cm	82.5	84.7	89.5	93.7	96.0	97.0
1.0 cm	94.0	90.0	92.6	96.4	98.7	98.9
D_{max} depth (cm)	1.4	2.2	2.9	2.9	2.9	2.2
D_{90} depth (cm)	1.8	2.8	3.9	4.8	5.4	5.8

[a]Measurements given in this table were taken with an Attix chamber whose front electrode is 0.025 mm thick, 4.8 mg/cm^2 Kapton (Ref. 130).
[b]Defined as 0.5 mm depth on the central axis.

and lateral to the stoma, but pointed out that the impact of such effects is moderated by the low dose usually prescribed for such boosts.

VI.B. Dose calculation accuracy

As described above, the accuracy of an electron dose calculation in the presence of heterogeneities is primarily a property of the algorithm. Electron beam dose calculation algorithms in currently available commercial treatment planning systems can be divided into two types: Those based on pencil-beam approximations and those based on stochastic Monte Carlo methods such as VMC (Refs. 112 and 113) and MMC.[114,115]

Because pencil-beam algorithms are available in most commercial treatment planning systems, it is worthwhile to discuss the limitations and general accuracy that can be achieved under heterogeneous conditions. These have been the subjects of many investigations,[38,88,89,116,117] some of which found quite significant differences between measured and calculated doses. However, the heterogeneities investigated were not always clinically realistic, e.g., aluminum as a bone substitute. For realistic high-density heterogeneities, the accuracy of the pencil-beam algorithms is as good as 3%–7%.[89] In the presence of air cavities, larger differences are noted.[89,116,117] If the algorithm models tissue inhomogeneities as infinite slabs, deeper heterogeneities are not modeled as well as shallower ones.

Stochastic algorithms such as VMC, MMC, and super-Monte Carlo[118] promise to be more accurate than traditional pencil-beam approaches. The first two algorithms have been implemented in commercially available treatment planning systems. The accuracy of a commercial implementation of the VMC algorithm has been described by Cygler *et al.*[56] and Ding *et al.*[119] This algorithm showed superior agreement with measurement for a demanding 3D phantom with air and bone inhomogeneities with calculation times comparable to 3D pencil-beam implementations. Popple *et al.*[120] did a comprehensive evaluation of an implementation of the MMC algorithm using the updated version of the ECWG data set.[95] They found that with appropriate choices for algorithm parameters, accuracy to within 3% dose or 3 mm distance to agreement was achievable.

More advanced analytical algorithms, such as pencil-beam redefinition algorithm (PBRA) (Refs. 121–125) and phase space evolution,[126–129] are capable of dose calculation accuracy similar to that of the above Monte Carlo algorithms. Boyd[125] showed that for typical patient cases, the dose calculation accuracy of the PBRA is essentially the same as EGS4 Monte Carlo dose calculations. Therefore, the choice of Monte Carlo versus analytical algorithms will be as much a function of marketplace availability and the learning curve of clinical users as of absolute calculation accuracy.

VI.C. The use of bolus in electron beam treatments

Bolus is used for several reasons in electron beam treatments: To increase the dose on the skin surface, to replace missing tissue due to surface irregularities, and as compensating material to shape the coverage of the radiation to conform as closely as possible to the target volume while sparing normal tissue. For modern linear accelerators, the surface dose can be as low as 70% of that at d_{max}. Table VI gives the dose at the surface, 0.5 and 1.0 cm for electrons for a Varian 2300 C/D linac. Measurements given in this table were taken with an Attix chamber[130] whose front electrode is 0.025 mm thick, 4.8 mg/cm^2 Kapton. To encompass the target within the 90% isodose surface, bolus would be required in all cases where the target has superficial extent.

The ideal electron bolus material would be equivalent to tissue in both stopping power and scattering power. Additionally it should be flexible and moldable to closely conform to the variations in surface topology of the patient. Several commonly available materials can be used as bolus material. These are paraffin wax, polystyrene, acrylic (polymethylmethacrylate), Super Stuff™, Superflab™, and Superflex™. Solid sheets of thermoplastic materials (3 mm thick) conform very well to the skin surface and are transparent when hot. They can be held in place to fit the skin surface

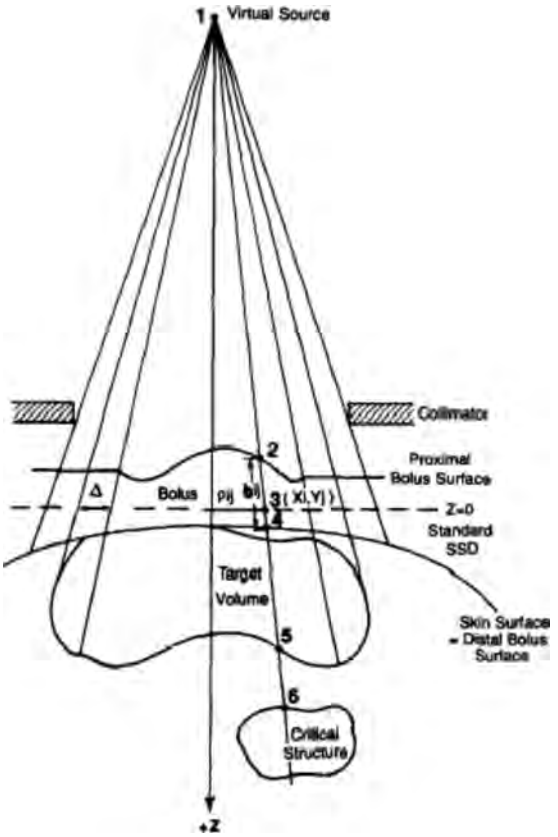

FIG. 4. Schematic representation of the patient contour, target volume, and compensating bolus designed to optimize the coverage of the target while minimizing the dose to the underlying critical structure. [Reprinted with permission from D. A. Low *et al.*, Med. Phys. 19, 117 (1992). Copyright 1992, American Association of Physicists in Medicine.]

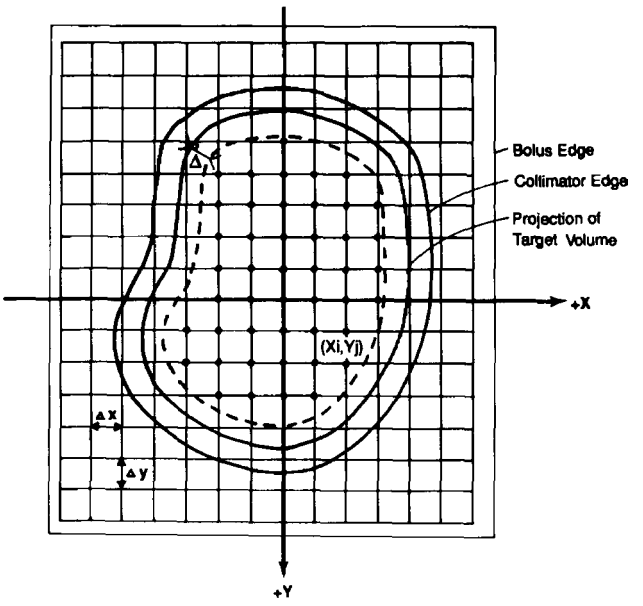

FIG. 5. Compensating bolus diagram for construction and placement of the bolus for patient treatment. [Reprinted with permission from D. A. Low *et al.*, Med. Phys. 19, 117 (1992). Copyright 1992, American Association of Physicists in Medicine.]

exactly and are rigid when cool. A nearly perfect outline of the patient's surface results and additional bolus can be added easily after the material solidifies.

Custom compensating bolus can be designed for complex situations to eliminate or decrease the effect of tissue heterogeneities, irregular patient surface structure, distance or curvature effects, or other parameters that would affect the production of an optimal dose distribution. Custom bolus can be designed by hand using individual CT scans[131] and/or ultrasound imaging[132] of the region to be treated. The electron energy is selected so that it covers the deepest extent of the target to be treated to at least 90% of the given dose. Bolus is added to the entrance surface of each CT slice to create an equal depth of penetration along fan lines on all scans to cover the target (Fig. 4). The proposed bolus is added to each individual CT scan and a computerized treatment plan is completed to ascertain the acceptability of the bolus design. The technique is repeated until final acceptable bolus design and plan are achieved. A grid describing the bolus location on the patient and the thickness of the bolus at those locations is produced and the compensator is made to these specifications (Fig. 5). The grid also serves as an alignment tool so that the compensating bolus can be placed accurately on the patient from one treatment to the next. This manual technique has several limitations. It is iterative in nature, is time consuming, is one-dimensional in nature which neglects multiple Coulomb scattering, does not accurately portray the dose at sharp edges, and does not account for the full three-dimensional nature of the problem.[96,133] If the edges of the bolus are sharp rather than tapered, high doses at the edges inside the treated field along with cold spots at the edges under the bolus can result. If a small strip of bolus is to be used, such as to increase the surface dose to a surgical scar, then the bolus must be wide enough (at least 2 cm) to ensure that the dose to the skin actually is increased rather than decreased due to outscattering from the bolus and by edge effects.

Computer-based techniques[96] have been devised to address these difficulties and limitations. The distribution in Fig. 6 gives an idea of the capabilities of these approaches in covering the target volume and limiting the high-dose regions.[97,98] The computerized bolus technique has been paired with electron intensity modulation to produce theoretical dose distributions for challenging target locations although currently there is no commercially available way to deliver the treatment.[134]

The manual method of compensating bolus fabrication is the primary means available to most clinics. It is hoped that the more advanced computer applications will be made available to a wider user base in future releases of commercial software.

VI.D. Electron field abutment

Matching electron fields on the skin surface requires special considerations. If the fields are abutted on the skin surface, then an overlap region with significant hot spots may result that can lead to unwanted clinical consequences. If the fields are separated on the surface, then a region of dose

FIG. 6. Isodose distribution (Gy) using the custom 3D electron bolus technique. A dose of 50 Gy was prescribed to 100% of the given dose using 16 MeV electrons, and the bolus was designed to deliver 90% of the given dose to the target volume. The plan shows dose minimization to the ipsilateral lung and underlying cardiac tissues. The isodose lines represent 20 Gy, 30 Gy, 40 Gy, 45 Gy, and 50 Gy. [Reprinted with permission from G. H. Perkins *et al.*, Int. J. Radiat. Oncol., Biol., Phys. 51, 1142 (2001). Copyright 2001, American Society for Radiation Oncology.]

deficit will be produced that can lead to inadequate coverage of a target in the region of the match. The size of the overlap region and the magnitude of the dose in the overlap region are dependent on the individual beams, their associated isodose curves [Figs. 7(a) and 7(b)], and the angle of incidence of the two beams with respect to each other.

If electron fields are to be abutted, moving the junction location between the beams provides a safe means by which to reduce the magnitude of the high-dose region. The number of junction changes depends on the total dose, the size of the high-dose region, and how high the dose is in the overlap region. A shift in the junction of 1 cm is adequate in most instances but the absolute amount depends on the size of the overlap region and the number of junction shifts to be made. It is recommended that the junction be moved a sufficient number of times and by a sufficient amount to ensure that the high-dose region does not exceed the prescription dose by more than 15%–20% when prescribed to d_{max}. Usually a 1 cm shift every 1000 cGy will accomplish this goal.

Matching electron fields on a curved surface that often exist in clinical situations usually increases the magnitude of the overlap region, as each of the electron fields is usually

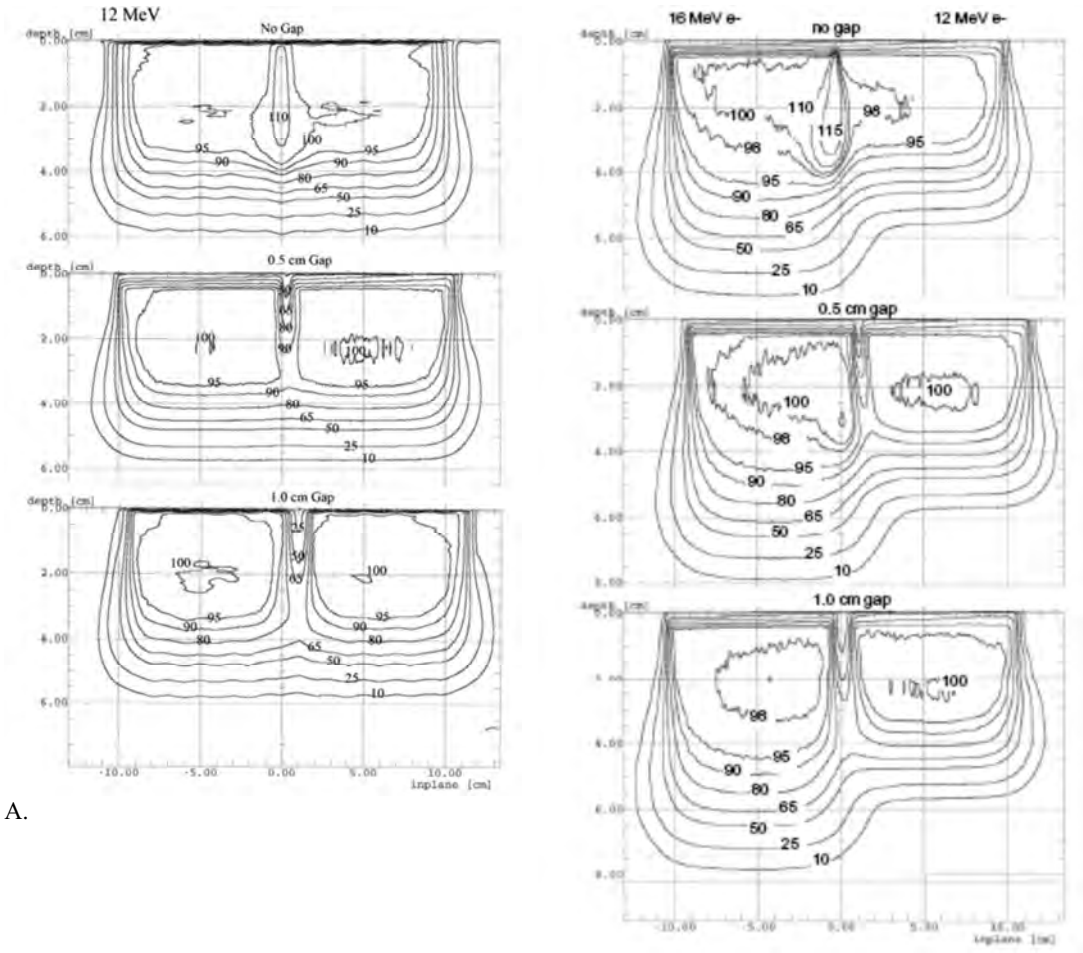

A.

B.

FIG. 7. Electron field matching for a Varian 2100c, 10×10 cone, 100 SSD, (a) two 12 MeV fields and (b) 16 MeV (left), 12 MeV (right) fields with no gap on the skin surface (top), 0.5 cm gap on the surface (middle), and 1. 0 cm gap on the surface (bottom). Isodose values are 10%, 25%, 50%, 65%, 80%, 90%, 95%, 100%, and 110%. Data were taken using Kodak XV-2 film in a solid water cassette and scanned using a Wellhofer isodensitomer and WP700 software.

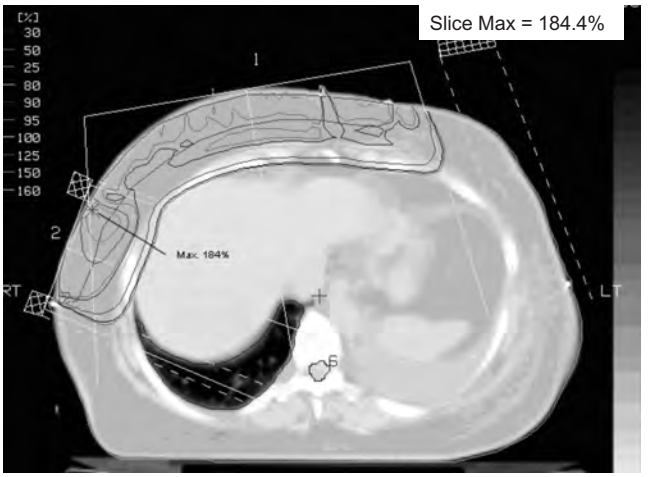

FIG. 8. Representation of the magnitude of the high-dose regions when two electron fields abut at the skin surface. Both beams are perpendicular to the skin surface. Represented are 12 MeV electron fields using Varian CadPlan beam model.

oriented perpendicular to the skin surface. The dose in the overlap region increases with decreasing radius of curvature of the external body contour. Situations such as those illustrated in Fig. 8 should be closely monitored in the clinic and the location of the junction should be repositioned with sufficient frequency to limit the risk of a complication. Figure 9 shows a clinical example of abutting electron fields in chest wall treatment. The dose homogeneity is acceptable at the border of the internal mammary chain and medial chest wall fields because the central axes are parallel, the field widths are small, and the field overlap is small. However, the dose homogeneity is unacceptable at the border of the medial and lateral chest wall fields because central axes are converging. The bottom figure of Fig. 8 shows the smoothing effect of moving the junction by 1 cm twice during the treatment. A 50% high-dose region (shown in the top figure of Fig. 8) was reduced to +27% by moving the junction in this manner (Fig. 8 bottom figure).

VII. CONCLUSIONS

TG-70 report is a supplement to the TG-25 report meant to enhance the material given in the TG-25 report by including procedures for obtaining data to commission a treatment planning computer and to determine dose in irregularly shaped electron beam fields and the procedures for commissioning of sophisticated special procedures using high-energy electron beams. Many clinical applications, though not exhaustive, of electron beams are also included in the full TG-70 report, available on the AAPM website (http://www.aapm.org/pubs/reports). The descriptions of the techniques in the clinical sections give key elements of the procedure and how to proceed toward initiation of these programs in a clinical setting. Since there have been no major changes since the TG-25 report relating to flatness and symmetry, surface dose, virtual source, air gap corrections, and oblique incidence, these topics are not readdressed in this new report.

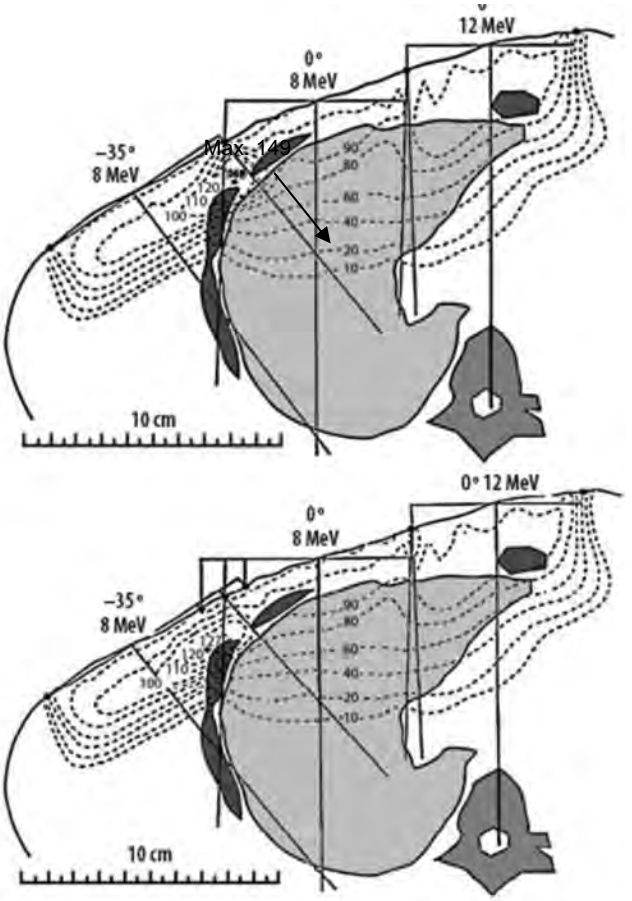

FIG. 9. Clinical examples of abutting electron fields in chest wall treatment. Dose homogeneity is acceptable at the border of the internal mammary chain and medial chest wall fields because central axes are parallel and field widths are small. Dose homogeneity is unacceptable at the border of the medial and lateral chest wall fields because central axes are converging. Bottom figure: Dose homogeneity is improved in this region by moving the match line twice during treatment by 1 cm. [From K. R. Hogstrom, Principles and Practice of Radiation Oncology. Copyright © 2004 by Lippincott, Williams and Wilkins. Reprinted by permission of Lippincott, Williams and Wilkins.]

VIII. LIBRARY OF CLINICAL EXAMPLES

VIII.A. Intact breast

VIII.A.1. Tangent photon fields plus internal mammary node electrons

VIII.A.1.a. Introduction. For treatment of the postlumpectomy (intact) breast patient, an electron field is sometimes used to treat the involved internal mammary nodes (IMNs) while avoiding excessive irradiation to the heart and mediastinum.[135–139] Photon-only methods can also be used to treat the breast plus IMN—most notably, partially wide tangents (PWTs). This is a CT-planning-based technique where a greater width is irradiated by the tangential beams in the superior part of the field in order to cover the IMN while the width is reduced to conventional tangent width below the nodal chain.

VIII.A.1.b. Prerequisites. CT planning is desirable for these techniques, as the electron beam energy or the PWT field shape is chosen to cover the nodes, which are most

conveniently visualized by CT scans. The lung dose can best be assessed by CT planning with inhomogeneity correction.

VIII.A.1.c. Planning and delivery. The patient is immobilized as for treating breast tangents. The CTV is the ipsilateral breast and the IMN; the physician defines the PTV to account for setup error and respiratory motion. The direction of the electron IMN field is often chosen to be straight AP, with the medial border matched on the skin to the medial edge of the tangential field and the shape designed to follow the ipsilateral IMN with adequate margin (total width: ~6–7 cm). The match line should be located so that breast tissue at risk is not included in the "cold triangle" between the tangents and the IMN field. Alternatively, the IMN beam can be angled approximately parallel to the medial tangent using the dose distribution visualized in the treatment planning system to assure adequate coverage of tissues at risk and for acceptable hot spots. To improve skin sparing, an electron beam angled to match the divergence of the tangential breast fields may be combined with a photon field weighted to give ~20% of the total dose [Figs. 10(a) and 10(b)]. Junction shifts may be used to even out the dose distribution.[139] Two recent comparison studies[139,140] find that, when carefully implemented with 3D-CT planning methods, both the combined electron-photon and the PWT method provide acceptable normal tissue protection but the PWT provides better coverage of the IMN.

VIII.A.1.d. Quality assurance. No special physics QA is required beyond a well commissioned planning system and the periodic linac QA recommended by TG-25, TG40, and this task group.

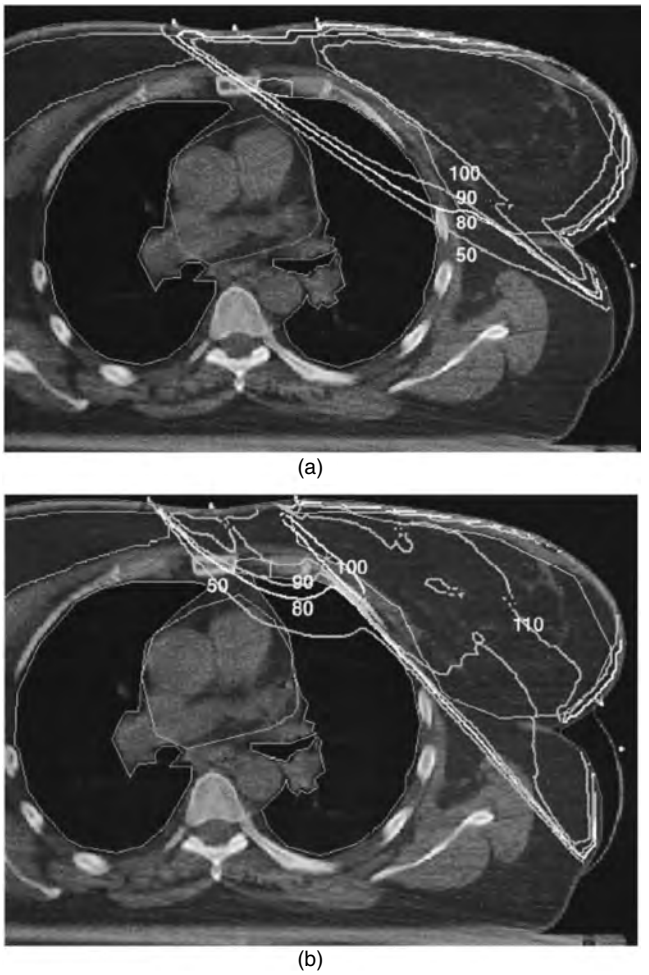

FIG. 10. Dose distribution with PWTs vs photon/electron (P/E) illustrating difference in position of hot spots. Left lung, heart, IMC, left breast or chest, and right breast were outlined. The 50%, 80%, 90%, 100%, 110%, and 120% isodose lines are displayed. (a) Dose distribution with intact breast and PWT. (b) Dose distribution with intact breast and P/E. [Reprinted with permission from D. Severin *et al.*, Int. J. Radiat. Oncol., Biol., Phys. 55, 633 (2003). Copyright 2003, American Society for Radiation Oncology.]

VIII.A.2. Electron boost to intact breast

VIII.A.2.a. Introduction. Following treatment of the postlumpectomy breast with photon tangents, the tumor bed and surgical scar are often boosted with electrons (10–20 Gy at 2 Gy/fraction) or, for a deep tumor bed (>4 cm), an interstitial implant. A discussion of the medical indications for a boost and literature comparing brachytherapy with electron boost is given by Perez *et al.*[141]

VIII.A.2.b. Prerequisites. It is important to know clearly the extent of the target volume so that it can be covered adequately. This is best done if the surgeon places radiopaque surgical clips that are visualized on radiographs and/or CT. Computerized treatment planning of the electron boost is not considered necessary, and the electron boost field is often designed clinically.[141] However, CT simulation images, if available, are very useful in selecting the electron energy and designing the shape of the field.[142,143]

VIII.A.2.c. Planning and delivery. The patient is usually immobilized in the same manner as when treating tangential photon fields. The beam should be directed enface, so that it is incident as nearly perpendicular to the surface as possible. An extended SSD (~110 cm) may be required for clearance. The energy and the lateral margins should be adequate to encompass the target volume within at least 90% of the prescription dose. The energy is usually chosen between 9 and 16 MeV; too low an energy will miss the deeper parts of the target while too high an energy may give excess lung dose for small-breasted patients.[142] In determining the cutout size and shape for clinically designed fields, it is necessary to allow margin for the electron beam penumbra, the constriction of the high percentage isodose lines at depth for electrons above 10 MeV, and the possibility of breast motion due to respiration.

VIII.A.2.d. Quality assurance. No physical QA is recommended beyond the periodic QA for electron beams recommended by TG-40. If the boost is designed as a clinical setup, a senior physician should attend the setup session and the monitor unit calculation and treatment instructions (both hard-copy and electronic entries in R&V system) should be reviewed in a timely fashion, as recommended by TG-40.[144]

VIII.B. Chest wall electrons

VIII.B.1. Introduction

Postmastectomy chest wall recurrences are frequently treated with electrons or a mixture of electrons and photons

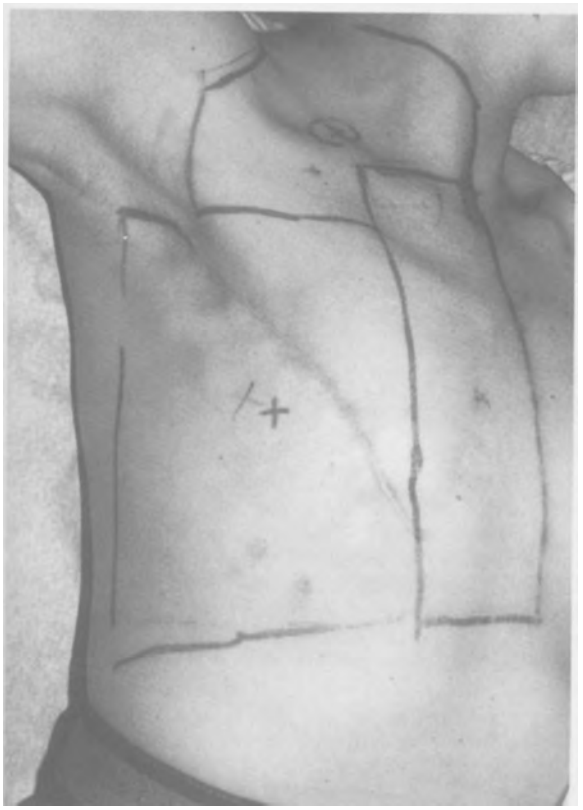

FIG. 11. Complicated arrangement of abutting electron fields for the treatment of postmastectomy chest wall. [From M. D. McNeese *et al*., Levitt and Tapley's Technological Basis of Radiation Therapy, Practical Clinical Applications. Copyright © 1992 by Lea and Febiger. Reprinted by permission of Lea and Ferbiger.]

to reduce lung and heart doses. The CTV is the remaining breast tissue on the ipsilateral chest wall and often the IMN. Although electron arc therapy is a well documented procedure, fixed field methods are simpler and are used more frequently.

VIII.B.2. History and description

One common method[135,136,145] employs an AP electron field to treat the anterior chest wall matched on the skin to a lateral-oblique electron field which has an approximately en-face entrance on the lateral portion of the chest wall and an additional anterior electron field to treat the IMN. Photons are used to treat the supraclavicular nodes (Fig. 11). Recently, a different method was described which uses a single beam direction, approximately normal to the curved chest wall, and matched cutouts to improve coverage at the target edges.[146] A third method combines tangential photon fields with an electron IMN field, similar to treatment of the intact breast and IMNs. In all cases, photons are used to treat the supraclavicular nodes.

VIII.B.3. Prerequisite

CT-based treatment planning with tissue inhomogeneity correction is highly desirable to determine the best technique for treating the residual breast tissue while sparing the underlying lung and heart.

VIII.B.4. Planning and delivery

The patient is immobilized as for breast tangents. For the electron-based methods, the energy of each electron beam is chosen to give adequate dose at the lung-chest wall interface. Tissue inhomogeneity corrections are necessary to evaluate the lung dose from the treatment plan. Bolus may be required both to increase the skin dose (for lower-energy electrons) and to provide lung protection where the chest wall is particularly thin. Extended SSD (up to 110) is often needed for clearance. It is common to shift the junctions at least once during treatment to reduce dose inhomogeneity. Two recent papers[147,148] compare a variety of electron-only, mixed electron-photon, and photon-only methods for treating the chest wall using 3D-treatment planning and inhomogeneity corrections. Both conclude that, at this disease site, the best technique depends strongly on individual features of patient anatomy.

In general, it is important to evaluate the effect of tissue inhomogeneity for an electron field at a site where substantial low-density tissues exist. Since lung density is approximately 30% that of soft tissue, an electron beam penetrates three times farther into lung tissue than it does in unit density material (muscle). Thus, the lung inhomogeneity has significant impact on the lung and heart doses in chest wall and IMN treatments and it must be taken into account in the choice of beam energy and evaluation of the overall dose distribution.

VIII.B.5. Quality assurance

The planning system should be well commissioned and capable of handling custom bolus. Care is required to assure that bolus is correctly and reproducibly placed. Since large areas of the chest wall are involved, *in vivo* dose verification is recommended if the technique is new to the clinic, if custom compensating bolus is used for the treatment, if extended SSDs are used for the treatment, or to determine the dose at the junctions if several electron fields are used. A collection of TLD chips placed on the skin surface through the treated field and into the contralateral breast provides a reliable means by which to ensure that the correct dose is being delivered to the region. If a large strip of paper tape with the TLD packets attached is prepared in advance, the accurate placement of a large number of TLD chips can be done with little inconvenience to the patient or the therapist staff.

VIII.C. Electron arc treatments

VIII.C.1. History and description

Electron arc therapy gained popularity as a mechanism to deliver a uniform and superficial dose over a curved or irregular surface of very large dimensions. Treatment of the chest wall is a primary example of the application of the electron arc and was developed to a high level in the early 1980s. The technique remains essentially unchanged since its inception,[99,149] except that the use of CT for treatment plan-

ning has replaced external contours. The dosimetry, treatment planning techniques, and details continue to be improved.[150,151]

Two approaches have been developed for electron arc therapy. One approach is called the electron pseudoarc approach,[152] which employs a series of overlapping stationary electron fields and the second uses a continuously rotating electron beam. The former is simpler to commission and current treatment planning systems can represent accurately the dose distribution from these beam arrangements. The amount of time and effort required to perform continuously rotating electron beam arc therapy is considerably greater due to the unique characteristics of this treatment technique.

VIII.C.2. Treatment planning and delivery

Electron arc therapy is most appropriate when the area to be treated presents a constant radius of curvature since the rotational isocenter needs to be placed at a constant distance from the surface if possible. Changes in the radius of curvature at other locations in the treatment region can lead to increased or decreased dose delivered in those regions. The dose to the skin surface for rotational electron arc treatments is also lower than what would be expected for fixed electron beams. This is due to the "velocity effect" where points closer to the isocenter are exposed to the beam longer than shallower points resulting in dose concentration at depth. Special measurements need to be performed before treatment initiation along with the fabrication of specific treatment devices that are unique to individual patients. These include superficial (skin) field collimation (tertiary collimation) and a custom secondary beam defining geometry for the electron applicator to deliver an appropriate field shape and the impact of oblique angles on the dose distribution. Attention should be paid to the electron energy and the potential for a focused bremsstrahlung dose at the rotational isocenter that is non-negligible when developing an electron arc procedure. An excellent overview of all aspects of electron arc treatment is given in the AAPM 1990 Summer School Proceedings.[153]

Special shielding devices have to be fabricated to ensure that only the area of interest is treated, to ensure that an accurate dose is delivered, and to ensure that areas outside of the treated area are shielded from scattered radiation. The procedure requires that the exact region of the body to be irradiated is defined by the physician. A treatment position that allows the entire area to be treated in one rotation is defined and the region is then outlined with radio-opaque markers. A treatment planning CT is taken for the determination of the rotational isocenter and to define clearly the target region (PTV). The scan series is essential to document the different curvatures existent within the treatment region. From these data, the secondary and tertiary shieldings can be designed and fabricated (Fig. 12). Current linear accelerators have electron arc options that automatically set the adjustable collimators to a fixed size when in that mode. Rotational fields can be of any size with smaller field width producing lower dose per monitor unit with greater photon contamination per dose delivered.[154,155] However, smaller field widths result in almost normal beam incidence which simplifies the dosimetry.[156] Recommended field widths are between 4 and 8 cm.

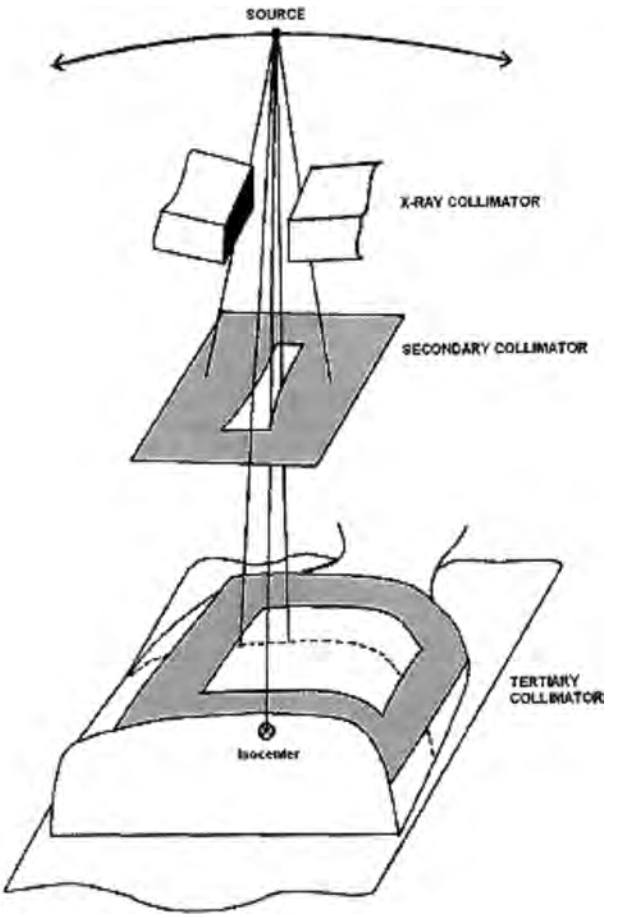

FIG. 12. Diagram of the field definition components required to perform electron arc irradiation. The secondary collimation device is placed at a distance and can vary in width to optimize the dose distribution at the patient surface. The tertiary collimation is required to restrict the electron spray to only the regions being treated. [Reprinted with permission from F. M. Khan *et al.*, Radiology 124, 497 (1997). Copyright 1997, Radiological Society of North America.]

Secondary collimation is designed to produce optimal dose distribution throughout the treated volume. For chest wall treatments, the radius of curvature of the chest wall generally decreases superiorly. As a result, the dose to this region is greater due to the focusing of electrons in this region.[157] Reducing the width of the opening in the secondary collimator that corresponds to this region can lead to a more uniform dose throughout the field (Fig. 12).

Tertiary collimation is placed on the patient's skin surface far from the secondary beam defining apparatus. Thus the dose falloff at the borders of the treatment field is gradual due to air scatter compared to ordinary static electron fields. The electron arc must be extended beyond each end of the treatment arc by approximately 15° to re-establish a sharper dose falloff. A tertiary shield is fabricated to not only sharpen the edges of the treatment area but also to protect the uninvolved regions that would be irradiated by the extended arc. Figure 13 shows an example of an electron arc distribution

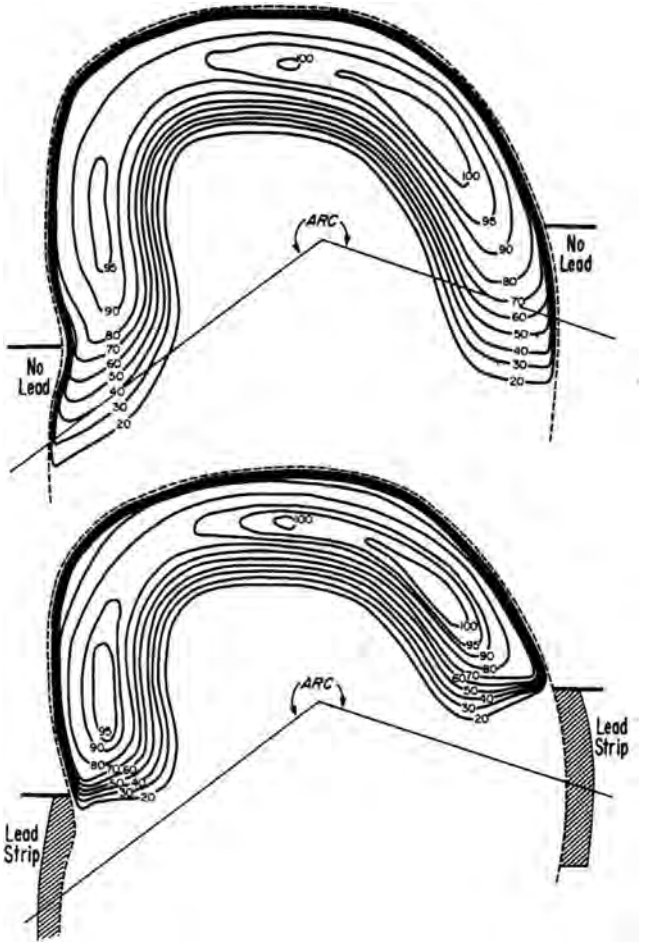

FIG. 13. Electron arc isodose distributions showing the rotational distribution without lead shielding to define the end of the treatment region (top) along with the edge sharpening effect of lead at the end of the arc (top). The distribution is representative of 10 MeV electrons and an average radius of curvature of 10 cm as measured using a Rando phantom. [From K. R. Hogstrom, Principles and Practice of Radiation Oncology. Copyright © 2004 by Lippincott, Williams and Wilkins. Reprinted by permission of Lippincott, Williams and Wilkins.]

both with and without a lead tertiary shield in place.[154] The tertiary shield can be made from sheets of lead or poured cerrobend. The thickness of the shield must be adequate for the electron energy being used. Because of the amount of shielding material required, these shields can be very heavy and of concern for therapists and the patient. In addition, scattering off the edges of the lead sheets that produces local high-dose regions needs to be taken into account.[156] Calibration of the dose rate for electron arc therapy can best be accomplished by direct measurement using an ionization chamber in a cylindrical phantom of polystyrene, acrylic, or solid water. Holes are drilled at d_{max} in the phantom to accommodate the chamber and standard corrections are applied to convert the integrated charge into dose.[156] Alternatively, the integrated charge measured in the cylindrical phantom can be compared to the integrated charge measured at d_{max} for a 10×10 cm^2 cone or the calibration cone size. The radius of curvature for the cylindrical phantom need only be approximately (within 2–3 cm) the same as the radius of curvature for the treatment situation but the depth of the rotational isocenter below the phantom surface must be the same as that used for treatment.[158] TLDs can be placed on the surface of the phantom to quantify the surface dose for the treatment.

VIII.C.3. Quality assurance

This is a very important aspect of the treatment since current treatment planning systems can only give an approximate dose distribution to represent the complex interplay of secondary and tertiary shieldings, variations in radius of curvature through the treatment region, and effects of inhomogeneous material. Thermoluminescent dosimeters should be placed on the skin surface to verify the dose in the treated region and outside of the treated region to assess the effectiveness of the shield and to ensure that uninvolved tissue is not being irradiated.

VIII.D. Total scalp

VIII.D.1. Introduction

Occasionally a patient presents with a cancer such as cutaneous lymphoma, squamous cell carcinoma, or angiosarcoma that involves the skin of the scalp and forehead to a depth of ~5 mm but does not invade the skull or underlying brain. The challenge is to give a reasonably uniform dose to the skin while sparing bone and brain.

VIII.D.2. History

Initially, an electron-only method was used. Able *et al.*[159] described a treatment using six abutted, approximately enface, low-energy (6–7 MeV) beams. The junctions are shifted by 2 cm halfway through the treatment course to improve dose uniformity, thus requiring a total of 12 different fields. However, a simpler method was developed by Akazawa.[160] and further enhanced by Tung *et al.*[161] that combined the use of both photon and electron fields.

VIII.D.3. Description

Akazawa's method uses a pair of parallel-opposed lateral low-energy photon beams (6 MV or less) and a matched pair of parallel-opposed lateral low-energy electron beams. The beam arrangement is shown schematically in Fig. 14. The photon fields treat a medial sagittal rind of scalp, with the brain being largely blocked. The remainder of the scalp is treated by the electron beams. In this study, the electron beam weights were 100% and the photon weights were 60%. Tung *et al.* found that an approximately 3 mm overlap between the adjacent photon and electron fields improves dose uniformity compared to the original technique of simple abutment. A 1 cm shift is performed at least once during treatment to feather the junction. Tung *et al.* advised that the first phase field junction be placed just inside the inner table of the skull and that the subsequent junction shift reduces the area covered by the electrons. Bolus (~6 mm) is used to increase the skin dose in the buildup region and to further protect the brain from the electron fields. Phantom and *in*

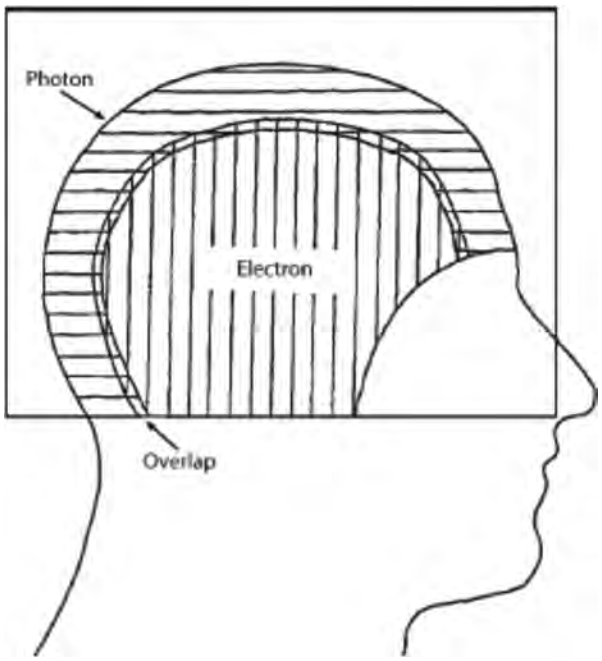

FIG. 14. Combination of right-left lateral photon fields with abutting electron fields to treat the entire scalp region. The overlap between the photon and electron fields is approximately 3 mm. [Reprinted with permission from S. S. Tung *et al.*, Int. J. Radiat. Oncol., Biol., Phys. 27, 153 (1993). Copyright 1993, American Society for Radiation Oncology.]

vivo TLD measurements show this method to be superior in dose uniformity (as well as simplicity) to the electron-only method.

VIII.D.4. Prerequisites

Prone positioning with good immobilization is advised. Although the apertures can be designed from simulator films, three-dimensional treatment planning is preferable, as it allows the planner to decide on the best beam weights and electron energy, to guard against unexpected hot spots in brain, and to customize bolus to accommodate different depths of disease. Bolus fabricated from a hard material (e.g., wax) provides the most secure placement.

VIII.D.5. Quality assurance

For physics QA, the routine linac quality assurance is sufficient. However, the therapist should pay particular attention to the field junctions at each setup especially since shifting field borders are involved.

VIII.E. Parotid

VIII.E.1. Introduction and purpose

In the past, electron beams were often used for treating lateral target volumes such as the postsurgical parotid bed.[162] However, the large penumbra and a lack of accuracy in planning electron treatments have led to less use of electron beams for this site. In the more recent past, intensity-modulated x-ray therapy (IMXT or IMRT) has caused electrons to be considered even less of an option for these cases.

VIII.E.2. History and description

The traditional photon beam arrangement for treating the parotid bed is a wedged pair, which has the advantage of sparing the contralateral side of the oral cavity. However, the treated volume on the ipsilateral side can be excessive compared to the extent of the PTV. More accurate dose calculations for electron beam treatment planning systems combined with advanced technology implies that electron beams can be considered for these treatments. For target volumes very near the surface, especially, lower surface dose for photon beams and uncertainty in the accuracy of treatment planning systems to calculate the dose near the surface imply that using x rays may be less than optimal for these patients. An in-depth study comparing nine different non-IMRT techniques to treat the parotid area[163] concluded that only three techniques met the objectives of providing a homogeneous dose through the target region, minimizing the dose to sensitive normal structures, and not producing an unacceptably high dose to the skin surface. These three techniques were the ipsilateral wedge pair technique, the three field, 6 MV photon technique (anterior wedged, posterior wedged, and lateral), and the mixed lateral beam technique consisting of 6 MV photons and 16 MeV electrons in a 1:4 weighting. Even without bolus, the surface dose for electron beams is much higher than for photon beams. Combined with customized bolus, such as described by Kudchadker *et al.*,[98] the dose distribution can be made to be much more conformal than the traditional wedged pair, and the skin dose can be higher than for x-ray treatments. The primary advantage of electrons for this type of treatment is the finite range of the electrons, sparing tissues distal to the target volume. Often patients are treated with their head turned to the side to ensure that the treatment couch does not interfere with the electron applicator.

VIII.E.3. Prerequisites

There is no commercial software currently available for designing customized electron bolus, such as the approach of Low *et al.*[96] Without this software, it can be very tedious, but possible, to design such a bolus by trial and error in the treatment planning system. Furthermore, fabrication of the designed bolus is difficult. With appropriate software to design the bolus, commercial fabrication is available, as described by Kudchadker *et al.*[98] If advanced electron techniques such as these are desired in the clinic, users are encouraged to solicit their treatment planning vendor to implement necessary software into the planning system.

VIII.E.4. Treatment delivery

Assuming that the electron bolus can be designed and fabricated, it is possible that the electron field will be incident on the auditory canal. In that case, the auditory canal should be filled with a liquid bolus, such as warm water, to avoid hot spots of up to 173% in the middle ear, resulting from electrons scattered into the ear canal from surrounding tissues.[164] Using this bolus reduces the hot spot significantly and moves it away from the sensitive middle-ear structures.

VIII.E.5. Quality assurance

If customized electron bolus is used, the patient should be CT scanned in the treatment position with the customized electron bolus in place. This verifies that the bolus fits the patient as intended, and a dose calculation for the electron beam on this CT scan verifies the intended dose distribution. To aid in reproducing the placement of the customized bolus for each fraction, the extent of the bolus on the patient's skin surface should be marked after fitting the bolus for the second CT scan.

VIII.F. Nose

VIII.F.1. Introduction

In the past, patients with carcinoma in the nasal vestibule often received a boost using electron beams, which could be combined with photon beams to reduce the skin dose.[106] Even with widespread use of IMRT for head and neck cancers, electron beams are still useful for patients whose target volumes are restricted to depths that can be treated using electron beams.

VIII.F.2. History and description

Chobe *et al.*[106] reviewed a series of 32 patients receiving radiation therapy in the pre-CT era, 21 of which received a combination of electron beams and cobalt-60 irradiation. As mentioned above, one of the patients developed necrosis of the upper mandible, attributed to a hot spot from the electron beam. They also described how modern methods incorporating computerized treatment planning can eliminate hot spots.

VIII.F.3. Treatment planning and delivery

Computerized treatment planning with heterogeneity corrections is essential when treating volumes in the nasal region because the combination of the irregular external surface and internal heterogeneities leads to hot and cold spots that are very difficult to predict. To reduce the hot spots, bolus is also essential. To compensate for the external surface, a beeswax bolus can be built using a positive mold of the patient.[106] Another approach is to use a customized bolus designed using the algorithm of Low *et al.*,[96] as described by Kudchadker *et al.*[98] The latter approach allows shaping of the dose distribution inside the patient to match the target volume. With either approach, inserting a bolus into the nasal passages[106] may be desirable to deliver adequate dose to the nasal septum. Without the bolus, electrons are scattered into the adjacent air cavities. Traditional pencil-beam dose calculation algorithms used in most treatment planning systems can show this effect qualitatively but have been shown to underestimate the dose to the nasal septum by as much as 10% for anterior beams.[38]

VIII.F.4. Quality assurance

If bolus is fabricated, the patient should be CT scanned with the bolus in place to verify that the dose distribution with the fabricated bolus irradiates the target volume adequately. Marks on the patient can be used to facilitate reproducible placement of the bolus for each treatment fraction.

VIII.G. Eye

VIII.G.1. Eyelid and other small, superficial lesions

VIII.G.1.a. Introduction. Skin and other superficial lesions may be treated effectively with low-energy photons (superficial or orthovoltage x rays) or with low-energy (6 or 9 MeV) electrons. The surface dose of 75%–80% for these low-energy electron beams must be kept in mind if a high dose is required at the skin surface. Bolus is almost always required to achieve greater than 90% of the maximum dose at the surface. The depth of the 90% isodose on the decreasing part of the curve must be deeper than the target when the bolus is included in the treatment. Due to the dosimetric properties of small electron fields described in Sec. III G above and in TG-25, such fields may not provide adequate coverage in depth and/or lateral extent. It may be necessary to add an additional margin (at least 1 cm) around the region to be treated to ensure adequate coverage. In some instances, skin collimation can be used to sharpen the penumbra and avoid unnecessary exposure to surrounding tissues (Fig. 15). Measurements and/or a planning system verified by measurements to correctly handle small field dosimetry should be used to assure correct treatment of small skin lesions.

Another typical application is the treatment of lesions on the eyelid or the cheek. In such cases, the lowest energy electron beam is selected, usually 4–6 MeV, which covers the distal surface of the lesion with acceptable dose. It is also necessary to use shielding to eliminate any dose beyond the PTV that might cause normal tissue sequelae. Extreme caution should be used when designing and implementing "internal" shields. Off-the-shelf shields for the eye exist for low-energy photon treatments but they should not be used for electron shielding. These photons shields are not appropriate or effective in reducing the penetration of low-energy electrons (Fig. 16). Appropriate shields can be found and should be investigated dosimetrically prior to using them in the clinic.[165,166] The combination of appropriate energy and bolus may be used to pull isodoses toward the surface.

VIII.G.1.b. Quality assurance. Measurements made with high spatial resolution detection systems such as film or radiochromic media may be necessary to fully describe the dose distribution in these applications. Output measurements taking into consideration the techniques detailed in Sec. III of this report are also recommended.

A critical consideration in using high-Z materials for internal shielding is electron backscatter which increases the dose to the tissue near the shield. This effect has been discussed in the literature and can amount to a 30%–70% dose enhancement for incident electron energies of 1–20 MeV. The magnitude of the backscatter is greater for low-energy electrons and increases with increasing Z. The range of the backscattered electrons for particular radiation conditions is a key consideration. In general, the dose enhancement decreases exponentially with increasing distance from the

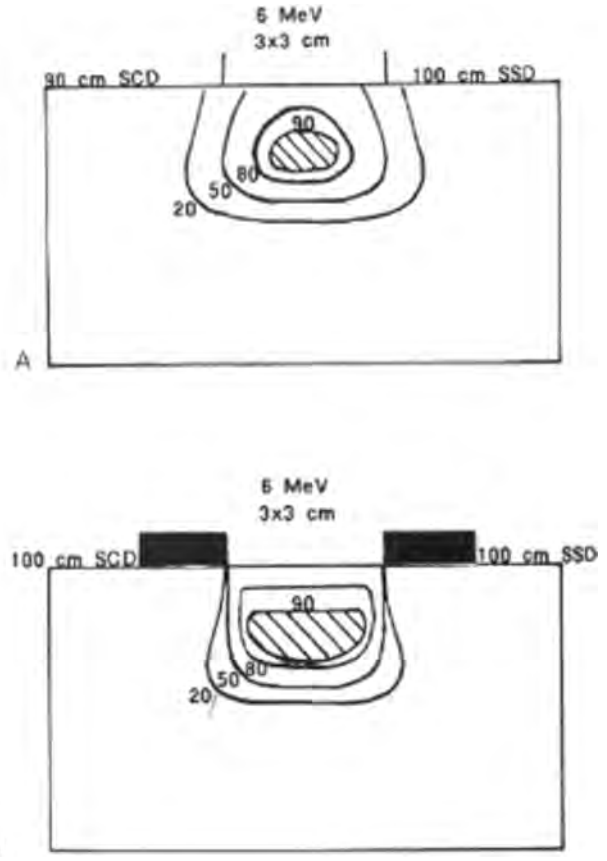

FIG. 15. Computer simulated effect of collimation location on isodose distributions of small 6 MeV electron fields in water. (a) A 3×3 cm^2 100 cm SSD field formed by an applicator insert placed 10 cm above the surface. (b) A 3×3 cm^2 field at 100 cm SSD produced by putting the shielding directly on the surface while using a 6×6 cm^2 cone insert 10 cm above the phantom surface. [From K. R. Hogstrom, Principles and Practice of Radiation Oncology. Copyright © 2004 by Lippincott, Williams and Wilkins. Reprinted by permission of Lippincott, Williams and Wilkins.]

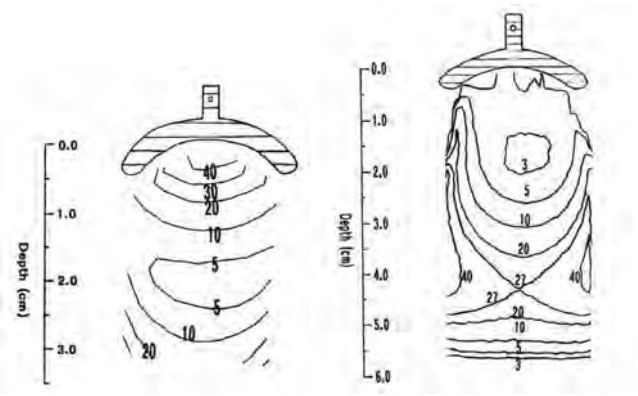

FIG. 16. Penetration of a 6 MeV electron field through a commercially available lead eye shield designed to be used with orthovoltage radiation (left diagram). Reduction in dose provided by a tungsten eye shield for a 9 MeV incident electron beam (right diagram). [Reprinted with permission from A. S. Shiu *et al.*, Int. J. Radiat. Oncol., Biol., Phys. 35, 599 (1996). Copyright 1996, American Society for Radiation Oncology.]

high-Z surface of the shield. To lower the impact of this backscatter to the patient, a low-Z material such as wax, an acrylic coating, or similar material can be added to the surface of the shield. 2–3 mm of low-Z material may be all that is required to reduce the backscatter dose from low-energy electrons, while 20–25 mm may be required for higher-energy beams ranging from 14 to 25 MeV. To keep the overall thickness of the shield to proportions that can actually be used for patients, a composite shield can be constructed of a high-Z material such as lead, topped by a lower Z material such as aluminum, then coated by an even lower Z material such as wax or acrylic. An excellent discussion of this topic along with examples for shield design can be found in the literature.[156]

VIII.G.2. Retinoblastoma

VIII.G.2.a. Introduction. Retinoblastoma is a rare cancer but is the most common primary pediatric cancer of the eye. It is most often present in very young children (<4 years of age) and the current 5 year survival is 98%.[167] About 75% of the cases are unilateral while 25% are bilateral (and usually associated with hereditary factors). In view of the young patient age and good survival, tumor control and normal tissue protection, including, if possible, preservation of vision, are of great importance. So radiation therapy of retinoblastoma shares all the technical complications of orbital treatments together with the problems involved in pediatric treatment. Typical treatment doses range from 35 to 50 Gy.

VIII.G.2.b. History. External beam radiation therapy is a primary treatment in patients with a good chance of vision preservation. A common and effective technique, which also provides lens sparing for patients with posterior disease, utilizes the D-shaped lateral single (unilateral disease) or parallel-opposed (bilateral disease) low-energy (4–6 MV) photon fields described above. In a comparison of outcomes for patients treated with the above-mentioned lateral method and those treated with combined D-shaped lateral and lens-blocked anterior photon fields, patients treated with the lens block were found to have a higher recurrence rate and no advantage in preventing cataract formation.[167,168]

VIII.G.2.c. Mixed electron-photon methods. To spare contralateral structures for patients with unilateral disease, 1/3 of the photon treatment may be replaced by a D-shaped electron beam. Three-dimensional planning is used to determine the optimum beam energy.

A more technically demanding method is described by Steenbakkers *et al.*[169] This technique employs a pair of electron beams rotated 26° medial and lateral of the axis of the optic nerve. The lens plus a 0.25 cm margin is blocked for each beam. TLD measurements in an anatomical phantom were found to agree with calculations of an in-house planning system and 9 MeV was found to deliver excellent target coverage and lens sparing for typical children up to 5 years of age. For small children, voluntary fixation of the lens is not possible. The authors suggest either daily positioning of the lens block to cover the lens of the anesthetized child or use of a suction-cup system described by Schipper[170] to immobilize the eye and thus the lens.

VIII.G.2.d. Treatment planning, delivery, and quality

assurance. The same requirements and cautions apply to the treatment of retinoblastoma as were described for the general treatment of orbital disease.

VIII.G.3. Eye or orbit treatments

VIII.G.3.a. Introduction. Radiation treatment of one or both orbits is performed for some cancers, including orbital lymphomas, rhabdomyosarcoma, and orbital metastases. Normal tissues including brain and (for unilateral disease) the contralateral eye and if possible the lacrimal gland and eyelid should be protected. Some techniques also strive to keep the lens dose below the threshold for cataract formation (2–8 Gy depending on dose fractionation and other biological variables). Lens protection is difficult if it is also necessary to deliver an approximately uniform prescription dose to the orbit, as the adult orbit is ~2.5–3.5 cm deep while the lens is 0.5–1 cm deep and ~0.8 cm in diameter.

VIII.G.3.b. History. Photon-only, electron-only, and mixed photon-electron treatments have all been implemented for the treatment of the eye or orbit. For unilateral posterior orbital tumors, a single low-energy (4 or 6 MV) D-shaped lateral photon field with a nondivergent anterior edge (half the field is blocked) is often used; for bilateral tumors, a parallel-opposed pair is used. The anterior edge is just posterior to the lens. This method is simple but cannot handle more anterior lesions and irradiates centrally located normal tissue and (for unilateral tumors) the contralateral eye.

Several methods for lens-sparing treatment of the orbits[171] or conjunctiva[172] use an AP electron beam with a central block, either alone[171,172] or in combination with a lateral photon field.[137,168] In designing these beams, the depth and diameter of the lens as well as the dimensions of the tumor must be well defined. Requesting a compliant patient to look at the block aids in immobilization of the eye which is crucial to achieving an acceptable outcome.[137,168,172] Unaccounting for eye motion has been reported to result in both cataracts and tumor recurrence.[137,168]

VIII.G.3.c. Description of electron and mixed electron-photon methods. In mixed photon-electron treatments, the photon beam is designed to compensate for the dose deficit caused by the lens block. Arthur *et al.*[137] described a technique where 6 MV photon beams, blocked at the central axis to achieve a nondivergent edge, are matched to the 50% isodose line of an AP 6 MeV electron beam. For bilateral orbital disease, the photon beams are opposed right and left laterals while for unilateral disease, the contralateral photon beam is replaced by a vertex beam, thus sparing the contralateral optic structures. Customized wax bolus is designed to provide a flat, tissue equivalent entrance surface for the electron beam and the bolus also holds the lens block. Eye position beneath the bolus is verified with a dental mirror before inserting the lens block into the hole in the bolus. To improve dose uniformity, the photon beam penumbra is broadened; a suggested method is to step the collimator defining the anterior edge of the photon beam through three positions during each treatment. The dose distribution was investigated with film dosimetry and the technique has been applied to patients. Ideally, this technique can achieve excellent dose uniformity. However, a 2 mm setup error can cause a dose variation of ±18%.

Borger *et al.*[171] used an AP electron beam with a central steel block (2 cm thick, 9 mm diameter) protecting the lens to treat the orbit. For the mixed electron-photon treatments, the posterior half of the orbit is treated with lateral photon beams and 6 MeV electrons are used for the lens-sparing AP field. The block is suspended within 1 cm of the lens and the beam is further modified by the presence of two ~1.6 mm thick plastic spoilers at 3 and 15 cm from the patient's surface. Scattering from the spoilers improves the dose distribution below the lens although there is still a dose deficit in the shadow of the lens block. Ion chamber, TLD, and film dosimetry for 17 MeV electrons were described. In these studies, the maximum dose beneath the lens block was 85% of the dose at the unblocked field d_{max} and occurred at a depth of ~4.5 cm.

For electron-only treatments in adults, medium- (12 MeV) (Ref. 172) to high-energy (17 MeV) beams[171] are needed to cover the full depth of the orbit. Rykers *et al.*[172] described using a single Cerrobend lens block of similar dimensions to treat a conjunctival lymphoma, with a 12 MeV beam. The block was glued to a thin, rigid plastic sheet within the electron insert. Since this target volume is shallow, the dose-deficit beneath the lens was not of concern.

VIII.G.3.d. Prerequisites. All the lens-sparing methods described above require excellent external immobilization of the head and patient cooperation in voluntary immobilization of the eye.[137,168,172,173] Securely mounting the lens block can provide a challenge.

VIII.G.3.e. Planning, delivery, and QA. Meticulous care in patient positioning is crucial to achieve adequate tumor coverage and lens protection. The patient's head should be well immobilized and it is recommended that a physician verify the setup for each treatment.[137,171] CT-based planning is useful in determining the best electron energy to use, but the ability of the planning system to accurately reproduce the dose distribution (depth and profiles) of the small field and the effect of the small central lens block should be verified with phantom measurements. Since bone surrounds the globe, the planning system should have a well-studied inhomogeneity correction. The output factor should also be measured unless output factor calculations by the planning system have been validated against experiment or if previously measured data for this situation do not exist.

VIII.H. Boost treatment for posterior cervical neck nodes

VIII.H.1. Introduction and purpose

Even with the advent of IMRT, electrons remain an essential component when high-dose head and neck radiotherapies are delivered with shaped, static lateral fields. After spinal cord tolerance has been reached, off-cord photons are matched to appropriate energy electrons to deliver full dose to the PTV while sparing the spinal cord. Dosimetric characteristics of these electron fields depend on the treatment

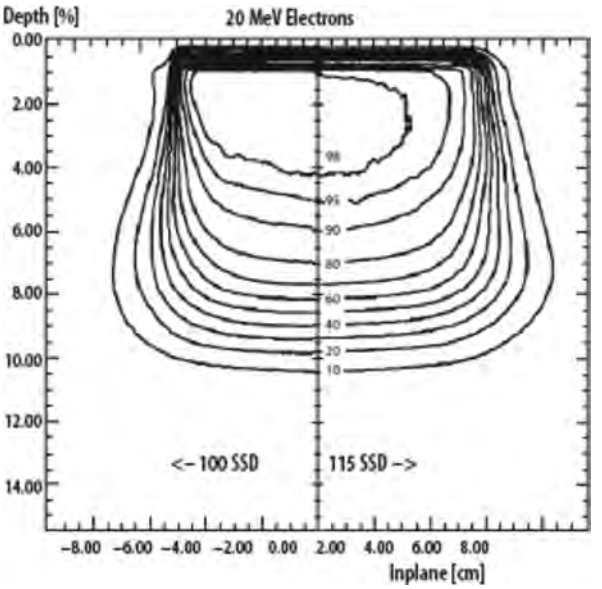

FIG. 17. Changes in electron isodose curves brought about by changing the SSD from 100 cm (left side of figures) to 115 cm (right side of figures). The isodose curve is for a 20 MeV electron beam using a 10×10 cm^2 electron cone. Isodose values represented are the 98, 95, and 90 to 10 by steps of ten isodose levels. Data are taken using Kodak XV2 film in solid water phantom and scanned using a Wellhofer WP700 system.

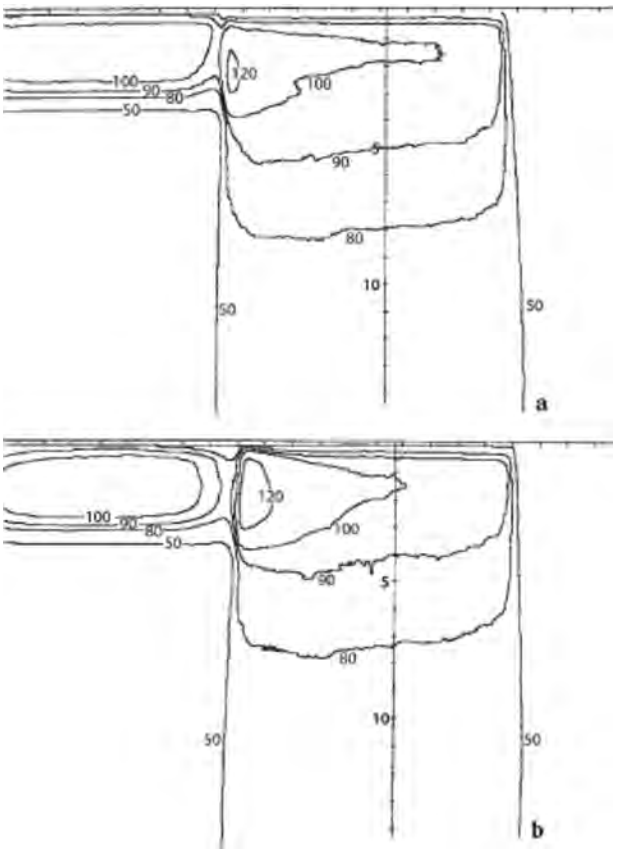

FIG. 18. Isodose curves in a plane perpendicular to the junction line between abutting photon and electron fields. 9 MeV electron beam; field size=10 $\times10$ cm^2; 6 MV photon beam; SSD=100 cm. (a) Electron beam at standard SSD of 100 cm. (b) Electron beam at extended SSD of 120 cm. [Reprinted with permission from J. M. Johnson *et al.*, Int. J. Radiat. Oncol., Biol., Phys. 28, 741 (1994). Copyright 1994, American Society for Radiation Oncology.]

geometry, SSD, and matched photon field and require special attention. In particular, treatment planning systems may not be commissioned for the conditions under which patients are being treated and care must be taken.

VIII.H.2. History and description

In non-IMRT head and neck tumor treatments, the treatment of posterior cervical nodes to a therapeutic dose represents a challenge for photon-only treatments. Historically, the additional necessary therapeutic dose has been delivered by matching electron fields to off-cord photon fields after cord tolerance has been reached in standard opposed photon fields. The electron fields are usually abutted with the edge of the lateral photon fields. The electron energy is selected on the basis of the cord depth and the distal surface of the cervical nodes.

VIII.H.3. Prerequisites

Commissioning and preparation for posterior cervical nodal boosts are essentially covered by routine commissioning tests done for blocked electron fields. Two specific additional considerations should be evaluated and documented for these fields. First, due to potential anatomical constraints, rectangular, rather than square, applicators may be used or extended SSD geometries may be required. Changes in the SSD will affect the shape of the dose distribution in a nontrivial manner and measurements in near clinical conditions should be made (Fig. 17). As shown in Fig. 18,[174] electron-photon field junctions using electrons at an extended distance can result in hot spots significantly larger than those experienced when matching fields at shorter treatment SSDs. In addition, the coverage in the electron field is also reduced because of loss of lateral electronic equilibrium at these extended distances. In any case, commissioning measurements that represent the range of clinical conditions under which patients will be treated should be made and if possible should be available in the treatment planning system.

Second, these fields in many cases are narrow and thus lateral electronic equilibrium may not be maintained. For these cases, additional commissioning measurements can be made that span the range of field widths and energies (and SSDs) expected to be used clinically. If it is not possible to enter this information directly and usably into the treatment planning system, graphs of profiles and depth doses for the clinical range of field sizes and energies should be made and be readily available.

VIII.H.4. Treatment planning and delivery

Depending on the anatomy and clinical conditions, the hot and cold areas within the match region need to be evaluated critically. To the extent possible this should be accomplished on the treatment planning system. As noted above, specific additional information is required in the planning system to properly plan and evaluate unique applicators, extended dis-

tances, and narrow field dosimetry. In some cases, and particularly where the planning system has not been explicitly commissioned for the conditions being planned (or the accuracy under these conditions is not known), it will be necessary to make phantom measurements to confirm adequate nodal coverage (and spinal cord sparing). The delivery of posterior neck node electrons requires good immobilization and localization for each patient as well as an evaluation of correct geometric field setup (SSD especially) for each treatment fraction. To keep the treatment SSD shorter, the posterior neck electron field often has to be offset from the central axis of the beam to the posterior half of the electron cone. Phantom measurements need to be done for these offset fields to ensure that cutout and air gap factors and dose profiles are accurately described by measurements taken for centered cutouts of similar dimensions. Individuals involved with these treatments should be aware of these important clinical factors that can impact dose delivery.

VIII.H.5. Quality assurance

Proper commissioning of the planning and delivery system for nodal electrons in any contemplated geometry, SSD, energy, and field size combination in the treatment planning system is the initial quality requirement. In addition, tabular and/or graphical data may also represent essential reference materials needed. Routine systematic quality assurance should be accomplished during monthly or annual planning system checks. These tests, as detailed in other reports (e.g., TG-53) should be done to include the special conditions considered for nodal electron therapy. Patient-specific quality assurance utilizing phantom measurements may be indicated in situations where the treatment plan goes beyond the conditions under which the treatment planning system is known to be accurate and where no prior measurements exist in the clinical database. Because of the effects of extended distances and narrow fields the specific conditions under which each patient is treated should be evaluated carefully. Use film dosimetry to measure the doses in the junction region and to assess the accuracy of the planning system junction doses.

VIII.I. Craniospinal irradiation using electrons

VIII.I.1. Introduction

Craniospinal irradiation is used to manage brain tumors that seed along the entire length of the cerebral spinal fluid. Medulloblastoma, malignant ependymoma, germinoma, and infratentorial glioblastoma are all candidates for this irradiation approach.[175] Commonly employed techniques treat the patient in a prone position and use right/left lateral photon beams to treat the brain in addition to a posteriorly directed photon beam to treat the spinal cord.[176,177] Replacement of the posterior photon field with a high-energy electron field can reduce greatly the exit dose to the upper thorax region, especially the heart, and the lower digestive tract. This is especially important for very young pediatric patients and results in reductions in both acute and late complications. Key challenges in the use of this technique involves matching of the right/left lateral photon fields with the posterior

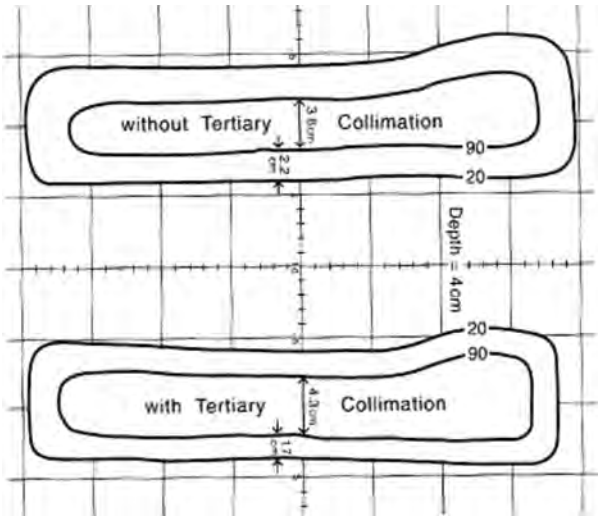

FIG. 19. Isodose curves demonstrating therapeutic and penumbra widths at the approximate deepest depth of a child's spinal cord (4 cm) 16 MeV, 120 cm SSD. Top illustration is for the field without tertiary collimation, while the bottom is with tertiary collimation in place. [Reprinted with permission from D. M. Roback *et al.*, Int. J. Radiat. Oncol., Biol., Phys. 37, 1187 (1997). Copyright 1997, American Society for Radiation Oncology.]

electron spine fields, selection of the proper electron energy to cover adequately the spinal canal all along its length, and the production of a posterior electron field of adequate length to treat the entire involved region.

VIII.I.2. History

Techniques have been published addressing these concerns with consequent solutions to the above stated problems.[175,178,179] The first two techniques using high-energy electrons employ conventional treatment distances for the posterior spine field of 110 and 115 cm SSDs and use two adjacent electron fields if one field is not adequate. The technique of Roback *et al.* for the production of a larger posterior electron field uses an extended SSD of approximately 120 cm. Special considerations in the application of this technique hinge on the change in the isodose distributions exhibited at the extended SSD. Figure 19 shows the difference in the sharpness of the electron field both with and without tertiary collimation at the depth of 4. This approach can be extended to larger treatment distances (140 cm SSD) provided that adequate dosimetry is performed at this distance. The adequacy of the user's planning system to handle complex spinal geometry can be an issue.[116] However, a recent study comparing TLD measurements in a pediatric (5-year-old) anatomic phantom with calculations of a pencil-beam-based commercial system showed moderately good agreement.[180]

VIII.I.3. Treatment setup and delivery

Figure 20 shows the basic field arrangement for the M.D. Anderson technique.[175] The lateral photon fields are rotated through an angle Θ to match the divergence of the posterior electron field. The central axis of the photon beams is placed

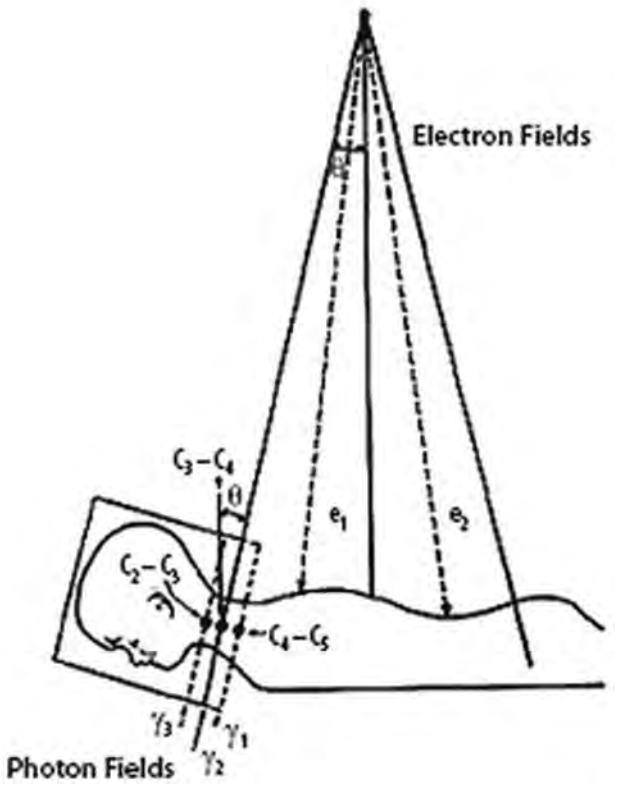

FIG. 20. Prone craniospinal field arrangement showing the orientation of the right/left lateral photon fields with respect to the posterior electron fields. Two electron fields are illustrated above to cover the entire spine of a larger patient. Some patients may be small enough such that one posterior electron field covers adequately the entire spine. The lateral photon fields are rotated through an angle θ to match the divergence of the posterior electron field. The superior field edge of electron field $e1$ is not moved during the treatment but the inferior border of the photon fields is shifted 9 mm to feather the junction location (positions $y1$, $y2$, and $y3$). The central axis of the photon beams is placed as close to the junction region as possible to eliminate divergence in the superior-inferior direction. [From K. R. Hogstrom, Principles and Practice of Radiation Oncology. Copyright © 2004 by Lippincott, Williams and Wilkins. Reprinted by permission of Lippincott, Williams and Wilkins.]

as close to the junction region as possible to eliminate divergence in the superior-inferior direction. The superior field edge of electron field e_1 is not moved during the treatment but the inferior border of the photon fields is shifted 9 mm to feather the junction location (positions y_1, y_2, and y_3). To achieve the most uniform dose per fraction in the region of the junction, one-third of the photon treatments are delivered with the inferior border of the two photon fields coincident with the electron field edge. The next one-third of the photon treatments are delivered with the edge of one photon field moved 9 mm superior to the electron field edge and the edge of the second photon field moved 9 mm inferiorly to the electron field edge. The final one-third of the photon treatments are delivered with the edges of the photon fields reversed from their previous position.

The overall length of the cord to be treated often exceeds the field size that can be covered using a 25×25 cm^2 cone at either 110 or 115 cm SSD. A small increase in overall field size can be accomplished by rotating the collimator 45° to produce a field size of approximately 30–35 cm in length. If the entire length of the cord cannot be covered in one electron field, then a second posterior field must be abutted to the inferior border of the first electron field. The addition of this second field requires that the couch be rotated 90° and that the angle of the two electron fields be rotated by an angle Θ (Fig. 20) to account for the divergence of each of these electron fields and to produce a common field edge.[175]

A simulation of the patient is done to establish the treatment position and to properly place the photon and electron fields and to provide documentation for subsequent patient treatment. A lateral radiograph is taken to define the depth of the cord along its entire length and to show the changes in the SSD along the length of the cord. A computerized treatment plan of this sagittal plane can be done easily using this information.

The electron energy is selected so that the 90% isodose surface covers the target to be treated. The energy should be selected such that the 90% isodose should exceed the maximum depth of the cord by 7 mm: 4 mm to account for the increased absorption of bone and 3 mm for a margin of error to ensure coverage of the target. If the depth of the spinal cord or the SSD to the patient skin surface varies significantly, then bolus can be added to the spinal cord to conform to the 90% isodose surface to the anterior border of the cord. With modern 3D-treatment planning computers, the overall plan can be calculated before treatment is begun. For the method described by Maor *et al.*[175] the dose in the junction region reaches a maximum of 36–37 Gy and a minimum of 27 Gy when 30 Gy is given to the posterior electron field, 30 Gy to the whole brain, plus 20 Gy to a posterior-fossa boost. Roback *et al.*[179] found that tertiary collimation reduces the hot spot at the junction from 115% to 105% with zero skin gap in the example cited.

VIII.I.4. Quality assurance

The capabilities of the treatment planning system in this setting should be well understood. Since this technique involves very complex arrangements of both photon and electrons fields, some at extended treatment distances, it is essential that both the staff physician and physicist are present at the first treatment. They are to ensure that all aspects of the treatment are performed as expected and to ensure that the therapist staff is fully aware of all of the intricacies associated with the treatment. In addition, all documentation in the treatment chart, whether paper or electronic, should be reviewed to ensure that it describes adequately the treatment to be performed. If the posterior field is treated using an electron field at an extended treatment distance, then tertiary blocking is required to reduce the width of the penumbra.[179] Since this field involves both an extended treatment distance and tertiary blocking, a special calibration of the output should be performed. If a special calibration was performed for the posterior electron field, *in vivo* dosimetry using either diodes or TLD should also be performed. This is because these fields are used predominantly for pediatric patients and the posterior spine of the patient is curved when the patient is

prone as compared to the calibration situation which uses a flat phantom.

VIII.J. Intraoperative radiation therapy

VIII.J.1. Introduction and purpose

The use of electrons to deliver a high dose to the tumor bed immediately following surgical resection remains an effective radiation therapy treatment option. This is particularly true for gastrointestinal and gynecological cancers. In these cases large doses of electrons can be delivered to the tumor bed in a geometry that maximizes tumor doses and also maximizes the sparing of normal tissues through the use of distance and temporary shielding.

VIII.J.2. History and description

The physical aspects of intraoperative electron procedures have been initially detailed by AAPM TG-48.[181] The initial report was dedicated to the use of a stationary (conventional linac-based) process. The ability to deliver intraoperative electron therapy has seen a revival and improvement to access with the development of mobile, specialized electron treatment machines. Thus, a recent document (TG-72) provides an update to TG-48 and a thorough description of the specific physical issues involved in the application of mobile electron intraoperative electron machines.[182]

VIII.J.3. Prerequisites

Whether using conventional linear accelerators modified for electron intraoperative treatment or a mobile machine, extensive commissioning is required due to the custom, small field applicators and short distances to the treatment target that are involved. In particular, understanding dose distributions under the unique scatter conditions with intraoperative cones with varying end shapes, distances, energies, and shieldings is essential and requires a significant investment in time to perform these special measurements.

Typically, commissioning will include measurement and graphical/tabular organization of beam profiles at multiple depths, leakage profiles (outside of cones), applicator output factors, air gap factors, and absolute calibration using TG-51. Since the patient is under anesthesia, the process needs to be as efficient as possible without sacrificing quality. To this end, isodose tables and graphs for each applicator and energy combination should be produced and be readily available, as well as output factors for each possible clinical condition.

It should be understood that commissioning for a mobile intraoperative radiation therapy (IORT) machine may differ from that for stationary conventional machines due to mobility, dose rate, and mechanical differences. These are detailed in AAPM TG-72.[182]

VIII.J.4. Treatment planning and delivery

As noted in TG-48 (Ref. 181) and TG-72,[182] dose prescription and specification are done in the operating room. While a standard prescription method is not defined, TG-72 recommends specifying the dose at the 90% isodose and reporting the 90% dose and the d_{max} dose. Thorough and well organized tabular and graphical data are referred to by the treatment team as prepared in commissioning. ICRU Report 71 also provides direction for the special electron beam technique of IORT. The CTV is defined as accurately as possible by both the surgeon and the radiation oncologist during the procedure. All devices specific to IORT need to be reported such as the IORT applicator system including type, shape, bevel angle, and size of the applicator. The ICRU reference point for reporting is always selected in the center or central part of the PTV and, when possible, at the level of the maximum dose on the beam axis.

The ICRU recommended that the following dose values be reported for IORT:[103]

- "peak absorbed dose to water, in reference conditions, for each individual beam (if the beam axis is perpendicular to the tissue surface);
- for oblique beam axis, the maximum absorbed dose in water on the "clinical axis" (i.e., the axis perpendicular to the surface of the tissues, at the point of intersection of the central axis of the beam with the tissue surface);
- location of, and dose value at the ICRU Reference Point (if different from above);
- best estimate of the maximum and minimum dose to the PTV. Usually the irradiation conditions (electron energy, field size, etc.) are selected so that at least 90 percent of the dose at the ICRU Reference Point is expected to be delivered to the entire PTV."[103]

The Radiation Therapy Oncology Group (RTOG) has traditionally specified that the 90% isodose line is to cover the target volume for IORT. ICRU Report 35 recommends that the dose be prescribed at d_{max}. Taking these two recommendations into account, TG-48 of the AAPM recommended that the dose be prescribed at d_{max} and both the 90% dose and the maximum dose be reported.[181] Observing that most groups performing IORT prescribe to the 90% isodose line, TG-72 recommends that the dose be prescribed at the 90% isodose level and that the dose be reported at both the 90% level and at d_{max}.[182] This task group stresses that prescribing dose and reporting dose are two completely different functions and recommends the approach taken by TG-72. Specifically for IORT, the dose should be prescribed at the 90% isodose level and the dose should be reported at both the 90% level and at d_{max}.

VIII.J.5. Quality assurance

Quality assurance should follow TG-40 (or current AAPM standards) and as usual sample a variety of essential data and characteristics acquired at acceptance and commissioning. These are well documented in TG-72 and TG-48 and include output constancy, depth dose, flatness and symmetry, applicator output ratios, output versus gantry angle, monitor chamber linearity, and docking mechanism. Additional (and sometimes more frequent) tests may be required for mobile units to verify calibration and geometric stability.[182]

VIII.K. Total skin electron therapy

VIII.K.1. Introduction and purpose

TSET continues to be used for treating large areas (whole body, hemibody) of very superficial diseases of the skin, such as cutaneous T-cell lymphomas (mycosis fungoides). The aim is to irradiate the total skin surface as homogeneously as possible. For patients with superficial disease, TSET can be delivered with one electron energy. In other clinical situations, the thickness of the skin disease may vary with stage, pathology, and location on the body surface. For such cases, several CTVs need to be identified and different beam penetrations have to be used. For each anatomical site, an ICRU reference point for reporting at or near the center of the PTVs/CTVs should be selected. The reference point may be at the level of the peak dose if it is located in the central part of the PTV. In addition, an ICRU reference point, clinically relevant and located within the PTV, can be selected for the whole PTV.

For TSET treatments, reporting of the following dose values are recommended:

- "peak absorbed dose in water for each individual electron beam;
- location of, and dose value at the ICRU Reference Point for each anatomical area (the ICRU Reference Point may or may not be at the level of the peak dose);
- best estimate of maximum and minimum dose to each anatomical area;
- location and absorbed dose at the ICRU point for the whole PTV, and best estimate of the maximum and minimum dose for the whole PTV;
- any other dose value considered as clinically significant."[103]

VIII.K.2. History and description

These techniques, although largely unchanged from the original Stanford technique,[183–193] continue to evolve.[194] Excellent discussions of the steps to consider in this technique can be found in task group reports and textbooks.[156,192,195]

VIII.K.3. Prerequisites

Commissioning for TSET requires the development of a treatment field of adequate size along with measurements of beam characteristics in the treatment position from the combination of fields used to treat the patient. The treatment machine is utilized without standard applicators at a much extended distance to accommodate the large field size necessary. The use of beam spoilers is also common both to degrade the energy of the beam and to help make the dose more uniform around the periphery of the patient. Since much of the dose comes from scattered electrons, both from the spoiler and from outside of the (light field defined) field, dosimetric validation must be performed at multiple points within the useful beam. Techniques continue to be developed to improve the resolution and efficiency of dosimetric measurements for large field electron treatments.[78,79]

Specialized hardware is required for TSET. A suitable treatment stand is used to elevate the patient off of the floor, which can absorb electrons and reduce the dose to the inferior portion of the body. The treatment stand can also be a suitable place to mount a beam spoiler, which is useful for improving the dose uniformity. It may also be necessary to add an energy degrader or additional scattering material on the linear accelerator treatment head. Other investigators described how to design an appropriate beam geometry for TSET.[196]

VIII.K.4. Treatment planning and delivery

Computerized treatment planning is not done for TSET. In general, patients are treated at a constant, large SSD, and the dose rate at the skin surface is almost the same for each patient. Variations in dose delivery can occur because of patient size and their ability (or lack thereof) to be able to maintain an appropriate treatment position. With appropriate TSET beam design, dose delivery can be quite uniform (better than $\pm 20\%$ for most points), although dose deficits usually exist for the axilliary folds, perineum, and soles of the feet. *In vivo* dosimetry is usually used to determine the dose deficits for a given patient since the deficits vary depending on the patient height, weight, and ability to be positioned appropriately.[197]

VIII.K.5. Quality assurance

Delivery of a uniform dose for TSET requires that the TSET beam properties well control both the dose output and beam profile. The former can be accomplished through a simplified setup, e.g., with a lateral gantry setting to perform routine constancy with an appropriate dosimeter and phantom. Cylindrical ion chambers are not suitable for calibration of low-energy electron beams; therefore, it is recommended that a small-volume parallel plate ionization chamber be used to determine the dose output of the TSET beam. AAPM Report 23 dealing with total skin electron therapy technique and dosimetry should be followed when commissioning this technique for clinical use.[192] Appropriate ADCL calibration of the ion chamber or cross calibration versus another ADCL-calibrated ion chamber in a high-energy electron beam is recommended. Of critical importance is the fact that cable effects can be significant when performing total skin electron calibrations at large treatment distances where a large amount of the chamber's cable could be irradiated. The polarity effect, which is usually less than $\pm 2\%$ at 100 SSD, can easily differ by more than $\pm 5\%$ at large SSDs under large field conditions. As such, great effort needs to be taken to either shield the cable from the electron beam or otherwise reduce the amount of cabling exposed to radiation.[198] Ongoing quality assurance may be accomplished through a simplified setup, e.g., with a lateral gantry setting to perform routine constancy with an appropriate dosimeter and phantom. A large volume ion chamber can be useful for daily constancy checks, since polarity effects are greatly reduced.

As mentioned above, patient positioning is critical to ensure that a uniform dose is delivered. Therefore, *in vivo* do-

simetry is a routine procedure for many institutions that provide TSET therapy. Weaver *et al.*[199] and Antolak *et al.*[197] described their use of *in vivo* TLD for ongoing quality assurance of TSET. The latter is particularly useful because they tabulated dosimetric data for a large series of patients treated using similar TSET techniques on two different linear accelerators. Comparison of *in vivo* dosimetry to these data is useful to ensure consistent TSET delivery.

VIII.L. Total limb irradiation

VIII.L.1. Clinical applications

Total limb irradiation can be useful in management of superficial cancers of the limbs, which include melanoma, lymphoma, and Kaposi's sarcoma.

VIII.L.2. Overview of technique

The target volume is typically the superficial tissues lying at a depth of 2 cm or less around the circumference of the limb. Parallel-opposed x-ray beams would needlessly irradiate bone and serial or spiral tomotherapy, although a potential alternative has yet to be proven useful for this treatment. Such treatment would likely require having a reproducible immobilization system and daily image-guided verification. Also, bolus would likely be required, and x-ray treatment planning systems must accurately calculate superficial dose. An alternate solution is electron total limb irradiation, which applies the principles of total skin electron irradiation technique. This technique has been discussed by Wooden *et al.* who applied it to irradiating the lower calf of a patient with Kaposi's sarcoma.[200]

VIII.L.3. Prerequisites for treatment planning and delivery

This technique can be delivered using a standard electron therapy machine. Thin lead sheets might be required for skin collimation, and thin flexible bolus is sometimes used to control the depth of penetration. Occasionally, custom immobilization devices might be required. In treating the arm, a custom holder that orients, immobilizes, and extends the arm perpendicular to the couch is useful (Fig. 21).

VIII.L.4. Treatment planning

Similar to total skin irradiation, the treatment technique uses six to eight equally spaced, low-energy (5–9 MeV) beams around the circumference of the extremity. Each beam will have sufficient falloff so that the portion of the limb receiving treatment lies completely inside the penumbra of each beam. The beams are delivered iso-SSD, meaning that the same SSD is selected for each beam and the central axes of all beams intersect at a common point. Figure 22, which illustrates the dose distribution using 5 MeV electrons for a 9 cm diameter water cylinder simulating the calf, has three significant characteristics. First, 90% of the given dose penetrates 8–10 mm, reduced from the value of 15 mm for a single beam incident normally on a flat surface. Second, the surface dose has increased to 90% or greater of average maximum dose compared with approximately 70% of given dose for a single beam incident normally on a flat surface. Both of these effects are characteristics of grazing radiation[1,201] when applied to treat a cylindrical geometry with broad beams.[202] Third, the average maximum dose along each radius is approximately 2.55 times the given dose of each of the six fields for the linac in this study and 5 MeV electrons.[200] Hence, the monitor units (U) for each of the six single fields to deliver the prescription dose ($D_{\text{prescribed}}$) to the $X\%$ isodose contour can be given by

FIG. 21. Patient in treatment position for total arm irradiation. The setup aid allows the arm to be positioned such that it is fully extended in a reproducible dorsal position. The angle of the arm is adjusted to be elevated from horizontal to allow gantry clearance for the beam 60° inferior to the 0° gantry angle.

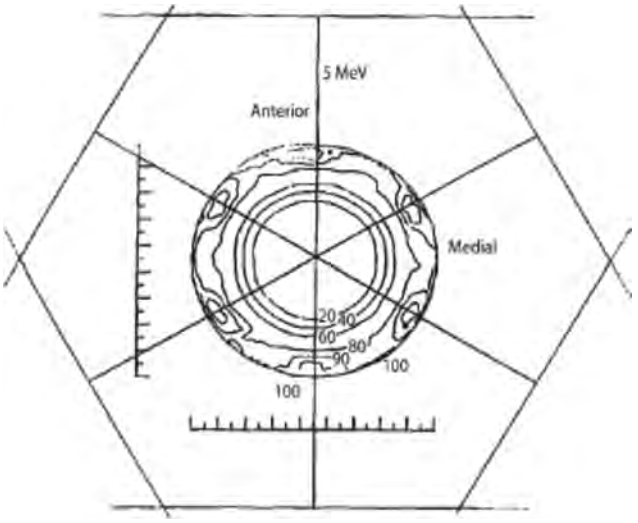

FIG. 22. Dose distribution for total limb irradiation. Six equally spaced 17 cm wide, 5 MeV electron beams are used to irradiate a 9 cm diameter cylinder. 100% equals 2.55 times the given dose from a single field. [Reprinted with permission from K. K. Wooden *et al.*, Med. Dosim. 21, 211 (1996). Copyright 1996, American Association of Medical Dosimetrists.]

$$U = \frac{D_{\text{prescribed}}/X\%}{2.55 \times (D/U)_s}, \tag{20}$$

where $(D/U)_s$ is the absorbed dose per monitor unit for the single, 105 cm SSD, 17×31 cm^2, 5 MeV electron beam incident on a flat water phantom. It must be stressed that the factor of 2.55 in Eq. (20) is only applicable to the linac, accessories, and beam energy associated with the quoted study[200] and can differ significantly from this value. This factor must be measured for each particular radiation situation with the accessories that are to be used and a phantom whose cylindrical size approximates the limb to be treated. It is recommended that a 3D or multiplanar 2D dose plan be generated using a treatment planning computer that uses a pencil-beam dose algorithm or one of equal or greater dose accuracy. The patient anatomy can be acquired by a CT, although it might not be possible to acquire the scan in the treatment position. In some cases, multiple manual contours might be acceptable. There can be slight differences in the dose distributions due to differences in patient diameter, which typically decrease near the end of the limb. The acceptability of the dose distribution resulting from such variations should be evaluated.

VIII.L.5. Treatment delivery

One of the challenges of this technique is patient setup and immobilization. Half of the fields are delivered with the patient in the prone position and half in the supine position. In some cases, it might be necessary to deviate slightly from six or eight equally spaced beams in order to avoid collision of the gantry with the patient or the table. In such cases beam weights can be adjusted to give the most uniform dose. In other cases, the length of the limb to be irradiated usually exceeds the maximum length of the treatment field, so two sets of fields can be abutted. Skin collimation is useful at the end of the treatment volume to protect normal tissue. This is usually required to protect the lower abdomen when treating the thigh.

VIII.L.6. Quality assurance

It is recommended that treatment aims be verified early in the treatment by measuring surface dose around the circumference of the limb using TLD or another appropriate dosimeter.

[a]Author to whom correspondence should be addressed. Electronic mail: gerbi001@umn.edu. Telephone: (612)-626-6154; Fax: (612)-626-7060.

[1]F. M. Khan, K. P. Doppke, K. R. Hogstrom, G. J. Kutcher, R. Nath, S. C. Prasad, J. A. Purdy, M. Rozenfeld, and B. L. Werner, "Clinical electron-beam dosimetry: Report of AAPM Radiation Therapy Committee Task Group No. 25," Med. Phys. **18**, 73–109 (1991).
[2]P. R. Almond, P. J. Biggs, B. M. Coursey, W. F. Hanson, M. S. Huq, R. Nath, and D. W. O. Rogers, "AAPM's TG-51 protocol for clinical reference dosimetry of high-energy photon and electron beams," Med. Phys. **26**, 1847–1870 (1999).
[3]International Commission on Radiation Units and Measurements Report No. 35, "Radiation dosimetry: electron beams with energies between 1 and 50 MeV," 1984.
[4]G. X. Ding, D. W. Rogers, and T. R. Mackie, "Calculation of stopping-power ratios using realistic clinical electron beams," Med. Phys. **22**, 489–501 (1995).
[5]G. X. Ding and D. W. Rogers, "Mean energy, energy-range relationships and depth-scaling factors for clinical electron beams," Med. Phys. **23**, 361–376 (1996).
[6]M. S. Huq, N. Yue, and N. Suntharalingam, "Experimental determination of fluence correction factors at depths beyond dmax for a Farmer type cylindrical ionization chamber in clinical electron beams," Med. Phys. **24**, 1609–1613 (1997).
[7]AAPM TG-21, "A protocol for the determination of absorbed dose from high-energy photon and electron beams," Med. Phys. **10**, 741–771 (1983).
[8]P. R. Almond, F. H. Attix, L. J. Humphries, H. Kubo, R. Nath, S. Goetsch, and D. W. O. Rogers, "The calibration and use of plane-parallel ionization chambers for dosimetry of electron beams: An extension of the 1983 AAPM protocol report of AAPM Radiation Therapy Committee Task Group No. 39," Med. Phys. **21**, 1251–1260 (1994).
[9]B. J. Gerbi and F. M. Khan, "The polarity effect for commercially available plane-parallel ionization chambers," Med. Phys. **14**, 210–215 (1987).
[10]S. Pai, I. J. Das, J. F. Dempsey, K. L. Lam, T. J. Losasso, A. J. Olch, J. R. Palta, L. E. Reinstein, D. Ritt, and E. E. Wilcox, "TG-69: Radiographic film for megavoltage beam dosimetry," Med. Phys. **34**, 2228–2258 (2007).
[11]V. M. Tello, R. C. Tailor, and W. F. Hanson, "How water equivalent are water-equivalent solid materials for output calibration of photon and electron beams?," Med. Phys. **22**, 1177–1189 (1995).
[12]D. I. Thwaites, A. R. DuSautoy, T. Jordan, M. R. McEwen, A. Nisbet, A. E. Nahum, and W. G. Pitchford, "The IPEM code of practice for electron dosimetry for radiotherapy beams of initial energy from 4 to 25 MeV based on an absorbed dose to water calibration," Phys. Med. Biol. **48**, 2929–2970 (2003).
[13]S. Agostinelli, S. Garelli, M. Piergentili, and F. Foppiano, "Response to high-energy photons of PTW31014 PinPoint ion chamber with a central aluminum electrode," Med. Phys. **35**, 3293–3301 (2008).
[14]R. C. Tailor, C. Chu, D. S. Followill, and W. F. Hanson, "Equilibration of air temperature inside the thimble of a Farmer-type ion chamber," Med. Phys. **25**, 496–502 (1998).
[15]K. A. Johansson, L. O. Mattsson, L. Lindborg, and H. Svensson, *National and International Standardization of Radiation Dosimetry* (IAEA, Vienna, 1978), Vol. 2, pp. 243–270.
[16]L. A. Buckley and D. W. Rogers, "Wall correction factors, Pwall, for parallel-plate ionization chambers," Med. Phys. **33**, 1788–1796 (2006).
[17]D. W. O. Rogers, in *Advances in Radiation Oncology Physics*, edited by J. A. Purdy (American Institute of Physics, New York, 1992), p. 181.
[18]D. W. Rogers, "A new approach to electron-beam reference dosimetry," Med. Phys. **25**, 310–320 (1998).
[19]D. Harder, "Einfluss der Vielfachstreuung von Elektronen auf die Ionisation in gasgefüllten Hohlräumen," Biophysik **5**, 157–164 (1968).
[20]IAEA, *Technical Report Series* (IAEA, Vienna, 1996).
[21]D. W. O. Rogers, in *Teletherapy: Present and Future*, edited by J. Palta and T. R. Mackie (Advanced Medical, Madison, 1996), p. 319.
[22]J. M. Fernandez-Varea, P. Andreo, and T. Tabata, "Detour factors in water and plastic phantoms and their use for range and depth scaling in electron-beam dosimetry," Phys. Med. Biol. **41**, 1119–1139 (1996).
[23]J. Antolak, "SU-FF-T-205: Ionization to dose for electron beams: A comparison of three approaches," Med. Phys. **32**, 1997–1997 (2005).
[24]D. T. Burns, G. X. Ding, and D. W. Rogers, "R_{50} as a beam quality specifier for selecting stopping-power ratios and reference depths for electron dosimetry," Med. Phys. **23**, 383–388 (1996).
[25]D. W. Rogers, "Accuracy of the Burns equation for stopping-power ratio as a function of depth and R50," Med. Phys. **31**, 2961–2963 (2004).
[26]L. L. Wang and D. W. Rogers, "Calculation of the replacement correction factors for ion chambers in megavoltage beams by Monte Carlo simulation," Med. Phys. **35**, 1747–1755 (2008).
[27]G. Rikner, "Characteristics of a p-Si detector in high energy electron fields," Acta Oncol. **24**, 71–74 (1985).
[28]R. K. Ten Haken, B. A. Fraass, and R. J. Jost, "Practical methods of electron depth-dose measurement compared to use of the NACP design chamber in water," Med. Phys. **14**, 1060–1066 (1987).
[29]K. Derikum and M. Roos, "Determination of radiation quality parameters for high energy photons and electrons using different types of detectors," in *Proceedings of Symposium on Measurement Assurance in Dosimetry* (IAEA, Vienna, 1994) pp. 323–331.
[30]C. McKerracher and D. I. Thwaites, "Notes on the construction of solid-state detectors," Radiother. Oncol. **79**, 348–351 (2006).

[31]I. J. Das, C. W. Cheng, R. J. Watts, A. Ahnesjo, J. Gibbons, X. A. Li, J. Lowenstein, R. K. Mitra, W. E. Simon, and T. C. Zhu, "Accelerator beam data commissioning equipment and procedures: report of the TG-106 of the Therapy Physics Committee of the AAPM," Med. Phys. **35**, 4186–4215 (2008).
[32]D. E. Mellenberg, R. A. Dahl, and C. R. Blackwell, "Acceptance testing of an automated scanning water phantom," Med. Phys. **17**, 311–314 (1990).
[33]G. G. Zhang, D. W. O. Rogers, J. E. Cygler, and T. R. Mackie, "Effects of changes in stopping-power ratios with field size on electron beam relative output factors," Med. Phys. **25**, 1711–1716 (1998).
[34]G. G. Zhang, D. W. O. Rogers, J. E. Cygler, and T. R. Mackie, "Monte Carlo investigation of electron beam output factors versus size of square cutout," Med. Phys. **26**, 743–750 (1999).
[35]I. J. Das, K. P. McGee, and C. W. Cheng, "Electron-beam characteristics at extended treatment distances," Med. Phys. **22**, 1667–1674 (1995).
[36]C. B. Saw, K. M. Ayyangar, T. Pawlicki, and L. J. Korb, "Dose distribution considerations of medium energy electron beams at extended source-to-surface distance," Int. J. Radiat. Oncol., Biol., Phys. **32**, 159–164 (1995).
[37]J. Cygler, X. A. Li, G. X. Ding, and E. Lawrence, "Practical approach to electron beam dosimetry at extended SSD," Phys. Med. Biol. **42**, 1505–1514 (1997).
[38]K. R. Hogstrom, M. D. Mills, J. A. Meyer, J. R. Palta, D. E. Mellenberg, R. T. Meoz, and R. S. Fields, "Dosimetric evaluation of a pencil-beam algorithm for electrons employing a two-dimensional heterogeneity correction," Int. J. Radiat. Oncol., Biol., Phys. **10**, 561–569 (1984).
[39]M. D. Mills, K. R. Hogstrom, and R. S. Fields, "Determination of electron beam output factors for a 20-MeV linear accelerator," Med. Phys. **12**, 473–476 (1985).
[40]D. Jones, P. Andre, J. T. Washington, and M. D. Hafermann, "A method for the assessment of the output of irregularly shaped electron fields," Br. J. Radiol. **63**, 59–64 (1990).
[41]P. A. Jursinic and R. Mueller, "A sector-integration method for calculating the output factors of irregularly shaped electron fields," Med. Phys. **24**, 1765–1769 (1997).
[42]F. M. Khan, P. D. Higgins, B. J. Gerbi, F. C. Deibel, A. Sethi, and D. N. Mihailidis, "Calculation of depth dose and dose per monitor unit for irregularly shaped electron fields," Phys. Med. Biol. **43**, 2741–2754 (1998).
[43]F. M. Khan and P. D. Higgins, "Calculation of depth dose and dose per monitor unit for irregularly shaped electron fields: An addendum," Phys. Med. Biol. **44**, N77–N80 (1999).
[44]K. R. Hogstrom, R. E. Steadham, P. F. Wong, and A. S. Shiu, in *Monitor Unit Calculations for External Photon and Electron Beams*, edited by J. P. Gibbons (Advanced Medical, Middleton, 2000), pp. 113–125.
[45]F. M. Khan and P. D. Higgins, "Field equivalence for clinical electron beams," Phys. Med. Biol. **46**, N9–N14 (2001).
[46]P. D. Higgins, B. J. Gerbi, and F. M. Khan, "Application of measured pencil beam parameters for electron beam model evaluation," Med. Phys. **30**, 514–520 (2003).
[47]K. R. Hogstrom, M. D. Mills, and P. R. Almond, "Electron beam dose calculations," Phys. Med. Biol. **26**, 445–459 (1981).
[48]M. D. Mills, K. R. Hogstrom, and P. R. Almond, "Prediction of electron beam output factors," Med. Phys. **9**, 60–68 (1982).
[49]A. Dutreix and E. Broit, in *The Computation of Dose Distributions in Electron Beams*, edited by A. E. Nahum (University of Umea, Umea, Sweden, 1990), pp. 242–270.
[50]I. A. Bruinvis, A. Van Amstel, A. J. Elevelt, and R. Van der Laarse, "Calculation of electron beam dose distributions for arbitrarily shaped fields," Phys. Med. Biol. **28**, 667–683 (1983).
[51]B. J. McParland, "A parameterization of the electron beam output factors of a 25-MeV linear accelerator," Med. Phys. **14**, 665–669 (1987).
[52]I. A. Bruinvis and W. A. Mathol, "Calculation of electron beam depth-dose curves and output factors for arbitrary field shapes," Radiother. Oncol. **11**, 395–404 (1988).
[53]B. J. McParland, "A method of calculating the output factors of arbitrarily shaped electron fields," Med. Phys. **16**, 88–93 (1989).
[54]R. K. Wu, W. Wang, and A. M. El-Mahdi, "Irregular field output factors for electron beams," in *Proceedings of the Ninth International Conference on the Use of Computers in Radiation Therapy*, edited by I. A. D. Bruinvis *et al.* (Scheveningen, Sweden, 1987), pp. 453–456.
[55]F. Verhaegen, C. Mubata, J. Pettingell, A. M. Bidmead, I. Rosenberg, D. Mockridge, and A. E. Nahum, "Monte Carlo calculation of output factors for circular, rectangular, and square fields of electron accelerators (6–20 MeV)," Med. Phys. **28**, 938–949 (2001).
[56]J. E. Cygler, G. M. Daskalov, G. H. Chan, and G. X. Ding, "Evaluation of the first commercial Monte Carlo dose calculation engine for electron beam treatment planning," Med. Phys. **31**, 142–153 (2004).
[57]D. I. Thwaites, D. T. Burns, S. C. Klevenhagen, A. E. Nahum, and W. G. Pitchford, "The IPEMB code of practice for electron dosimetry for radiotherapy beams of initial energy from 2 to 50 MeV based on an air kerma calibration," Phys. Med. Biol. **41**, 2557–2603 (1996).
[58]D. M. Galbraith, J. A. Rawlinson, and P. Munro, "Dose errors due to charge storage in electron irradiated plastic phantoms," Med. Phys. **11**, 197–203 (1984).
[59]L. O. Mattsson and H. Svensson, "Charge build-up effects in insulating phantom materials," Acta Radiol. Oncol. **23**, 393–399 (1984).
[60]D. I. Thwaites, "Charge storage effect on dose in insulating phantoms irradiated with electrons," Phys. Med. Biol. **29**, 1153–1156 (1984).
[61]W. G. Pitchford, "The HPA photon protocol and proposed electron protocol," Radiother. Oncol. **4**, 297–299 (1985).
[62]B. Thomadsen, C. Constantinou, and A. Ho, "Evaluation of water-equivalent plastics as phantom material for electron-beam dosimetry," Med. Phys. **22**, 291–296 (1995).
[63]A. Nisbet and D. I. Thwaites, "An evaluation of epoxy resin phantom materials for electron dosimetry," Phys. Med. Biol. **43**, 1523–1528 (1998).
[64]B. Nilsson, A. Montelius, P. Andreo, and J. Johansson, "Correction factors for parallel-plate chambers used in plastic phantoms in electron dosimetry," Phys. Med. Biol. **42**, 2101–2118 (1997).
[65]M. R. McEwen and D. Niven, "Characterization of the phantom material virtual water in high-energy photon and electron beams," Med. Phys. **33**, 876–887 (2006).
[66]G. X. Ding, D. W. O. Rogers, J. E. Cygler, and T. R. Mackie, "Electron fluence correction factors for conversion of dose in plastic to dose in water," Med. Phys. **24**, 161–176 (1997).
[67]E. A. Siegbahn, B. Nilsson, J. M. Fernandez-Varea, and P. Andreo, "Calculations of electron fluence correction factors using the Monte Carlo code PENELOPE," Phys. Med. Biol. **48**, 1263–1275 (2003).
[68]J. Dutreix and A. Dutreix, "Film dosimetry of high-energy electrons," Ann. N.Y. Acad. Sci. **161**, 33–43 (1969).
[69]A. S. Shiu, V. A. Otte, and K. R. Hogstrom, "Measurement of dose distributions using film in therapeutic electron beams," Med. Phys. **16**, 911–915 (1989).
[70]B. J. Gerbi and D. A. Dimitroyannis, "The response of Kodak EDR2 film in high-energy electron beams," Med. Phys. **30**, 2703–2705 (2003).
[71]C. G. Soares, "New developments in radiochromic film dosimetry," Radiat. Prot. Dosim. **120**, 100–106 (2006).
[72]A. Niroomand-Rad, C. R. Blackwell, B. M. Coursey, K. P. Gall, J. M. Galvin, W. L. McLaughlin, A. S. Meigooni, R. Nath, J. E. Rodgers, and C. G. Soares, "Radiochromic film dosimetry: Recommendations of AAPM Radiation Therapy Committee Task Group 55. American Association of Physicists in Medicine," Med. Phys. **25**, 2093–2115 (1998).
[73]M. J. Butson, T. Cheung, and P. K. Yu, "Weak energy dependence of EBT gafchromic film dose response in the 50 kVp-10 MVp X-ray range," Appl. Radiat. Isot. **64**, 60–62 (2006).
[74]T. Cheung, M. J. Butson, and P. K. Yu, "Independence of calibration curves for EBT Gafchromic films of the size of high-energy X-ray fields," Appl. Radiat. Isot. **64**, 1027–1030 (2006).
[75]F. C. Su, Y. Liu, S. Stathakis, C. Shi, C. Esquivel, and N. Papanikolaou, "Dosimetry characteristics of GAFCHROMIC EBT film responding to therapeutic electron beams," Appl. Radiat. Isot. **65**, 1187–1192 (2007).
[76]S. Devic, J. Seuntjens, E. Sham, E. B. Podgorsak, C. R. Schmidtlein, A. S. Kirov, and C. G. Soares, "Precise radiochromic film dosimetry using a flat-bed document scanner," Med. Phys. **32**, 2245–2253 (2005).
[77]S. Devic, J. Seuntjens, W. Abdel-Rahman, M. Evans, M. Olivares, E. B. Podgorsak, T. Vuong, and C. G. Soares, "Accurate skin dose measurements using radiochromic film in clinical applications," Med. Phys. **33**, 1116–1124 (2006).
[78]L. M. Gamble, T. J. Farrell, G. W. Jones, and J. E. Hayward, "Two-dimensional mapping of underdosed areas using radiochromic film for patients undergoing total skin electron beam radiotherapy," Int. J. Radiat. Oncol., Biol., Phys. **62**, 920–924 (2005).
[79]L. M. Gamble, T. J. Farrell, G. W. Jones, and J. E. Hayward, "Composite

depth dose measurement for total skin electron (TSE) treatments using radiochromic film," Phys. Med. Biol. **48**, 891–898 (2003).
[80]M. Ciocca, R. Orecchia, C. Garibaldi, E. Rondi, A. Luini, G. Gatti, M. Intra, P. Veronesi, R. Lazzari, G. Tosi, and U. Veronesi, "In vivo dosimetry using radiochromic films during intraoperative electron beam radiation therapy in early-stage breast cancer," Radiother. Oncol. **69**, 285–289 (2003).
[81]K. Al-Yahya, F. Verhaegen, and J. Seuntjens, "Design and dosimetry of a few leaf electron collimator for energy modulated electron therapy," Med. Phys. **34**, 4782–4791 (2007).
[82]B. Fraass, K. Doppke, M. Hunt, G. Kutcher, G. Starkschall, R. Stern, and J. Van Dyk, "American Association of Physicists in Medicine Radiation Therapy Committee Task Group 53: Quality assurance for clinical radiotherapy treatment planning," Med. Phys. **25**, 1773–1829 (1998).
[83]A. S. Shiu, S. Tung, K. R. Hogstrom, J. W. Wong, R. L. Gerber, W. B. Harms, J. A. Purdy, R. K. Ten Haken, D. L. McShan, and B. A. Fraass, "Verification data for electron beam dose algorithms," Med. Phys. **19**, 623–636 (1992).
[84]G. Starkschall, S. W. Bujnowski, L. L. Wang, A. S. Shiu, A. L. Boyer, G. E. Desobry, N. H. Wells, A. L. Baker, and K. R. Hogstrom, "A full three-dimensional radiotherapy treatment planning system," Med. Phys. **18**, 647 (1991).
[85]A. Brahme, I. Lax, and P. Andreo, "Electron beam dose planning using discrete Gaussian beams. Mathematical background," Acta Oncol. **20**, 147–158 (1981).
[86]A. Brahme and I. Lax, "Absorbed dose distribution of electron beams in uniform and inhomogeneous media," Acta Radiol. Diagn. (Stockh) **364**, 61–72 (1983).
[87]K. R. Hogstrom, in *Radiation Oncology Physics*, Medical Physics Monograph No. 15, edited by J. G. Kereiakes, H. R. Elson, and C. G. Born (American Institute of Physics, New York, NY, 1987), pp. 532–557.
[88]J. Cygler, J. J. Battista, J. W. Scrimger, E. Mah, and J. A. Antolak, "Electron dose distributions in experimental phantoms: A comparison with 2D pencil beam calculations," Phys. Med. Biol. **32**, 1073–1086 (1987).
[89]E. Mah, J. A. Antolak, J. W. Scrimger, and J. J. Battista, "Experimental evaluation of a 2D and 3D electron pencil beam algorithm," Phys. Med. Biol. **34**, 1179–1194 (1989).
[90]A. Brahme, "Current algorithms for computed electron beam dose planning," Radiother. Oncol. **3**, 347–362 (1985).
[91]K. R. Hogstrom and R. E. Steadham, in *Teletherapy: Present and Future*, edited by J. Palta and T. R. Mackie (Advanced Medical, Madison, 1996), pp. 137–174.
[92]P. J. Keall and P. W. Hoban, "A review of electron beam dose calculation algorithms," Australas. Phys. Eng. Sci. Med. **19**, 111–130 (1996).
[93]K. R. Hogstrom and P. R. Almond, "Review of electron beam therapy physics," Phys. Med. Biol. **51**, R455–R489 (2006).
[94]I. J. Chetty, B. Curran, J. E. Cygler, J. J. DeMarco, G. Ezzell, B. A. Faddegon, I. Kawrakow, P. J. Keall, H. Liu, C. M. Ma, D. W. Rogers, J. Seuntjens, D. Sheikh-Bagheri, and J. V. Siebers, "Report of the AAPM Task Group No. 105: Issues associated with clinical implementation of Monte Carlo-based photon and electron external beam treatment planning," Med. Phys. **34**, 4818–4853 (2007).
[95]R. A. Boyd, K. R. Hogstrom, J. A. Antolak, and A. S. Shiu, "A measured data set for evaluating electron-beam dose algorithms," Med. Phys. **28**, 950–958 (2001).
[96]D. A. Low, G. Starkschall, S. W. Bujnowski, L. L. Wang, and K. R. Hogstrom, "Electron bolus design for radiotherapy treatment planning: Bolus design algorithms," Med. Phys. **19**, 115–124 (1992).
[97]G. H. Perkins, M. D. McNeese, J. A. Antolak, T. A. Buchholz, E. A. Strom, and K. R. Hogstrom, "A custom three-dimensional electron bolus technique for optimization of postmastectomy irradiation," Int. J. Radiat. Oncol., Biol., Phys. **51**, 1142–1151 (2001).
[98]R. J. Kudchadker, J. A. Antolak, W. H. Morrison, P. F. Wong, and K. R. Hogstrom, "Utilization of custom electron bolus in head and neck radiotherapy," J. Appl. Clin. Med. Phys. **4**, 321–333 (2003).
[99]D. D. Leavitt, L. M. Peacock, Jr., F. A. Gibbs, and J. R. Stewart, "Electron arc therapy: Physical measurement and treatment planning techniques," Int. J. Radiat. Oncol., Biol., Phys. **11**, 987–999 (1985).
[100]D. D. Leavitt, J. R. Stewart, and L. Earley, "Improved dose homogeneity in electron arc therapy achieved by a multiple-energy technique," Int. J. Radiat. Oncol., Biol., Phys. **19**, 159–165 (1990).
[101]D. D. Leavitt and J. R. Stewart, "Electron arc therapy of the postmastectomy prosthetic breast," Int. J. Radiat. Oncol., Biol., Phys. **28**, 297–301 (1994).
[102]International Commission on Radiation Units and Measurements Report No. 29, "Dose specification for reporting external beam therapy with photons and electrons," 1978.
[103]International Commission on Radiation Units and Measurements Report No. 71, "Prescribing, recording, and reporting electron beam therapy," 2004.
[104]International Commission on Radiation Units and Measurements Report No. 50, "Prescribing, recording, and reporting photon beam therapy," 1993.
[105]International Commission on Radiation Units and Measurements Report No. 62, "Prescribing, recording, and reporting photon beam therapy (Supplement to ICRU Report No. 50)," 1999.
[106]R. Chobe, M. McNeese, R. Weber, and G. H. Fletcher, "Radiation therapy for carcinoma of the nasal vestibule," Otolaryngol.-Head Neck Surg. **98**, 67–71 (1988).
[107]M. Gosselin, E. B. Podgorsak, M. D. Evans, M. Pla, and G. Shenouda, "A technique using parallel-opposed high energy electron beams for reirradiation of tumors near the spinal cord," Int. J. Radiat. Oncol., Biol., Phys. **27**, 1207–1214 (1993).
[108]K. R. Hogstrom, R. E. Steadham, Jr., E. A. Strom, and M. D. McNeese, "Concerns regarding technique using parallel-opposed high-energy electron beams for reirradiation of tumors near the spinal cord (recurrent Hodgkin's lymphoma)," Int. J. Radiat. Oncol., Biol., Phys. **31**, 683–685 (1995).
[109]M. Gosselin, E. B. Podgorsak, M. D. C. Evans, M. Pla, and G. Shenouda, "Response to Hogstrom *et al.*," Int. J. Radiat. Oncol., Biol., Phys. **31**, 684–685 (1995).
[110]D. P. Fontenla, M. Ahmad, C. S. Chui, B. McCormick, D. H. Abramson, and G. J. Kutcher, "Effect of ocular implants of different materials on the dosimetry of external beam radiation therapy," Int. J. Radiat. Oncol., Biol., Phys. **32**, 1477–1480 (1995).
[111]E. D. Yorke, A. Kassaee, T. Doyle, L. A. Loevner, and D. I. Rosenthal, "The dose distribution of medium energy electron boosts to the laryngectomy stoma," J. Appl. Clin. Med. Phys. **2**, 9–20 (2001).
[112]I. Kawrakow, M. Fippel, and K. Friedrich, "3D electron dose calculation using a Voxel based Monte Carlo algorithm (VMC)," Med. Phys. **23**, 445–457 (1996).
[113]I. Kawrakow, "Improved modeling of multiple scattering in the Voxel Monte Carlo model," Med. Phys. **24**, 505–517 (1997).
[114]H. Neuenschwander and E. J. Born, "A macro Monte Carlo method for electron beam dose calculations," Phys. Med. Biol. **37**, 107–125 (1992).
[115]H. Neuenschwander, T. R. Mackie, and P. J. Reckwerdt, "MMC–A high-performance Monte Carlo code for electron beam treatment planning," Phys. Med. Biol. **40**, 543–574 (1995).
[116]G. X. Ding, J. E. Cygler, G. G. Zhang, and M. K. Yu, "Evaluation of a commercial three-dimensional electron beam treatment planning system," Med. Phys. **26**, 2571–2580 (1999).
[117]M. M. Glegg, "Electron dose calculations: A comparison of two commercial treatment planning computers," Med. Dosim. **28**, 99–105 (2003).
[118]P. J. Keall and P. W. Hoban, "Super-Monte Carlo: A 3-D electron beam dose calculation algorithm," Med. Phys. **23**, 2023–2034 (1996).
[119]G. X. Ding, J. E. Cygler, C. W. Yu, N. I. Kalach, and G. Daskalov, "A comparison of electron beam dose calculation accuracy between treatment planning systems using either a pencil beam or a Monte Carlo algorithm," Int. J. Radiat. Oncol., Biol., Phys. **63**, 622–633 (2005).
[120]R. A. Popple, R. Weinber, J. A. Antolak, S. J. Ye, P. N. Pareek, J. Duan, S. Shen, and I. A. Brezovich, "Comprehensive evaluation of a commercial macro Monte Carlo electron dose calculation implementation using a standard verification data set," Med. Phys. **33**, 1540–1551 (2006).
[121]A. S. Shiu and K. R. Hogstrom, "Pencil-beam redefinition algorithm for electron dose distributions," Med. Phys. **18**, 7–18 (1991).
[122]R. A. Boyd, K. R. Hogstrom, and I. I. Rosen, "Effect of using an initial polyenergetic spectrum with the pencil-beam redefinition algorithm for electron-dose calculations in water," Med. Phys. **25**, 2176–2185 (1998).
[123]R. A. Boyd, K. R. Hogstrom, R. A. White, and G. Starkschall, "Modelling pencil-beam divergence with the electron pencil-beam redefinition algorithm," Phys. Med. Biol. **46**, 2841–2856 (2001).
[124]R. A. Boyd, K. R. Hogstrom, and G. Starkschall, "Electron pencil-beam redefinition algorithm dose calculations in the presence of heterogeneities," Med. Phys. **28**, 2096–2104 (2001).

[125]R. A. Boyd, Ph.D. thesis, The University of Texas Graduate School of Biomedical Sciences, 2001.
[126]H. Huizenga and P. R. Storchi, "Numerical calculation of energy deposition by broad high-energy electron beams," Phys. Med. Biol. **34**, 1371–1396 (1989).
[127]J. J. Janssen, E. W. Korevaar, P. R. Storchi, and H. Huizenga, "Numerical calculation of energy deposition by high-energy electron beams: III-B. Improvements to the 6D phase space evolution model," Phys. Med. Biol. **42**, 1441–1449 (1997).
[128]D. Scora and B. A. Faddegon, "Monte Carlo based phase-space evolution for electron dose calculation," Med. Phys. **24**, 177–187 (1997).
[129]E. W. Korevaar, A. Akhiat, B. J. Heijmen, and H. Huizenga, "Accuracy of the phase space evolution dose calculation model for clinical 25 MeV electron beams," Phys. Med. Biol. **45**, 2931–2945 (2000).
[130]B. J. Gerbi, "The response characteristics of a newly designed plane-parallel ionization chamber in high-energy photon and electron beams," Med. Phys. **20**, 1411–1415 (1993).
[131]J. O. Archambeau, B. Forell, R. Doria, D. O. Findley, R. Jurisch, and R. Jackson, "Use of variable thickness bolus to control electron beam penetration in chest wall irradiation," Int. J. Radiat. Oncol., Biol., Phys. **7**, 835–842 (1981).
[132]J. L. Beach, C. W. Coffey, and J. S. Wade, "Individualized chest wall compensating bolus for electron irradiation following mastectomy: An ultrasound approach," Int. J. Radiat. Oncol., Biol., Phys. **7**, 1607–1611 (1981).
[133]J. A. Antolak, J. W. Scrimger, and E. Mah, "Optimization of a cord shielding technique for electrons," Australas. Phys. Eng. Sci. Med. **15**, 91–94 (1992).
[134]R. J. Kudchadker, K. R. Hogstrom, A. S. Garden, M. D. McNeese, R. A. Boyd, and J. A. Antolak, "Electron conformal radiotherapy using bolus and intensity modulation," Int. J. Radiat. Oncol., Biol., Phys. **53**, 1023–1037 (2002).
[135]M. D. McNeese, G. H. Fletcher, S. H. Levitt, and F. M. Khan, in *Levitt and Tapley's Technological Basis of Radiation Therapy, Practical Clinical Applications*, edited by S. H. Levitt, F. M. Kahn, and R. A. Potish (Lea and Febiger, Philadephia, 1992).
[136]G. C. Bentel, *Radiation Therapy Planning*, 2nd ed. (McGraw-Hill, New York, NY, 1996) (used for ACMP 2000 talks on immobilization and treatment techniques).
[137]D. W. Arthur, R. D. Zwicker, P. W. Garmon, D. T. Huang, and R. K. Schmidt-Ullrich, "Electron/photon matched field technique for treatment of orbital disease," Int. J. Radiat. Oncol., Biol., Phys. **37**, 469–474 (1997).
[138]T. Whelan, "Treatment of the internal mammary nodes in early breast cancer: Back to the future," Clin. Oncol. (R Coll. Radiol) **15**, 14–16 (2003).
[139]D. Severin, S. Connors, H. Thompson, S. Rathee, P. Stavrev, and J. Hanson, "Breast radiotherapy with inclusion of internal mammary nodes: A comparison of techniques with three-dimensional planning," Int. J. Radiat. Oncol., Biol., Phys. **55**, 633–644 (2003).
[140]D. W. Arthur, M. R. Arnfield, L. A. Warwicke, M. M. Morris, and R. D. Zwicker, "Internal mammary node coverage: An investigation of presently accepted techniques," Int. J. Radiat. Oncol., Biol., Phys. **48**, 139–146 (2000).
[141]C. A. Perez, M. E. Taylor, J. D. Bradley, D. Mansur, and M. M. Sanchez-Aragon, in *Principles and Practice of Radiation Oncology*, edited by C. A. Perez *et al.* (Lippincott Williams & Wilkins, Philadelphia, 2004).
[142]R. K. Benda, G. Yasuda, A. Sethi, S. G. Gabram, R. W. Hinerman, and N. P. Mendenhall, "Breast boost: Are we missing the target?" Cancer **97**, 905–909 (2003).
[143]P. M. Messer, I. C. Kirikuta, K. Bratengeier, and M. Flentje, "CT planning of boost irradiation in radiotherapy of breast cancer after conservative surgery," Radiother. Oncol. **42**, 239–243 (1997).
[144]G. J. Kutcher, L. Coia, M. Gillin, W. F. Hanson, S. Leibel, R. J. Morton, J. R. Palta, J. A. Purdy, L. E. Reinstein, G. K. Svensson, L. Wingfield, and M. Weller, "Comprehensive QA for radiation oncology: Report of AAPM Radiation Therapy Committee Task Group 40," Med. Phys. **21**, 581–618 (1994).
[145]S. J. Feigenberg, N. Price Mendenhall, R. K. Benda, and C. G. Morris, "Postmastectomy radiotherapy: Patterns of recurrence and long-term disease control using electrons," Int. J. Radiat. Oncol., Biol., Phys. **56**, 716–725 (2003).
[146]M. M. Spierer, L. X. Hong, R. T. Wagman, M. S. Katz, R. L. Spierer, and B. McCormick, "Postmastectomy CT-based electron beam radiotherapy: Dosimetry, efficacy, and toxicity in 118 patients," Int. J. Radiat. Oncol., Biol., Phys. **60**, 1182–1189 (2004).
[147]L. J. Pierce, J. B. Butler, M. K. Martel, D. P. Normolle, T. Koelling, R. B. Marsh, A. S. Lichter, and B. A. Fraass, "Postmastectomy radiotherapy of the chest wall: Dosimetric comparison of common techniques," Int. J. Radiat. Oncol., Biol., Phys. **52**, 1220–1230 (2002).
[148]Y. C. Ung, K. E. Sixel, and C. Bell, "The influence of patient geometry on the selection of chest wall irradiation techniques in post-mastectomy breast cancer patients," Radiother. Oncol. **57**, 69–77 (2000).
[149]B. Paliwal, *Proceedings of the Symposium of Electron Dosimetry and Arc Therapy* (American Institute of Physics, New York, 1982).
[150]M. Tobler, D. D. Leavitt, and J. K. Hayes, "Dosimetry and treatment planning of complex electron arc therapy," Med. Dosim. **20**, 229–235 (1995).
[151]M. Olivares-Pla, E. B. Podgorsak, and C. Pla, "Electron arc dose distributions as a function of beam energy," Med. Phys. **24**, 127–132 (1997).
[152]A. L. Boyer, G. D. Fullerton, and J. G. Mira, "An electron beam pseudoarc technique for irradiation of large areas of chest wall and other curved surfaces," Int. J. Radiat. Oncol., Biol., Phys. **8**, 1969–1974 (1982).
[153]D. D. Leavitt, J. R. Stewart, J. H. Moeller, and L. Earley, in *Advances in Radiation Oncology Physics: Dosimetry, Treatment Planning, and Brachytherapy*, Medical Physics Monograph No. 19, edited by J. A. Purdy (American Institute of Physics, Woodbury, NY, 1992), p. 430.
[154]F. M. Khan, G. D. Fullerton, J. M. Lee, V. C. Moore, and S. H. Levitt, "Physical aspects of electron-beam arc therapy," Radiology **124**, 497–500 (1977).
[155]K. R. Kase and B. E. Bjärngard, "Bremsstrahlung dose to patients in rotational electron therapy," Radiology **133**, 531–532 (1979).
[156]F. M. Khan, *The Physics of Radiation Therapy*, 3rd ed. (Lippincott Williams & Wilkins, Philadelphia, 2003) (used for ACMP 2000 talks on immobilization and treatment techniques).
[157]K. R. Hogstrom and D. D. Leavitt, in *Radiation Oncology Physics*, Medical Physics Monograph No. 15, edited by J. G. Kereiakes, H. R. Elson, and C. G. Born (American Institute of Physics, New York, NY, 1987), pp. 265–295.
[158]F. M. Khan, "Calibration and treatment planning of electron beam arc therapy," in *Proceedings of the Symposium of Electron Dosimetry and Arc Therapy*, edited by B. Paliwal (American Institute of Physics, New York, 1982), p. 249.
[159]C. M. Able, M. D. Mills, M. D. McNeese, and K. R. Hogstrom, "Evaluation of a total scalp electron irradiation technique," Int. J. Radiat. Oncol., Biol., Phys. **21**, 1063–1072 (1991).
[160]C. Akazawa, "Treatment of the scalp using photon and electron beams," Med. Dosim. **14**, 129–131 (1989).
[161]S. S. Tung, A. S. Shiu, G. Starkschall, W. H. Morrison, and K. R. Hogstrom, "Dosimetric evaluation of total scalp irradiation using a lateral electron-photon technique," Int. J. Radiat. Oncol., Biol., Phys. **27**, 153–160 (1993).
[162]N. D. Tapley, *Clinical Applications of the Electron Beam* (Wiley, New York, 1976).
[163]R. Yaparpalvi, D. P. Fontenla, S. K. Tyerech, L. R. Boselli, and J. J. Beitler, "Parotid gland tumors: A comparison of postoperative radiotherapy techniques using three dimensional (3D) dose distributions and dose-volume histograms (DVHS)," Int. J. Radiat. Oncol., Biol., Phys. **40**, 43–49 (1998).
[164]W. H. Morrison, P. F. Wong, G. Starkschall, A. S. Garden, C. Childress, K. R. Hogstrom, and L. J. Peters, "Water bolus for electron irradiation of the ear canal," Int. J. Radiat. Oncol., Biol., Phys. **33**, 479–483 (1995).
[165]R. D. Weaver, B. J. Gerbi, and K. E. Dusenbery, "Evaluation of eye shields made of tungsten and aluminum in high-energy electron beams," Int. J. Radiat. Oncol., Biol., Phys. **41**, 233–237 (1998).
[166]A. S. Shiu, S. S. Tung, R. J. Gastorf, K. R. Hogstrom, W. H. Morrison, and L. J. Peters, "Dosimetric evaluation of lead and tungsten eye shields in electron beam treatment," Int. J. Radiat. Oncol., Biol., Phys. **35**, 599–604 (1996).
[167]D. H. Abramson, B. McCormick, and A. C. Schefler, "Retinoblastoma," in *Textbook of Radiation Oncology*, edited by S. A. Leibel and T. L. Phillips (Elsevier, New York, 2004), Chap. 65.

[168]B. McCormick, R. Ellsworth, D. Abramson, B. Haik, M. Tome, E. Grabowski, and T. LoSasso, "Radiation therapy for retinoblastoma: Comparison of results with lens-sparing versus lateral beam techniques," Int. J. Radiat. Oncol., Biol., Phys. **15**, 567–574 (1988).
[169]R. J. Steenbakkers, M. D. Altschuler, D. A. GJ, J. W. Goldwein, and A. Kassaee, "Optimized lens-sparing treatment of retinoblastoma with electron beams," Int. J. Radiat. Oncol., Biol., Phys. **39**, 589–594 (1997).
[170]J. Schipper, "An accurate and simple method for megavoltage radiation therapy of retinoblastoma," Radiother. Oncol. **1**, 31–41 (1983).
[171]F. Borger, I. Rosenberg, S. Vijayakumar, R. Virudachalam, D. Schneider, V. Langmuir, and G. T. Chen, "An anterior appositional electron field technique with a hanging lens block in orbital radiotherapy: A dosimetric study," Int. J. Radiat. Oncol., Biol., Phys. **21**, 795–804 (1991).
[172]K. Rykers, G. Uden, and V. Thompson, "Orbital lymphoma: A simple treatment using electrons," Med. Dosim. **28**, 95–98 (2003).
[173]P. Zhou, A. K. Ng, B. Silver, S. Li, L. Hua, and P. M. Mauch, "Radiation therapy for orbital lymphoma," Int. J. Radiat. Oncol., Biol., Phys. **63**, 866–871 (2005).
[174]J. M. Johnson and F. M. Khan, "Dosimetric effects of abutting extended source to surface distance electron fields with photon fields in the treatment of head and neck cancers," Int. J. Radiat. Oncol., Biol., Phys. **28**, 741–747 (1994).
[175]M. H. Maor, R. S. Fields, K. R. Hogstrom, and J. van Eys, "Improving the therapeutic ratio of craniospinal irradiation in medulloblastoma," Int. J. Radiat. Oncol., Biol., Phys. **11**, 687–697 (1985).
[176]L. Dewit, J. Van Dam, A. Rijnders, G. van de Velde, K. K. Ang, and E. van der Schueren, "A modified radiotherapy technique in the treatment of medulloblastoma," Int. J. Radiat. Oncol., Biol., Phys. **10**, 231–241 (1984).
[177]R. Miralbell, A. Bleher, P. Huguenin, G. Ries, R. Kann, R. O. Mirimanoff, M. Notter, P. Nouet, S. Bieri, P. Thum, and H. Toussi, "Pediatric medulloblastoma: Radiation treatment technique and patterns of failure," Int. J. Radiat. Oncol., Biol., Phys. **37**, 523–529 (1997).
[178]M. H. Maor, K. R. Hogstrom, and R. S. Fields, in *Malignant Tumors of Childhood*, edited by B. F. Brooks (The University of Texas Press, Austin, 1986), pp. 245–254.
[179]D. M. Roback, J. M. Johnson, F. M. Khan, G. P. Engeler, and W. A. McGuire, "The use of tertiary collimation for spinal irradiation with extended SSD electron fields," Int. J. Radiat. Oncol., Biol., Phys. **37**, 1187–1192 (1997).
[180]C. Hood, T. Kron, C. Hamilton, S. Callan, S. Howlett, F. Alvaro, and M. Back, "Correlation of 3D-planned and measured dosimetry of photon and electron craniospinal radiation in a pediatric anthropomorphic phantom," Radiother. Oncol. **77**, 111–116 (2005).
[181]J. R. Palta, P. J. Biggs, J. D. Hazle, M. S. Huq, R. A. Dahl, T. G. Ochran, J. Soen, R. R. Dobelbower, and E. C. McCullough, "Intraoperative electron beam radiation therapy: Technique, dosimetry, and dose specification: Report of Task Force 48 of the Radiation Therapy Committee, American Association of Physicists in Medicine," Int. J. Radiat. Oncol., Biol., Phys. **33**, 725–746 (1995).
[182]A. S. Beddar, P. J. Biggs, S. Chang, G. A. Ezzell, B. A. Faddegon, F. W. Hensley, and M. D. Mills, "Intraoperative radiation therapy using mobile electron linear accelerators: Report of AAPM Radiation Therapy Committee Task Group No. 72," Med. Phys. **33**, 1476–1489 (2006).
[183]C. J. Karzmark, R. Loevinger, R. E. Steele, and M. Weissbluth, "A technique for large-field, superficial electron therapy," Radiology **74**, 633–644 (1960).
[184]C. J. Karzmark, "Large-field superficial electron therapy with linear accelerators," Br. J. Radiol. **37**, 302–305 (1964).
[185]C. J. Karzmark, "Physical aspects of whole-body superficial therapy with electrons," Front. Radiat. Ther. Oncol. **2**, 36–54 (1968).
[186]V. Page, A. Gardner, and C. J. Karzmark, "Patient dosimetry in the electron treatment of large superficial lesions," Radiology **94**, 635–641 (1970).
[187]G. R. Edelstein, T. Clark, and J. G. Holt, "Dosimetry for total-body electron-beam therapy in the treatment of mycosis fungoides," Radiology **108**, 691–694 (1973).
[188]B. E. Bjärngard, G. T. Chen, R. W. Piontek, and G. K. Svensson, "Analysis of dose distributions in whole body superficial electron therapy," Int. J. Radiat. Oncol., Biol., Phys. **2**, 319–324 (1977).
[189]R. T. Hoppe, Z. Fuks, and M. A. Bagshaw, "Radiation therapy in the management of cutaneous T-cell lymphomas," Cancer Treat. Rep. **63**, 625–632 (1979).
[190]R. T. Hoppe, R. S. Cox, Z. Fuks, N. M. Price, M. A. Bagshaw, and E. M. Farber, "Electron-beam therapy for mycosis fungoides: The Stanford University experience," Cancer Treat. Rep. **63**, 691–700 (1979).
[191]B. A. Fraass, P. L. Roberson, and E. Glatstein, "Whole-skin electron treatment: patient skin dose distribution," Radiology **146**, 811–814 (1983).
[192]American Association of Physicists in Medicine Report No. 23, "Total skin electron therapy: technique and dosimetry," 1987.
[193]R. T. Hoppe, "Total skin electron beam therapy in the management of mycosis fungoides," Front. Radiat. Ther. Oncol. **25**, 80–89 (1991).
[194]Z. Chen, A. G. Agostinelli, L. D. Wilson, and R. Nath, "Matching the dosimetry characteristics of a dual-field Stanford technique to a customized single-field Stanford technique for total skin electron therapy," Int. J. Radiat. Oncol., Biol., Phys. **59**, 872–885 (2004).
[195]F. M. Khan, in *Advances in Radiation Oncology Physics*, Medical Physics Monograph No. 19, edited by J. A. Purdy (American Institute of Physics, New York, 1992), pp. 466–479.
[196]J. A. Antolak and K. R. Hogstrom, "Multiple scattering theory for total skin electron beam design," Med. Phys. **25**, 851–859 (1998).
[197]J. A. Antolak, J. H. Cundiff, and C. S. Ha, "Utilization of thermoluminescent dosimetry in total skin electron beam radiotherapy of mycosis fungoides," Int. J. Radiat. Oncol., Biol., Phys. **40**, 101–108 (1998).
[198]I. J. Das, J. F. Copeland, and H. S. Bushe, "Spatial distribution of bremsstrahlung in a dual electron beam used in total skin electron treatments: Errors due to ionization chamber cable irradiation," Med. Phys. **21**, 1733–1738 (1994).
[199]R. D. Weaver, B. J. Gerbi, and K. E. Dusenbery, "Evaluation of dose variation during total skin electron irradiation using thermoluminescent dosimeters," Int. J. Radiat. Oncol., Biol., Phys. **33**, 475–478 (1995).
[200]K. K. Wooden, K. R. Hogstrom, P. Blum, R. J. Gastorf, and J. D. Cox, "Whole-limb irradiation of the lower calf using a six-field electron technique," Med. Dosim. **21**, 211–218 (1996).
[201]K. E. Ekstrand and R. L. Dixon, "The problem of obliquely incident beams in electron-beam treatment planning," Med. Phys. **9**, 276–278 (1982).
[202]K. R. Hogstrom, in *Principles and Practice of Radiation Oncology*, edited by C. A. Perez *et al.* (Lippincott Williams & Wilkins, Philadelphia, 2004), pp. 252–282.
[203]Netherlands Commission on Radiation Dosimetry Report No. 5, "Code of practice for the dosimetry of high-energy electron beams," 1989.
[204]H. Kubo, L. J. Kent, and G. Krithivas, "Determinations of Ngas and Prepl factors from commercially available parallel-plate chambers: AAPM Task Group 21 protocol," Med. Phys. **13**, 908–912 (1986).
[205]F. T. Kuchnir and C. S. Reft, "Experimental determination of fluence perturbation factors for five parallel–late ionization chambers," Med. Phys. **20**, 3331–335 (1992).
[206]R. P. Nair *et al.*, "Shaped field electron dosimetry for a Philips SL75/10 linear accelerator," Med. Phys. **10**, 356–360 (1983).
[207]H. Rashid *et al.*, "Small-field electron dosimetry for the Philips SL25 linear accelerator," Med. Phys. **17**, 710–715 (1990).
[208]M. S. A. L. Al-Ghazi and I. Tavaras, "Relative output factors for electron fields," Med. Phys. **20**, 886 (1993).
[209]A. Niroomand-Rad, "Film dosimetry of small elongated electron beams for treatment planning," Med. Phys. **16**, 655–662 (1989).